Insights into Genipin Dye Mechanisms and Colour Origins

Fiona Jeeva

A Thesis Submitted to the Faculty of Graduate Studies in Partial Fulfillment of the Requirements for the Degree of

MASTER OF SCIENCE

GRADUATE PROGRAM IN CHEMISTRY

York University

Toronto, Ontario

May 2021

Abstract

Genipin is a natural compound that forms colours when reacted with primary amines. Curiously, it contains a large amount of uncertainty surrounding its dye structure. It was previously believed that genipin reacts with primary amines to first form a red intermediate dye that polymerizes to form a blue dye when exposed to oxygen. We have determined that the dye colour can be altered by reacting genipin with aromatic amines, producing green dyes instead of blue dyes. In addition, we have found that these dyes are not polymers at all, and their characteristic blue colour is instead the result of a persistent radical, supported by NMR spectroscopy, MS, and EPR spectroscopy. Furthermore, we have shown that the oxidation of the allylic alcohol functionality can form the oxetane derivative via a 2,3-epoxyalcohol rearrangement that can alter the redox properties of the dye, and thereby halting the dye formation at its red intermediate.

Acknowledgements

First and foremost, I would like to thank my supervisor Professor Christopher Caputo for his invaluable guidance and support. I truly believe that I have grown immensely as a person and as a chemist under his supervision. A special thanks to everyone else in the Caputo group: Jordan and Lucas as my first friends here, Ian and Sanjay for their incredible help, and everyone else in the lab for their support. I am also grateful to my committee members, Professor Baumgartner and Professor Hili for their guidance that I appreciate deeply. To Billy, my parents and my sister: I'm so fortunate to have you for the emotional support that helped me get through some tough times. Finally, a special thanks to Dr. Howard Hunter and Dr. Karl Demmans for their counseling and technical help with NMR and EPR; my work would not have been possible without them.

Table of Contents

List of Figures

List of Schemes

List of Abbreviations

CHCA……α-cyano-4-hydroxycinnamic acid

COSY……..….correlated spectroscopy

CV.....cyclic voltammetry

CW ……...Continuous wave

DCM……...dichloromethane

DMSO……...dimethylsulfoxide

EB……..…emeraldine base

EPR……..electron paramagnetic resonance

ES…….emeraldine salt

ESI……..Electrospray ionization

EtOAc……...ethyl acetate

g……...……..Landé g-factor

G……gauss

GPC……gel permeation chromatography

HMBC…….heteronuclear multiple bond correlation

HOMO……..……..highest occupied molecular orbital

HSQC…….heteronuclear single quantum coherence

LA……..loganin aglycone

LUMO……Lowest unoccupied molecular orbital

MALDI……Matrix-associated laser desorption/ionization

mCPBA……*m*-chloroperbenzoic acid

MS……mass spectrometry

m/z……mass to charge ratio

NMR……nuclear magnetic resonance

PANI……polyaniline

ppm……parts per million

S/N……signal-to-noise ratio

TD-DFT……time dependant density functional theory

TLC……thin layer chromatography

UCP2……uncoupling protein 2

UV……ultraviolet light

Vis……visible light

Chapter 1. Introduction

Chapter 1.1 Blue — Nature's Elusive Dye

Considering the prevalence of the diverse array of colours that surround us in present day, it can be difficult to notice the inherent lack of blue in nature. As nature is a diverse term, referring not only to living organisms that occupy the Earth but also the landscape and products of the planet itself, it is therefore necessary to distinguish between the natural blue pigments formed from organic and inorganic compounds. Within the inorganic realm, blue pigments are far more accessible. Many have even been used for centuries: the ultramarine dye obtained from the rock *lapis lazuli*; cobalt(II) aluminate, used for blue in traditional Chinese ceramics; and the mineral chalcanthite, containing copper(II) sulfate. There are numerous other examples, as inorganic compounds have the ability to access these blues through charge-transfer transitions between metals and ligands, or more commonly, electronic transitions between nondegenerate d-orbitals.[1] Yet when it comes to organic compounds, blue is one of the rarest of colours; it is much more difficult to achieve absorption at longer wavelengths since it requires having very closely lying frontier orbitals, which generally involves an extensively conjugated system. When compared to transition metal complexes, a smaller difference in energy between the nondegenerate d-orbitals can be much more easily attained than the tuning of the HOMO-LUMO gap of an organic compound. Of course, the ability of a *naturally* occurring organic compound to achieve this is even more difficult; so difficult in fact that many of the blues we see in plants and animals are not the result of blue pigments at all. While the world is saturated with oranges, reds and yellows from the large abundance of cartenoids (λ_{max} ~ 400–500 nm) and anthocyanins (λ_{max} ~ 500–550 nm)[2], this colouration is derived from pigments: materials containing colours that are produced by the selective absorption of wavelengths.

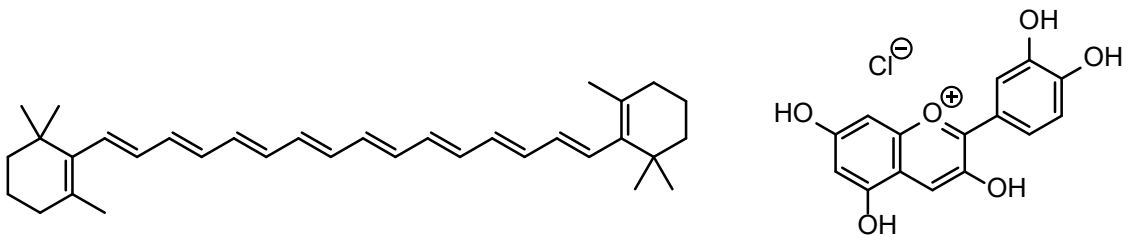

Figure 1. Structures of common natural colourants, β-carotene (a cartenoid) and cyanidin chloride (an anthocyanin).

However, regarding many of the blues seen in animals such as Bluejays or the famous blue Morpho butterflies, the colours we perceive are due to something other than pigments — a phenomenon known as structural colour. Structural colours achieve their colouration through nanostructured surfaces, exploiting the differential reflection and scattering of light[3,4]. Blue wavelengths are more efficiently scattered than reds and yellows; we see examples of this in our everyday lives — it is the answer to the age-old question "Why is the sky blue?" and explains the colours of blue and green eyes. Thus, in addition to blue already being an extremely rare colour, the majority are due to these structural colours, an entirely different process of colour perception when compared to traditional pigments. Nature seems to cheat its way into producing blue not only through these structural colours, but also in the compounds that are most commonly responsible for blue pigments in nature. Anthocyanins, as mentioned before, are commonly reddish in colour, however this pigmentation is seen at lower pH's. Under basic conditions, anthocyanins adopt their quinoidal base form, which absorbs at higher wavelengths than its flavylium counterparts.[5] Consequently, this results in the blues and purples of fruits like blueberries and blackberries. Yet even these blue pigments are not very stable on their own, and generally require co-pigments or even formation of metal complexes with metals like magnesium and calcium to maintain the stability of the blue hues.[6] Thus, finding a stable, naturally occurring blue pigment still proves to be a challenge. Albeit, not an impossible one. A famous example is

Indigo dye: a dark blue, naturally occurring indole derivative extracted from the plant *Indigofera tinctoria* that has been used throughout history. Its use dates back as far as 6000 years ago due to its distinct bright blue colour and great stability. In today's day and age, it is commonly known as the dye in blue jeans and is now being produced synthetically. Though uncommon, there are other examples of blue dyes that fit these criteria; and in the search for these compounds, the study of a much lesser-known candidate has grown in the past decade. Genipin: a naturally occurring iridoid that forms deep blue dyes with reportedly even greater photostability than Indigo.[7,8]

Chapter 1.2 Introduction to Genipin

Genipin is a naturally occurring compound isolated from plants around the world and has been used in a wide range of applications. In most plants where genipin is found, its parent compound, geniposide, is also abundant. Geniposide belongs to a class of compounds called iridoids, a type of monoterpenoid with a general structure of a cyclopentanopyran glycoside where the glycoside is most often a glucose molecule. Enzymatic hydrolysis of the glycosyl group from geniposide affords genipin and is therefore classified as a geniposide aglycone.

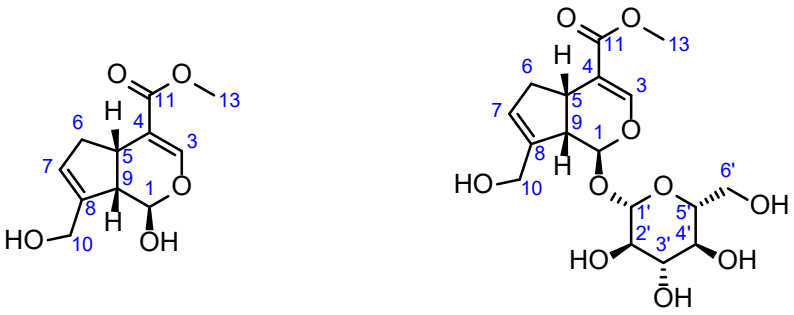

Genipin Geniposide

Figure 2. Molecular structures of genipin and geniposide with iridoid numbering.

Chapter 1.2.1. Applications of Genipin

While genipin has garnered a lot of interest for its dye properties, it has also been used over centuries for its therapeutic characteristics. Some of the oldest known uses of genipin is in traditional Chinese medicine as an anti-inflammatory and for hepatic disorder treatment. And while many tend to dismiss Chinese herbal remedies, significant amounts of research surrounding the therapeutic effects of genipin have been investigated in recent years. For example, this long history of genipin has been affirmed by research that has shown its significant impacts on treating liver diseases.[9,10] Initially, it was geniposide that was administered and demonstrated benefits for chronic liver injury, and while studies have shown that geniposide has therapeutic effects on liver disease, further research has revealed that that genipin also plays a large role in regulating hepatic toxicity.[9,11,12] The presence of β-glucosidase enzymes present in the bowel can hydrolyze geniposide to genipin. Consequently, by administering geniposide, therapeutic effects of both compounds can be achieved by generating genipin *in vivo*.[13] Interestingly enough, genipin exhibits benefits for other disorders as well, such as type 2 diabetes by stimulating insulin secretion from pancreatic islets, as well as an anti-cancer agent through a variety of pathways. Though it exerts its therapeutic responses via various mechanisms, one major mechanism of action appears to be its ability to inhibit Uncoupling Protein 2 (UCP2), resulting in positive effects with respect to liver disease, type 2 diabetes and cancer.[10,14–16] Aside from its potential to be used as a drug, genipin also offers benefits to applications in drug delivery.[17,18] Some drug delivery systems work by exploiting natural polymers such as chitosan, gelatin and other proteins as scaffolds for hydrogels due to their low toxicity and good biocompatibility. However, forming these hydrogels requires crosslinking of the biopolymers, usually by a crosslinking agent such as glutaraldehyde. Still, there is cause for concern around glutaraldehyde's toxicity, which can offset the benefits of the natural polymer's biocompatibility. Crosslinking of polymers such as chitosan work by reacting with the free amine groups formed after the deacetylation of chitin. Fortunately,

genipin reacts readily with primary amines and forms oligomers that react at multiple sites on the molecule, and is able to act as a crosslinking agent for these amine-containing biomolecules (**Figure 3**) with toxicity of 5000 – 10 000 times less than that of glutaraldehyde, making it an excellent candidate for a glutaraldehyde alternative.[12]

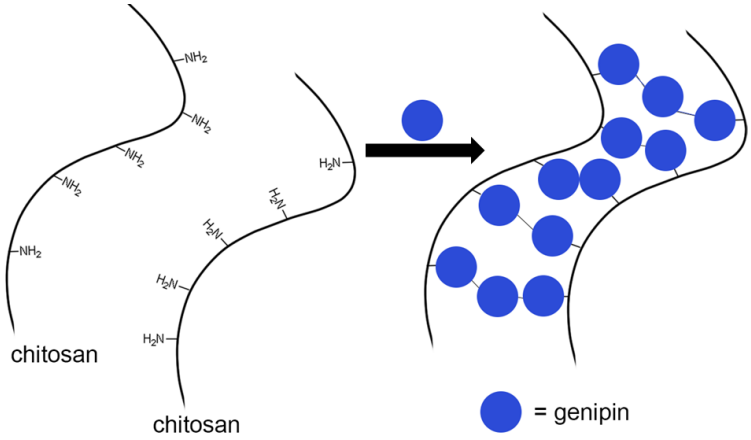

Figure 3. Simplified scheme of genipin oligomers crosslinking chitosan.

When undergoing this reaction with amines, the product forms a red dye intermediate that reacts readily with oxygen gas to produce a final dark blue dye.[19,20] These chromogenic properties are precisely what makes genipin a good reactive dye and shows that its diversity in applications reaches even further. Even outside of Asia, genipin has a long history: the *genipa americana* fruit has been used for centuries by South American tribes for body art by spreading the juices of the fruit on their skin, producing dark blue tattoos. We now know that this is the result of the genipin present in the fruit reacting with amines in the skin proteins. In recent years, its use as a temporary tattoo has grown in popularity and is even sold commercially as such.[21] These temporary tattoos develop over the course of 24 hours and can last as long as 2-3 weeks as the skin cells regenerate. Its utility as a reactive dye can extend even to textile applications for fabrics containing primary amines[22], where the colour persistence is not limited to cell turnover and can theoretically be applied indefinitely.

Chapter 1.2.2 Proposed Mechanisms of Genipin Dye Formation

The mechanism in which genipin reacts with primary amines has been under speculation for decades. Some of the earliest published research to open the gateway of genipin's use as a crosslinking agent was done by Fujikawa and coworkers who characterized a dimer formed from the reaction between genipin and glycine, where the primary amine appears to replace the ether oxygen in the hemiacetal ring to form a pyridine-type structure (**Figure 4**).[23] This compound, termed Genipocyanin G_1, was reportedly a blue compound which they believed likely dimerized via a radical pathway.

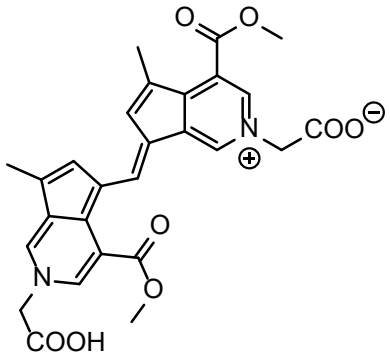

Figure 4. Structure of the genipin-glycine dimer, Genipocyanin G1, reported by Fujikawa et al.

Genipin reactions proceed with distinctive visual milestones: though genipin is colourless on its own, when reacted with primary amines it quickly develops into a red dye. This red dye subsequently converts rapidly to a blue dye if exposed to oxygen. In 1994, Touyama and coworkers further studied the red "intermediate" products formed from the genipin-amine reactions, and characterized the products formed from reacting genipin and methylamine in the absence of oxygen.[19,20] They found that under an argon atmosphere a number of red products can be isolated from this reaction including a variety of monomers, dimers, trimers and a tetramer shown as compounds **1**-**8** in **Figure 5**.

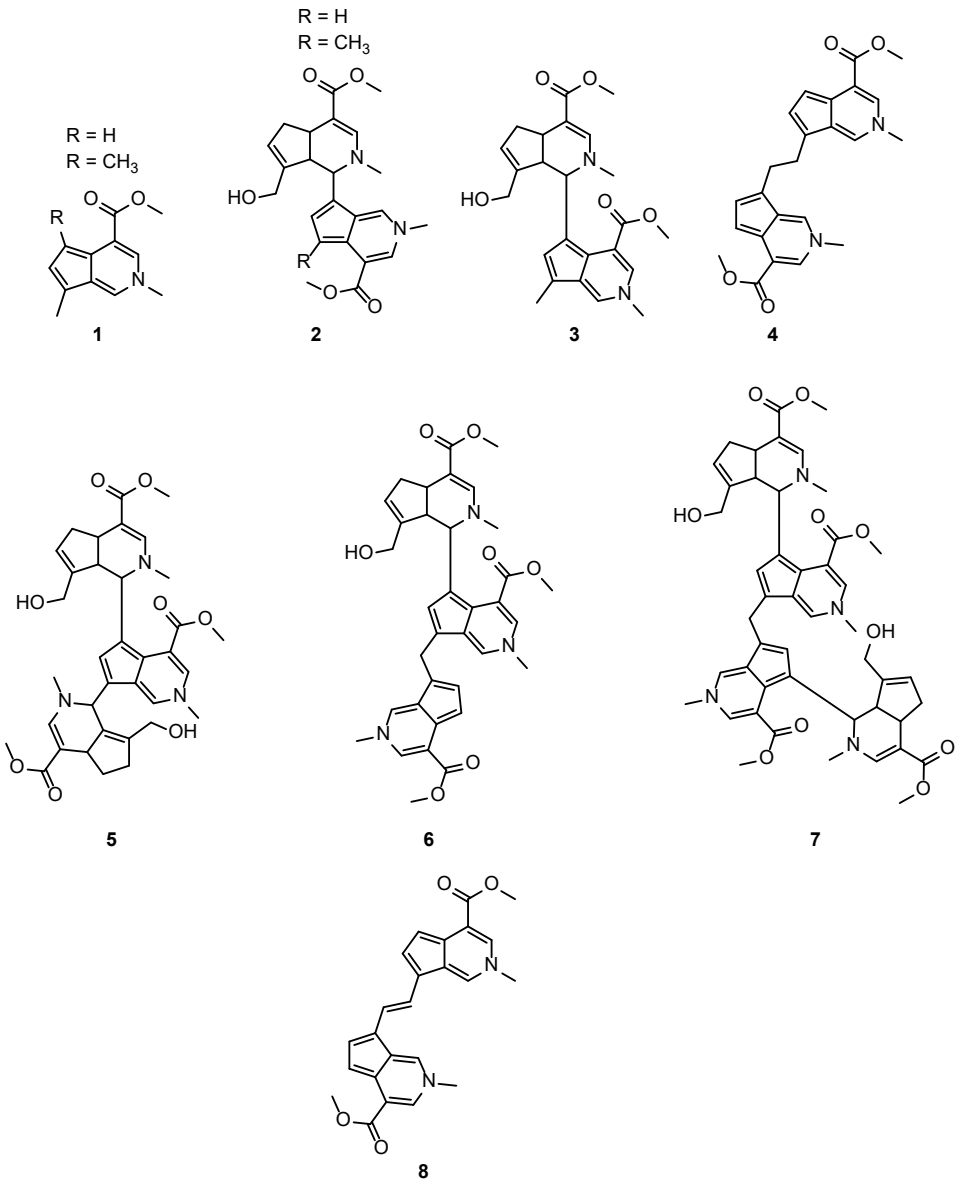

Figure 5. Structures of red products **1**-**7** formed from the reaction with genipin and methylamine in the absence of oxygen and the structure of compound **8** formed from dehydrogenation of compound **4** upon oxygen exposure.

As the red products are known to be unstable to oxygen, these compounds were subjected to bubbling with O_2. Osmotic pressure measurements of the resulting blue dye showed that the product was a mixture of polymeric structures averaging 8970 ± 600 g/mol, corresponding to an average of 40-44 genipin units. Compound **4** was also subjected to oxygen exposure, resulting in a dehydrogenation to produce a dark blue product, deemed to be compound **8.** UV Irradiation of

the genipin-methylamine reaction in the absence of oxygen also yielded a dark blue compound, and it was therefore concluded that formation of the blue pigments were the results of radical polymerizations/dehydrogenations initiated either by oxygen or UV light. Over the course of genipin research, there has been a great deal of debate over the mechanism in which this reaction with primary amines occurs. Both Touyama[19] and Butler[24] proposed similar mechanisms for the initial product formation, with a nucleophilic attack of the primary amine on the olefinic carbon 3 shown in **Scheme 1a** (mechanism **A**, Touyama — pathway I and Butler — pathway II). Mechanism **A** II demonstrates an unlikely scenario, with an S_N2 reaction on an sp^2-hydbridized carbon with the oxygen leaving group while retaining the alkene. Butler also proposes another mechanism for crosslinking between genipin and amine products, where the carbonyl carbon of the methyl ester undergoes a nucleophilic attack by the amine, shown in **Scheme 1b** (mechanism **B**), which would give products that are not observed by either Touyama[19] or Fujikawa[23].

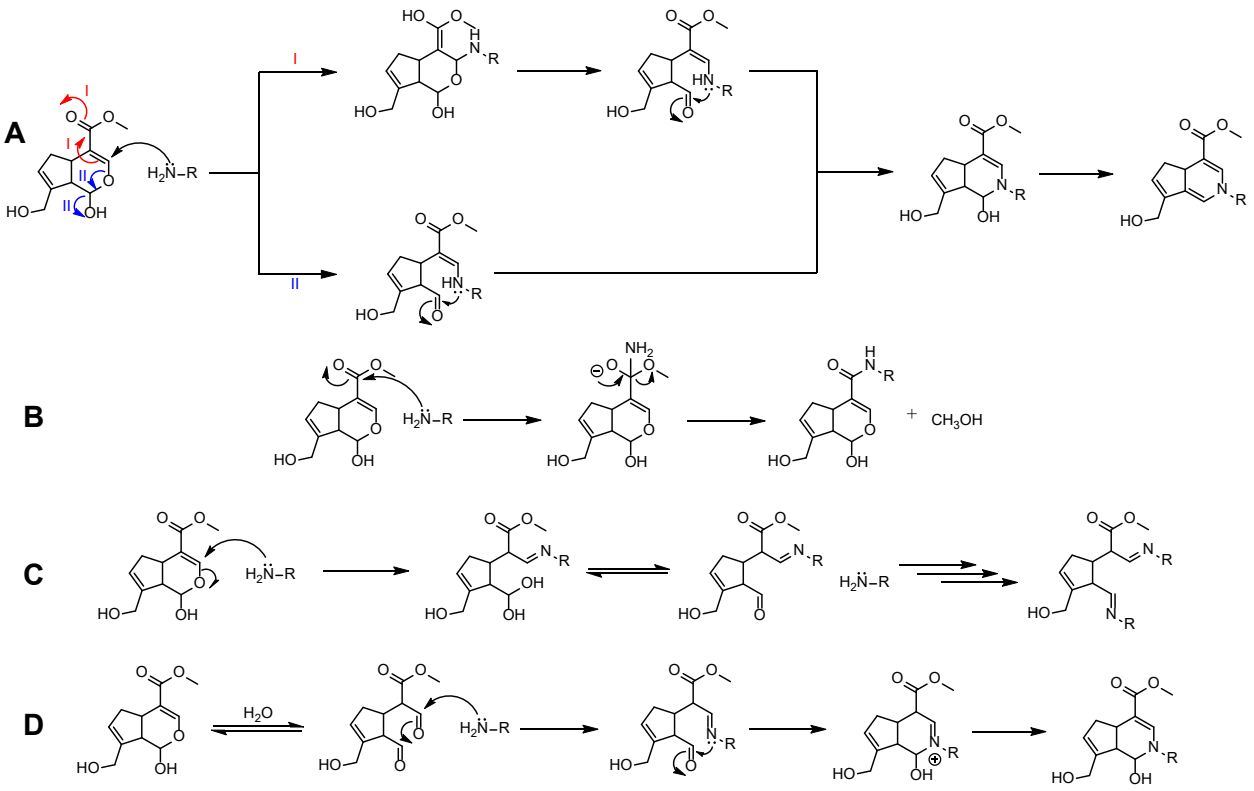

Scheme 1. Proposed mechanisms of **A** by Touyama (pathway I) and Butler (pathway II) of the genipin-amine crosslinking**,** mechanism **B** by Butler for genipin-amine crosslinking, mechanism **C** proposed by Zhu and Chan-Park and mechanism **D** proposed by Park and coworkers.

In 2007, Zhu and Chan-Park suggested another crosslinking mechanism (mechanism **C**), where only a single genipin molecule crosslinks two amine polymer chains.[25] They propose that after the ring-opening induced by the amine attack, a second amine condensation by another primary amine group would occur at the free aldehyde group shown in **Scheme 1c** and suggests that no ring closure occurs. This mechanism, like mechanism **B**, are unlikely to occur as it is inconsistent with any of the known structures characterized by Touyama[20] and Fujikawa[23]. Alternatively, Park and coworkers suggested the ring opening of the hemiacetal ring with water to form a dialdehyde as the initiated step (mechanism **D**).[26] This is supported by the lack of reactivity in the absence of water. **Scheme 1d** shows mechanism **D** where, in contrast to **A** and **B**, the amine attack occurs after the ring opening.

With the wide range of different proposed mechanisms for this reaction, Di Tommaso and coworkers turned to computational analysis of the genipin structure.[27] With respect to mechanism **D** put forward by Park in **Scheme 1d**, the ring opening tautomerization requires first an intramolecular proton transfer from the hydroxy group at C1 to the ether oxygen in the hemiacetal ring to form an intermediate of the ring opened tautomer. This is followed by a second intramolecular proton transfer to C4, yielding the final ring opened dialdehyde tautomer (**Scheme 2**).

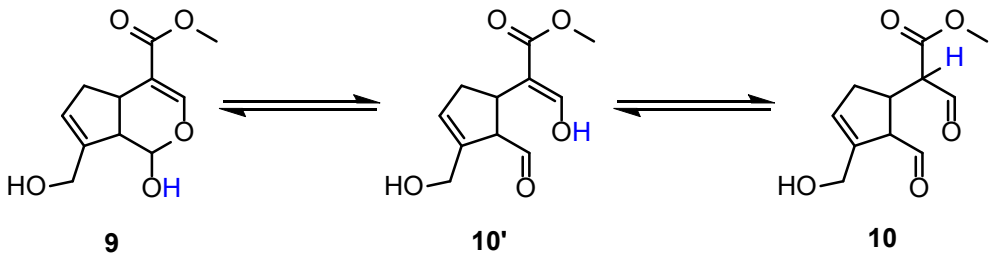

Scheme 2. Intramolecular proton transfers for the ring opening tautomerization of genipin.

DFT calculations reveal that the intramolecular proton transfer from **9** to **10'** is thermodynamically disfavoured, with a relatively large activation barrier of 47.9 kcal/mol and the overall ΔH being endothermic for 15.1 kcal/mol. However, as this ring opening tautomerization is likely water-catalyzed, addition of water molecules decreases the activation energy to 25.5 kcal/mol with the addition of one water molecule. A further decrease of the activation energy to 16.8 kcal/mol is seen with the addition of two water molecules, accompanied by a decrease in the ΔH to 5.6 kcal/mol, indicating that this water-catalyzed ring-opening tautomerization is energetically feasible (**Figure 6**). As these were calculated in the gas phase, the activation energy and enthalpy of the catalysis with two water molecules when calculated in ethanol decreased to 16.6 kcal/mol and increased to 6.2 kcal/mol, respectively. In terms of the second intramolecular proton transfer for **10'** to **10**, with no water molecules the reaction has an activation energy of 56.8 kcal/mol and is exothermic at -3.7 kcal/mol. The addition of one water molecule decreases the

activation energy to 32.6 kcal/mol but is endothermic by 4.4 kcal/mol, whereas the addition of two water molecules further decreases the activation energy to 22.3 kcal/mol and is exothermic at -1.8 kcal/mol in the gas phase. Calculations for ethanol solvation with two explicit water molecules gives a final activation energy barrier of 16.5 kcal/mol and is endothermic by 2.3 kcal/mol.

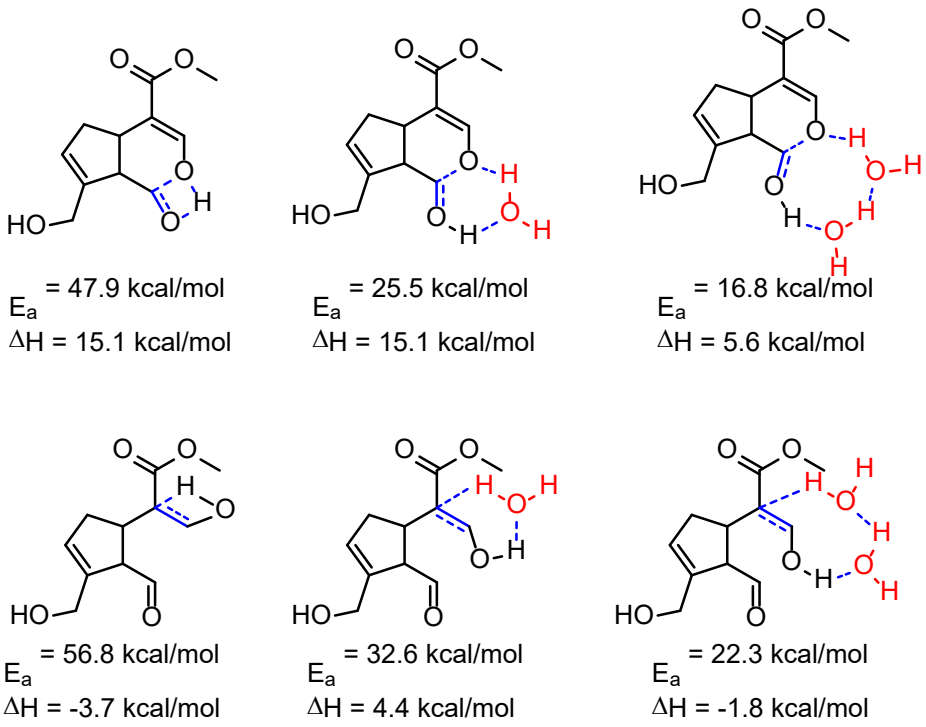

Figure 6. Structures with the activation energy and reaction enthalpy of **9** to **10'** catalyzed without water (top left), with one water molecule (top centre) and two water molecules (top right) in the gas phase and the same with the structures for **10'** to **10** in the bottom row.

Considering the number of mechanisms put forward, clarification on which pathway was most probable was provided by calculating the activation energy and reaction enthalpies of: the amine attack on the olefinic carbon; the amine attack on the aldehyde of **10'**; and amine attack on either of the aldehyde moieties of **10** and are shown in **Figure 7**.[28]

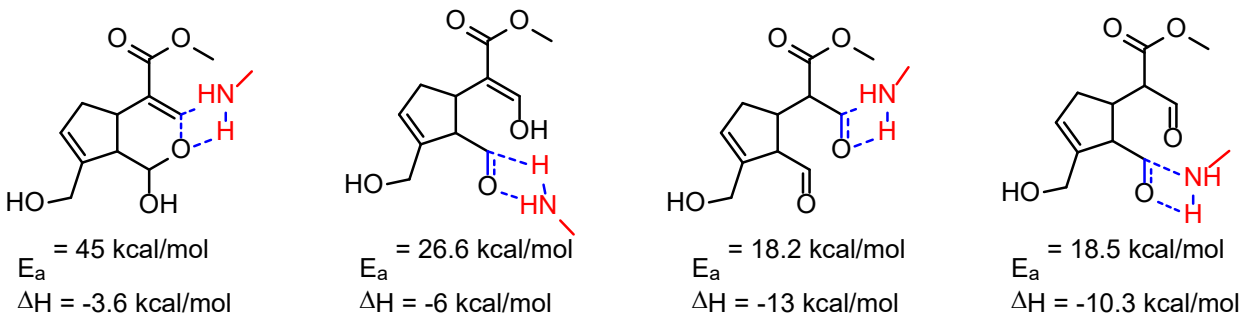

E_a = 45 kcal/mol
ΔH = -3.6 kcal/mol

E_a = 26.6 kcal/mol
ΔH = -6 kcal/mol

E_a = 18.2 kcal/mol
ΔH = -13 kcal/mol

E_a = 18.5 kcal/mol
ΔH = -10.3 kcal/mol

Figure 7. Transition-state structures of the various possibilities for the genipin and methylamine reaction with their respective activation energy and reaction enthalpy.

It can be clearly seen that the most favourable reaction pathway is that of the Schiff base amine condensation with either of the aldehyde moieties in the dialdehyde structure with activation energies of 18.2 kcal/mol and 18.5 kcal/mol and are both exothermic by -13 kcal/mol and -10.3 kcal/mol. Contrarily, mechanism **A**-II proposed by Butler has a significantly larger activation barrier at 45 kcal/mol and is only slightly exothermic at -3.6 kcal/mol. It can therefore be concluded that the reaction pathway most likely proceeds through the mechanism proposed by Park.

With two possibilities for the plausible amine condensation, the activation energies (E_a) and enthalpies of the individual steps in the reaction were calculated to determine the preferential pathway. While the calculations revealed that the energy profiles do not differ significantly from each other, the final dehydration of **14** or **14'** to **15** showed significant deviations (**Scheme 3**). The dehydration of **14** to **15** shows an activation barrier of 41.3 kcal/mol and is endothermic by 7 kcal/mol. Alternatively, **14'** to **15** shows an activation barrier of 26.3 kcal/mol and is endothermic by 6.5 kcal/mol. The activation barrier of **14'** to **15** is significantly lower than its parallel pathway due to activation of the C4 C-H bond by the ester moiety for the dehydration. Overall, both pathways are exothermic, where the amine attack on the C3 aldehyde is exothermic for 10.9 kcal/mol and the amine attack on the C1 aldehyde for 9.9 kcal/mol, suggesting that in terms of product stabilization, pathway **11** to **15** may be favourable. However, the activation barrier of **14**

to **15** is significantly larger, suggesting that despite being overall less exothermic, pathway **11'** to **15** might be more favourable.[28]

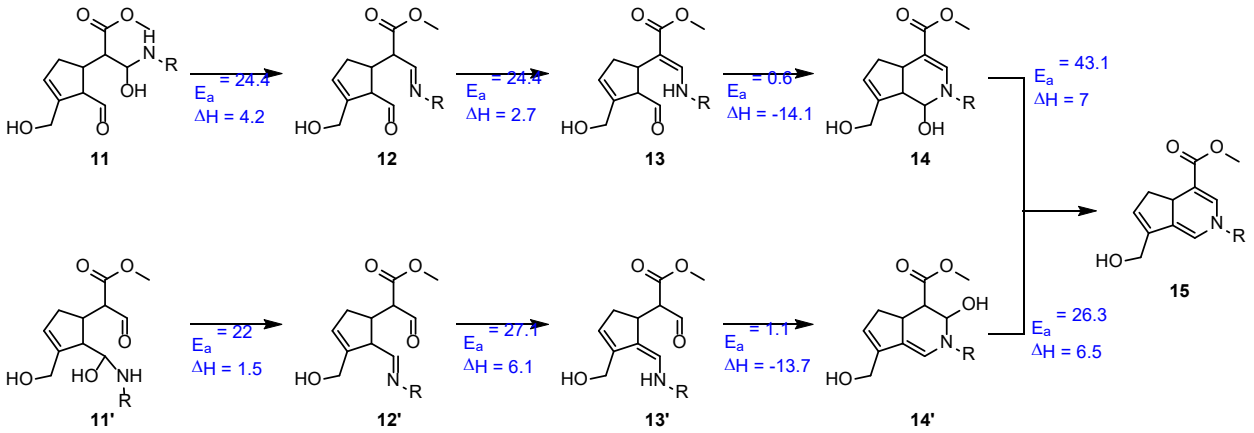

Scheme 3. Parallel reaction pathways by amine attack on either of the aldehydic moieties on genipin. E_a and ΔH in kcal/mol.

While the calculations shed some light on the condensation reactions of the hemiacetal ring, Adamo and coworkers[28] sought to further understand the observed dehydration of the cyclopentenyl allylic alcohol and consequently, formation of the fully unsaturated **16** (**Scheme 4**). The subsequent reaction of **15** to **16** forming the conjugated compound that is the building block for all the reported red intermediates first involves oxidation of **15** to **15ox** with a subsequent dehydration of the C10 allylic alcohol to form **16Me**. It is unknown what initiates the oxidation of **15**, however after the initial oxidation the reaction can be deemed self-promoted, as **16Me** can be reduced to **16** by **15** while simultaneously oxidizing **15** to **15ox** to continue the cycle.

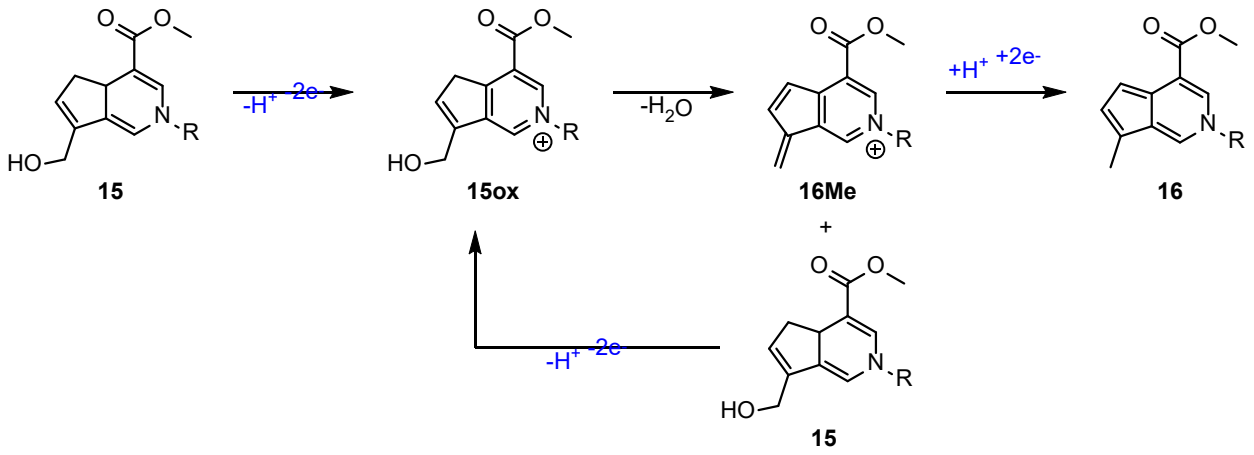

Scheme 4. Proposed catalytic pathway for formation of **16**.

Thus far it has been determined that the reaction mechanism between genipin and primary amines proceed first by a water-catalyzed ring-opening tautomerization with subsequent nucleophilic attack on one of the aldehyde moieties, undergoing a Schiff-base reaction. The genipin-amine product will then need to proceed through a redox cycle to produce the fully conjugated compound **16**. TD-DFT analysis showed that product **16** should have an absorption at around λ = 469 nm, corresponding to an orange pigment, supporting the findings of Touyama and coworkers who report this compound as a red solid. However, despite the clarification surrounding the genipin-amine condensation mechanism, the understanding of why these genipin-amine products turn blue is limited, and neither the polymerization mechanism nor the structures of any of these genipin-amine polymers have been elucidated.

Chapter 1.3 Polyaniline

Conjugated amines dyes are of no rarity, especially that of polyaniline (PANI) — a highly conjugated polymeric dye generated from the oxidative polymerization of aniline — which is widely known for its applications as a conductive polymer. The discovery of conductive polymers has been massively influential in the progress of optoelectronics. So much, in fact, that a Nobel Prize in 2000 was awarded to Heeger, Macdiarmid and Shirakawa for their contributions to conductive polymer discovery and development in 1977.[29] Today – more than 40 years later – these have not only been applied industrially, but also have aided in making dramatic strides in solar energy, batteries, sensors and many other sectors – even in the medical field.[30–34]

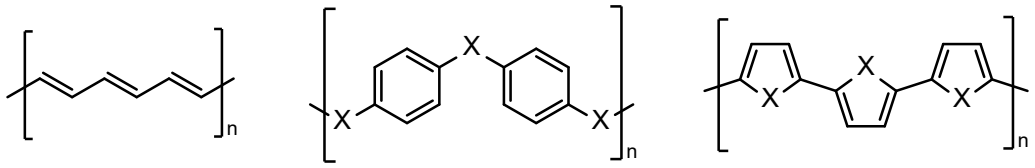

polyaniline: X = N
polyphenylene sulfide: X = S

polypyrrole: X = N
polythiophene: X = S

Figure 8. Commonly known conductive polymers. Polyacetylene (left), polyaniline (middle, X = N), polyphenylene sulfide (middle, X=S), polypyrrole (right, X=N), polythiophene (right, X=S).

Some common examples of conductive polymers are shown in **Figure 8**, where it can be seen that the minimum requirement of a conductive polymer is π-conjugation. This is due to the fact that in order for a polymer to be able to conduct electricity, electrons must be able to move freely throughout the molecule. This process is hindered in saturated polymers like polyethylene where only σ-bonds are present, as all carbons are sp^3 hybridized and thus cannot function as a conductive polymer. To initiate conductive properties of conjugated polymers, they are “doped” to change the oxidation state of the polymer to probe electron flow. Thus, the two types of doping are termed p-type (oxidation) and n-type (reduction), referring to whether the addition or removal of electrons is used to facilitate conductivity.[35]

PANI in particular has gathered lots of interest, and its history dates back to over a century ago when Letheby reported generation of a blue substance from the electrochemical oxidation of aniline sulfate.[36] Since then, a plethora of research has gone into PANI and its electrochemical properties due to the ease of synthesis and cheap cost of its building block, aniline. The synthetic procedure typically involves oxidative polymerization of aniline, either chemically or electrochemically. The chemical oxidation is most often done with ammonium persulfate (APS), however other oxidants can be used, and the reaction conditions (eg: pH) determines what form the PANI structure takes.[37] This is important to note, since its polymeric structure can exist in not one, but three oxidation states, all of which have different conductive and physical properties. Leucoemeraldine is the fully reduced state of polyaniline and is white or colourless, while pernigraniline is the fully oxidized state and is typically a blue/purple colour (**Figure 9**).[38] Emeraldine is the PANI form that is a good conductor. Commonly referred to as Emeraldine base (EB), it is the partially reduced state of PANI and exists as a blue substance. However, acid doping of EB leads to protonation of the imines of the diiminoquinone moieties, resulting in the green emeraldine salt (ES) (**Figure 9**).[39]

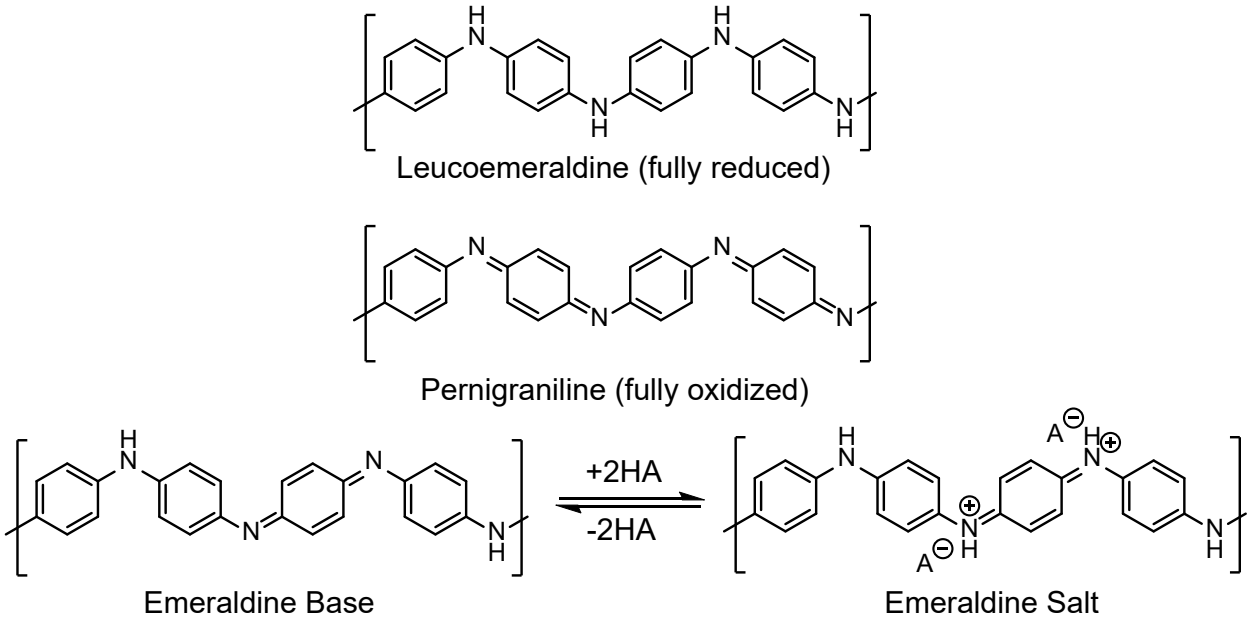

Figure 9. Molecular structures of leucoemeraldine, pernigraniline, emeraldine salt and emeraldine base

The doped ES has also shown to have significantly better conductive properties than EB. However, despite the knowledge surrounding the various PANI oxidation states, the particular structure of ES that is responsible for its impressive conductivity is still under debate. The polaron, bipolaron and polaron lattice forms (**Figure 10**) have all been put forward as the conductive state of PANI-ES; and while it has been recognized that they all exist, it is unclear which — if not equal — is the best conductor.[40]

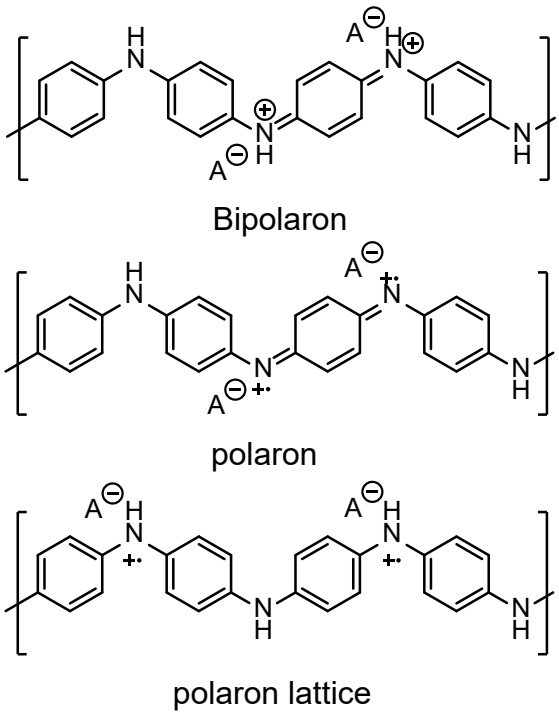

Figure 10. The bipolaron, polaron and polaron lattice forms of PANI-ES.

The UV-Vis spectra of PANI-ES and -EB can tell a lot about its structure. Typically, PANI-EB contains two peaks, which, depending on the solvent, arise around λ = 320 nm and 600-650 nm. The λ = 300 nm absorption is indicative of the π→π* transition of the benzene rings, and the λ = >600 nm absorption is the result of the quinoid exciton and is the feature responsible for the blue colour of EB. However, acid doping of EB to ES shows distinct shifts in the UV-Vis spectrum, with the decrease of the λ = ~600 nm absorption and the appearance of two new peaks, around λ = 400-450 nm and λ = 800-1000 nm.[41,42] These absorption features are indicative of PANI-ES as they correspond to the polaron and bipolaron transitions of the doped polymer. Consequently, the redox capabilities and distinct colour transitions of PANI helps lay the groundwork for insights into genipin polymers as blue/green nitrogen-containing, aromatic polymer systems.

Chapter 1.4 Study outline

Decades of work surround genipin-based research, yet the research involved tends to focus less on specific characterization of genipin products since many involve complex biomolecules that make characterization impossible. In addition, despite centuries of genipin use as a dye, little research has gone into investigation of the dye origins, and its potential to access a wider range of the visible light spectrum. The focus of this research was to gain further understanding of the fundamental knowledge surrounding genipin products: mechanistically, structurally and in terms of its dye properties. Since the studies by Touyama and coworkers have provided the foundation on general properties of genipin-methylamine products such as colour, average molecular weight and possible products, we decided to expand the amine substrate scope to determine if amines with different electronic and steric properties exhibit the same reactivity with genipin. This would allow us not only to determine if the colourimetric properties are tunable through the amine functionality, but also determine if similar sized polymers are formed. These results have since been submitted for publication.[43] Subsequently, we aimed to investigate how targeted synthetic modifications of genipin affect the resulting dye properties – with the hypothesis that we could inhibit the polymerization or by altering the absorptive properties.[44]

Chapter 2. Results and Discussion

Chapter 2.1 Impact of Amines on Colours Formed with Genipin-Based Dyes

As shown in the work done by Touyama and coworkers[19,20], as well as the many applications of genipin-crosslinked chitosan[17,24], the diversity of primary amines that can freely react with genipin has not been comprehensively examined, limited to only amino acids and aliphatic amines. In addition, to the best of our knowledge there have been no studies regarding the impact that the amine substituents have on the colour of the dye. Thus, we sought to examine the effects of extending the conjugation of the system, as we hypothesized that extension of the π-conjugation is likely to lead to a bathochromic shift (red shift) in the absorption spectrum (**Scheme 5**). Our goal was to ascertain if the proposed red-shifting of the polymeric absorption feature would be sufficient to access colours other than the characteristic blue.

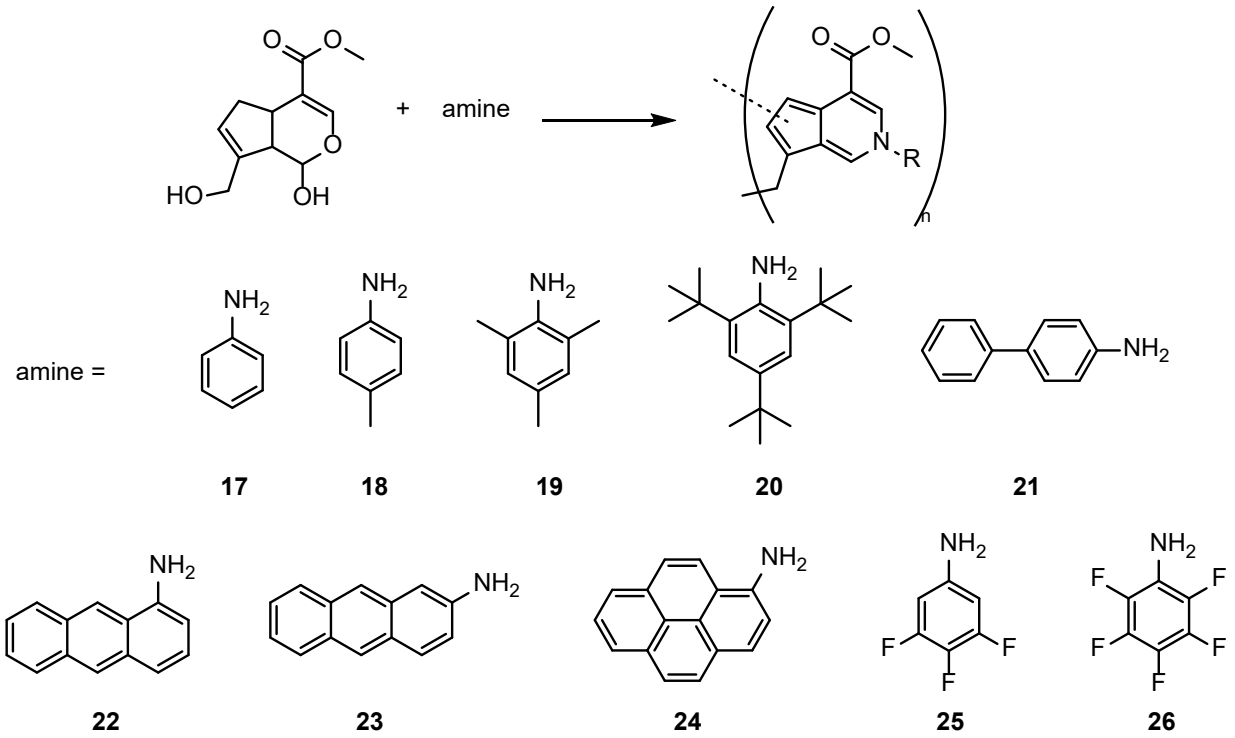

Scheme 5. Genipin reaction with amines, **17-26**.

The substrate scope began with the simplest of aromatic amines — aniline. As the reaction between genipin and primary amines readily occurs under ambient conditions, a methanolic equimolar solution of genipin and aniline were simply stirred together in an open vessel until a colour change was observed, which was approximately after 24 hours. The reaction of genipin with primary amines first generates a red dye, indicating formation of the pyridine-type intermediate, and subsequently darkens to a blue dye from oxygen exposure (λ_{max} = 590 nm).[19] The reaction between genipin and aniline (**17**) showed similar transitions, first with a colour change to reddish-brown, which subsequently turned into deep green (λ_{max} = 630 nm, **Figure 11**). The similar sequence in colour changes suggests that the reactivity of genipin with aromatic amines may indeed be similar to that of aliphatic amines. However, the deep green colour closely resembled that of the well-known PANI-ES, giving rise to suspicions that the green colour may arise from polymerizing aniline as opposed to a genipin dye.

A simple method to combat this issue was to employ a related aromatic amine without the ability to polymerize. PANI results primarily from polymerization of aniline at the *para*-position; therefore *p*-toluidine, an aniline derivative with a methyl group occupying that *para*-position should not be able to successfully polymerize to form PANI. The experiment was carried out with *p*-toluidine in place of aniline (**18**). As hoped, **18** underwent a strikingly similar reaction to **17**, with an initial colour change to reddish-brown and eventually to deep green (λ_{max} = 624 nm, **Figure 11**). Thus, formation of the dye while blocking the aniline polymerization site provided further credence to the product of the reaction with **17** being a green genipin-derived dye as opposed to PANI. Bearing in mind that the reaction of genipin with aromatic amines (where the N-atom of the aromatic amine is incorporated into the 6-membered genipin ring) is likely the green dye, it was imperative that the extent of this reactivity (how many different aromatic amines and containing which properties) was established.

To further expand this substrate scope, we chose to investigate the role of steric bulk around the amine group. 2,4,6-trimethylaniline (**19**) was added to a methanolic solution of genipin under and demonstrated that the two *ortho*-methyl groups did not inhibit reactivity (λ_{max} = 621 nm, **Figure 11**). However, reactivity did appear to be hindered as the reaction progressed visibly more slowly; no further observable colour change (indicating that the reaction was complete) took 48 hours — an extra 24 hours compared to **17** and **18**. Additional steric bulk was introduced with the bulkier *t*-butyl groups in 2,4,6-tri-*t*-butylaniline (**20**). Unlike **19**, **20** showed no reactivity with genipin, even when stirred for 72 hours and at refluxing temperatures. This demonstrates that while slight steric bulk around the amine group is tolerated, it does slow the reaction time and bulkier groups will completely prevent reactivity.

As it was noted that π-extension does in fact result in a redshift of the absorption spectrum, amine substrates featuring extended π-systems were investigated in analogous reactions with genipin (**21**-**24**, **Scheme 5**). Interestingly, while we do see a redshifted absorption when compared to aliphatic amines (λ_{max} = 590nm), the redshift does not appear to show a specific trend with respect to the number of aromatic rings as anticipated. While the product of the reaction of genipin with 1-aminopyrene (**24**) does have the largest π system and indeed exhibits the highest λ_{max} at 640 nm, the reaction of genipin with **22** (λ_{max} = 613 nm) and **23** (λ_{max} = 619 nm), both of which contain 3 fused aromatic rings, have a lower λ_{max} than the product of the reaction with the biphenyl derivative (**21**, λ_{max} = 629 nm). While **21** differs from the other polyaromatic amines in that its benzene rings are not fused, it still has approximately the same λ_{max} as the product from the reaction with **17** (λ_{max} = 630 nm), our simplest aromatic amine. Nonetheless, these polyaromatic systems do tend to have a greener appearance compared to the smaller anilines, which are more of a blueish-green tone.

It is, however, important to note that we do see a wider variation in the absorption features within the UV region of the respective spectra. A shift of ~30-50 nm in the λ = >600 nm absorbance

does appear to be relatively small considering the visually noticeable difference in colour, and observing a greener hue despite a smaller shift in the λ = ~600 nm absorbance is a curious occurrence. Since we do tend to see significant shifts in the UV region absorbances, it is likely that these contribute to the final green colour. These typically absorb around λ = 300 nm. However, while the λ_{max} is in the UV region, it is close enough to the visible light region that the higher wavelength portions of the peak results in slight absorption in the 400 nm region. This absorbance is comparably small to the λ = ~300 nm peak, however since the λ = ~600 nm peak is miniscule as well, it can have a noticeable effect on the overall colour. Absorptions around λ = 600 nm and λ = 400 nm would give a greener appearance, which is consistent with the variation in green hues displayed and is especially significant in explaining why the dyes that absorb at lower wavelengths in the 600 nm region still appear to exhibit greener hues than the higher-wavelength absorbing dyes. In addition, with respect to the differences in absorption intensity of the λ = ~600 nm absorption features, this variation cannot be exclusively attributed to greater or lower molar absorptivities of their respective dyes. Due to the complex mixture of products, accurate concentrations cannot be properly measured and thus, molar absorptivies cannot be measured; thus the samples (0.025 mM) were prepared relative to the amount of initial genipin added.

As sterics were shown to impede genipin reactivity, we sought to explore the electronic effects of the amine group. The potential to employ chromophores on the amine substituent might extend the range of colours we can access from genipin even further. Based on the mechanism being a Schiff-base reaction, the most prominent question would be whether electron withdrawing groups (EWGs) hinder the formation of genipin dyes by slowing or preventing the Schiff base reaction. Thus, fluorinated anilines (3,4,5-trifluoroaniline — **25** and pentafluoroaniline — **26**) were added to solutions of genipin under analogous conditions. Compound **25** was first used to investigate EWGs while minimizing the potential for steric interference, as none of the fluorine

atoms occupied an *ortho*-position. Under standard conditions, genipin showed no reactivity with **25**, however upon refluxing did produce a green dye (λ_{max} = 633 nm, **Figure 11**), thus demonstrating that the three fluorine atoms withdraw sufficient electron density to inhibit reactivity under ambient conditions, however it is still reactive when heated. Conversely, **26** with genipin showed no colour change at room temperature or when refluxed, indicating no reactivity. Thus, genipin dyes with electron withdrawing groups on the amine substituent appear to be accessible but only to a limited extent.

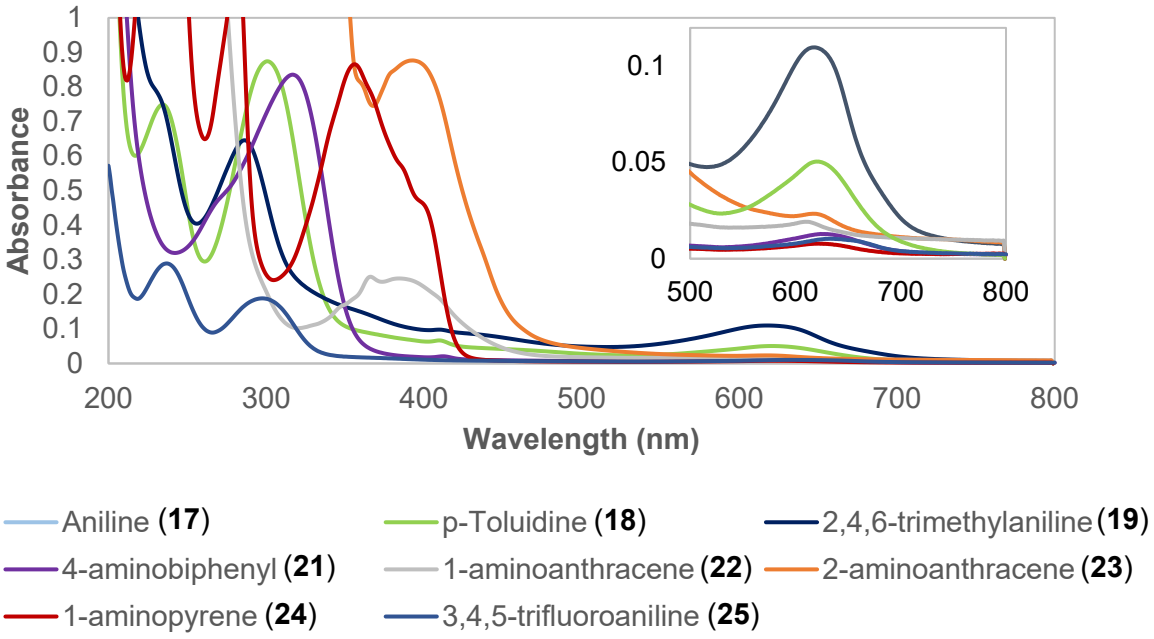

Figure 11. UV-Vis spectra of genipin dyes **17-24**. Inset: region of polymeric peak.

Chapter 2.2 Investigation of Amine Impact on Genipin Polymers

Generating genipin-based dyes with aromatic amines proved successful. However, in addition to the lack of literature on the possible variety in genipin dyes, there is also very limited research available on the polymers formed from the reaction between genipin and amines. This probed us to ask: how does switching the amine group from aliphatic to aromatic affect the structure, molecular weight and length of the polymer? It was still unknown to us whether the resulting polymer would be similar to the reported genipin polymers in terms of length (~44 genipin units) and molecular weight (~9000 g/mol)[19], or be completely different in both regards. Touyama and coworkers employed osmotic pressure measurements to determine the molecular weight of the polymer, however we found Gel Permeation Chromatography (GPC) to be a more appropriate technique. Thus, we began to explore this by employing GPC to measure the molecular weights of the products formed by reaction of genipin with **17** and **18**, the simplest of the aromatic amines. Despite the clear dye formation with aniline derivates that cannot polymerize, it was unknown if **17** still formed some amount of PANI. However, much to our surprise, the GPC revealed that no polymers were formed in either **17** or **18** (**Figure 12**). Any compounds present eluted with the system peak, which indicates that only small molecules were present.

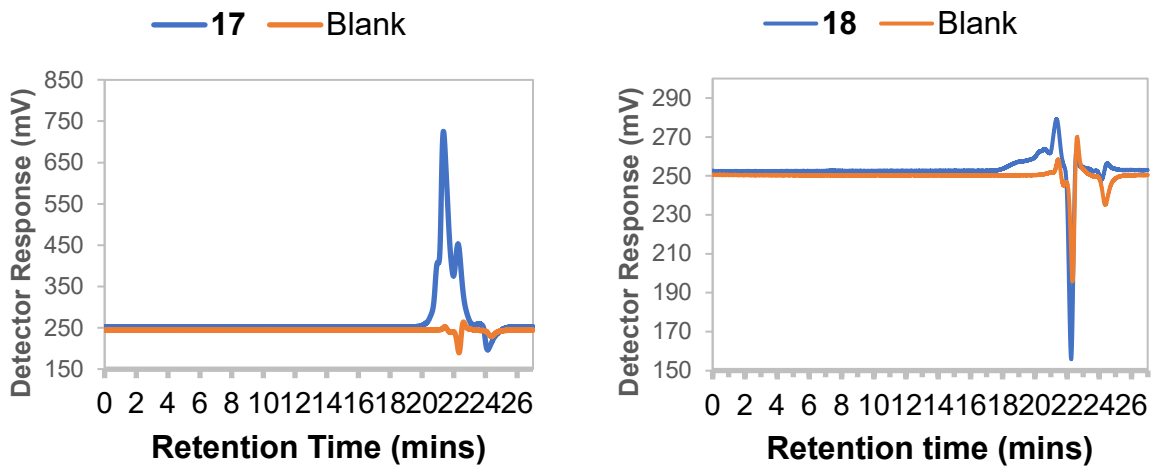

Figure 12. GPC chromatograms for products formed from reacting genipin with **17** and **18**

As this was found for the products of the reactions of both **17** and **18** with genipin, it seemed to indicate that while genipin does react with the aromatic amines, the green colour was not the result of polymers, unlike its blue, aliphatic amine counterparts. This was unexpected, as they appeared to proceed through the same stages — first formation of the reddish-brown intermediate, which indicated the Schiff-base and condensation reactions had occurred to produce the pyridine-type ring as in **16**. According to literature, exposing **16** to oxygen is what initiates a radical polymerization event, resulting in the blue dye (~590 nm); however, in our case exposure of the reddish-brown intermediate to oxygen results in a green dye (>600 nm) that is not a polymer.

Now knowing that the green dye did not arise from polymers (genipin or aniline), the genipin dye that has been characterized by Touyama and coworkers was a good starting point for investigating where the differences in the reactions arise, despite similar observed reactivity. The genipin-methylamine dye (**27**) was synthesized according to their procedure[19] (**Scheme 6**). It was reported in literature that for **27** in particular, the blue colour arises from the polymer, and therefore obtaining this deeply coloured product is a direct indication that the correct product was formed. To eliminate any of the uncertainty surrounding the product of the reaction the product of the reaction of genipin with **18** (p-toluidene) was chosen as the representative dye of the aromatic amine-genipin dyes for any comparative experiments between them and **27** (methylamine). However, dyes generated from genipin and amines **17**-**24** were made by simply stirring genipin and the corresponding amine together at room temperature until the colour indicated a complete reaction. The synthetic procedure of **27** was more controlled, involving first generating the red dye in air-free conditions, and subsequently polymerizing by bubbling with air. To eliminate the possibility that the lack of polymers formed was due to the difference in preparation, **18** was remade (**28**) according to the procedure of **27** (**Scheme 6**).

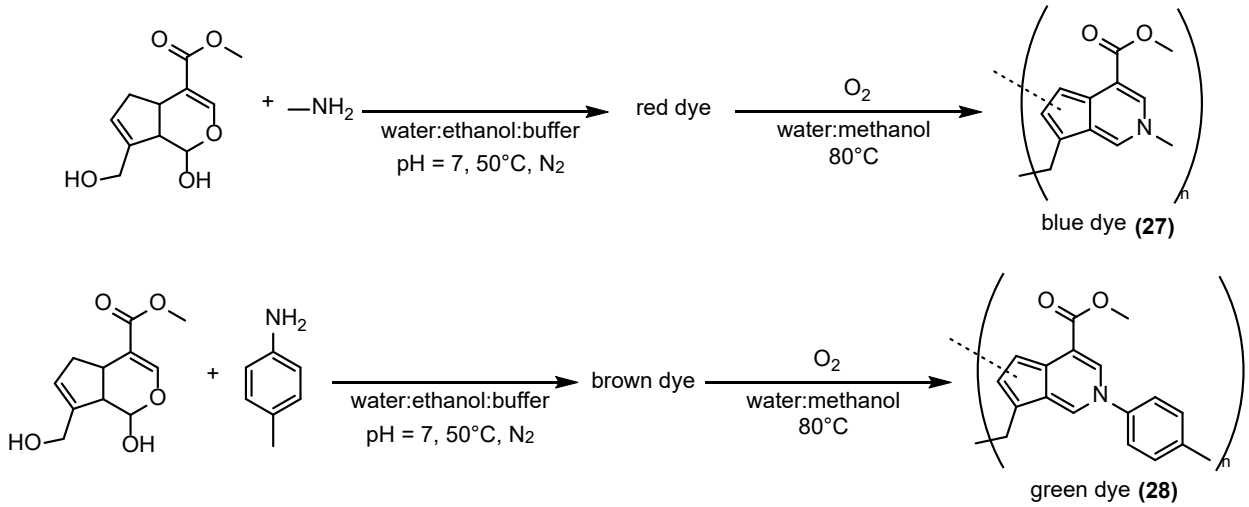

Scheme 6. Synthetic procedures of **27** (top) and **28** (bottom).

To follow up after the GPC results, MALDI-TOF was run on **27** and **28** to affirm that no polymers were formed in the event that there was some unexpected interaction between the GPC column and the polymer that prevented it from properly eluting. Fortunately, the MALDI also showed that no polymers were formed for **28**, and that all peaks were below 1000 m/z. Shockingly, the MALDI of **27** also revealed that no polymers were present. However, since MALDI was used to confirm the absence of polymers, the peaks observed are all below 1000 m/z and thus cannot be definitively assigned as product peaks due to possible overlap with the matrix-cluster peaks of the CHCA. ESI-MS was easily employed instead and showed that the largest molecule in the reaction mixture from the reaction presumed to form **27** had a m/z of 831.35. If the molecular weight of a genipin-methylamine monomer product is expected to be around 200–220 g/mol, then it is expected that an oligomer between 800-900 g/mol would correspond to that of a tetramer**.** Interestingly, the largest oligomer reported by Touyama (aside from the ~9000 g/mol polymers) was the red tetramer **7** with the approximate m/z of the largest molecule observed in the reaction mixture of **27** (**27a**, **Figure 13**). Likewise, as they reported that various dimers and trimers are formed with varying linkages, the distribution of peaks in the ESI-MS seem to be consistent with the molecular weights of monomers (with an expected range of approximately 200–220 g/mol),

dimers (~400–440 g/mol) and trimers (~600–660 g/mol) as well. However, the actual masses may extend slightly outside of these ranges, depending on the linkages between the monomeric units. The proposed structures of some of the notable peaks in the ESI-MS spectra for **27** and **28** can be seen in **Figure 13**. The ESI-MS of **28** shows a similar trend with the clusters of peaks around the m/z that resemble the monomers (~280–300 g/mol), dimers (~560–600 g/mol) and trimers (~840–900 g/mol). The largest peak of 831 m/z (**28a**, **Figure 13**) corresponds to a trimer, suggesting that it is molecular weight, not number of repeating monomeric units, that determines the length of the oligomer.

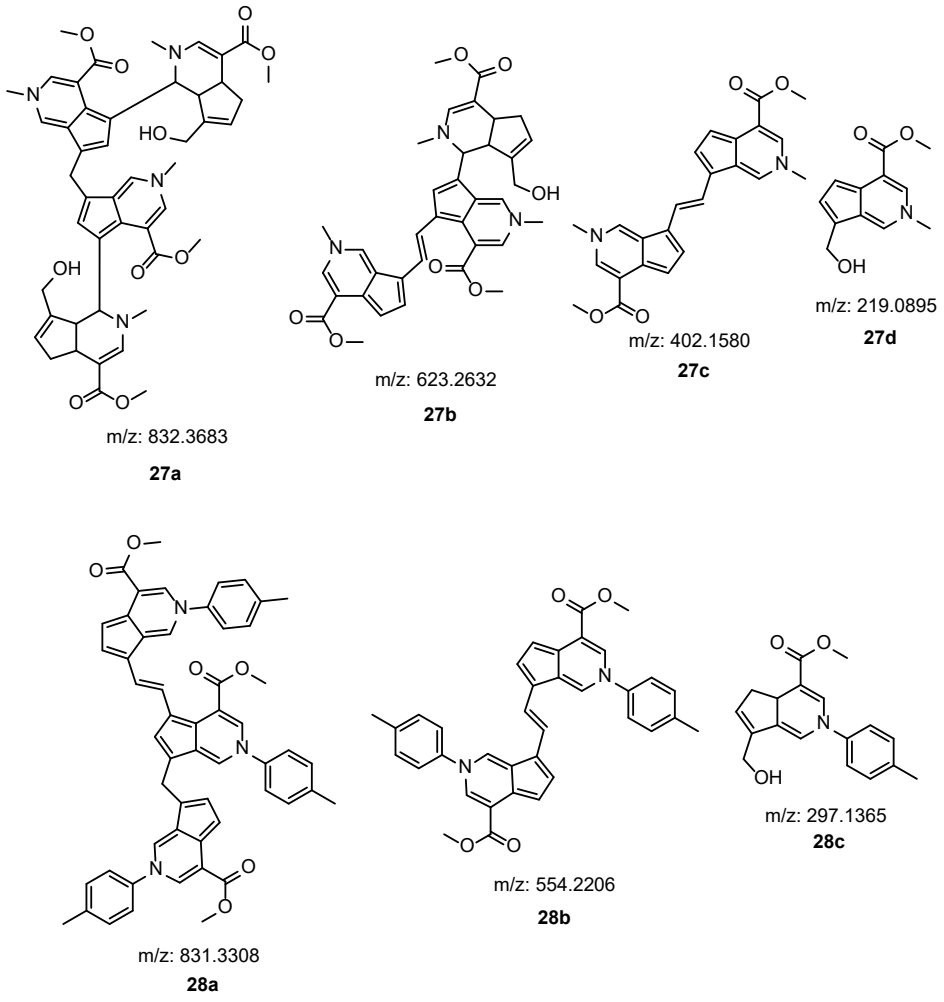

Figure 13. Proposed structures of molecules in **27** and **28** corresponding to the ESI-MS m/z values.

Taking into account that the blue colour is reported to be the product of polymerization, it was extremely unlikely that an alternate product with the same features was formed by these reactions. Going back to the initial paper by Touyama and coworkers who determined the average molecular weight of the polymers, it is important to note that the method used was osmotic pressure measurements; this method was not ideal for those conditions, considering the presence of small molecules that can freely pass through the membrane, as well as the possibility of charged species which can increase the osmotic pressure prevents accurate measurements of molecular weight.[45] Thus, its likely that the product reported by Touyama and coworkers was not a polymer at all. While this clears up the discrepancy between the aromatic amines and aliphatic amine dyes with genipin, this raises another question — *what is responsible for the deep blue colour of genipin dyes if not polymers?*

Chapter 2.3 Investigating the Origin of the Dye Colours

Since the mixture of polymers and oligomers proposed by Touyama consisted of varying linkages and products, NMR spectroscopy was originally thought to be less useful in discerning reactivity of these type of compounds, as NMR spectra of these mixtures could be so complex as to be not useful due to the inconsistent linkages. However, knowing that polymers are not present, NMR spectroscopy on the blue/green products could prove fruitful. Compound **27** required no further purification, as upon work-up, the dye product could be extracted from the organic phase into the aqueous phase easily. However, due to the aromatic substituent, the green dye of **28** differed in solubility of the final product and therefore could not be separated from any other compounds (various reddish-brown intermediates) without purification by column chromatography. While the reddish-brown components were present based on thin-layer chromatography (TLC), the spots quickly darkened to a deep green upon separation. Likewise, the corresponding reddish-brown fractions obtained from the column quickly turned green in solution. When both **27** and the purely green fraction of **28** were attempted to be analyzed via ^{1}H and ^{13}C NMR, it was surprising to find that the NMR spectra were both completely absent of signals, except for the solvent peaks (**Figure 14**, Appendix **Figure A15**, **A16**). While the lack of polymers despite the deeply coloured products was unexpected, the complete silence in the NMR spectrum suggested an unpaired electron could be present in the product, convincing us further that the true molecular structure of the dyes were drastically different than previously thought.

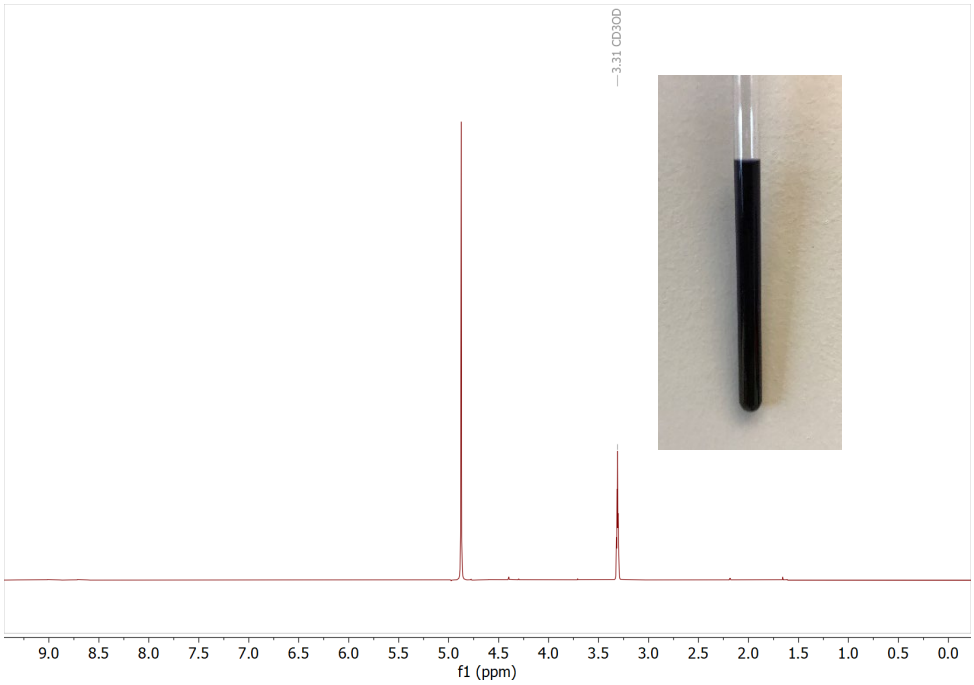

Figure 14. ^{1}H NMR spectrum of **27** in methanol-d4. Inset: Photograph of sample.

Electron paramagnetic resonance (EPR) spectroscopy was undertaken to validate this theory. EPR spectroscopy on **27** was run in the solid state due to poor solubility in solvents with lower dielectric constants. EPR spectroscopy indicated that an unpaired electron was indeed present, showing a signal at g = 2.002 (where g is the Landé g-factor) — the expected region for a nitrogen- or carbon-centered radical (**Figure 15**).

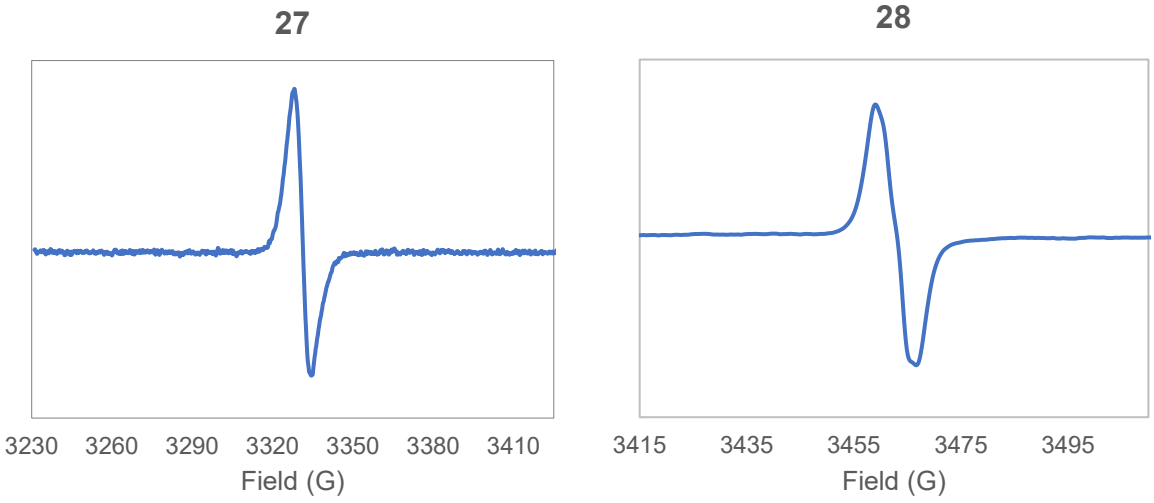

Figure 15. EPR Spectrum of **27** in the solid state (g = 2.002) and **28** in DCM (g = 2.002)

EPR spectroscopy was also run on **28**, showing a similar spectrum as **27** (**Figure 15**). However, while **27** shows a relatively sharp singlet, the signal in the spectrum of **28** appears slightly broader and appears to be a poorly resolved signal that is not simply a singlet. While this could be the result of hyperfine coupling demonstrated by the additional peaks, there still is the possibility that this could arise from multiple unpaired electrons. As the product is a mixture of compounds that can be very similar, it is possible that what appears to be poorly resolved hyperfine coupling could arise from overlapping signals of multiple radicals with varying intensities. The g-value of **28** was the same as **27** (2.002), which was expected since the environment of the unpaired electron should be the relatively similar.

The EPR spectrum for **17** contained a significant amount of noise compared to the other spectra (**Figure 16**). The reason for this is unclear, however as the sample is a mixture of products as opposed to one compound and with the difficulty purifying this mixture, it was unfeasible to prepare samples of the same concentration. Therefore, it is possible that this sample was more dilute than the others, resulting in a lower S/N ratio.

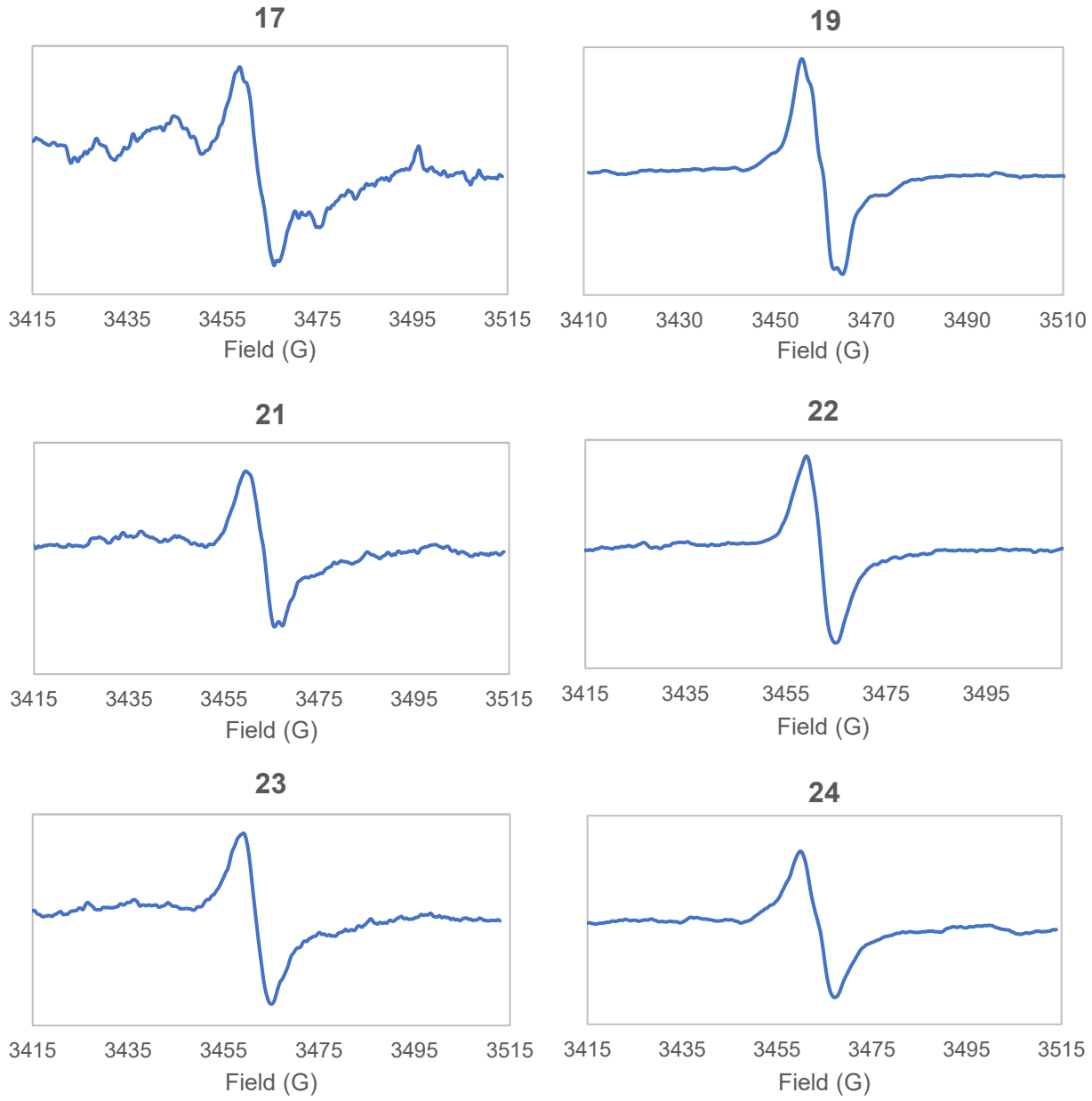

Figure 16. EPR spectra of **17** (g = 2.002), **19** (g = 2.002), **21** (g = 2.002), **22** (g = 2.002), **23** (g = 2.002) and **24** (g = 2.001) in DCM.

As with **28**, all the EPR spectra that were obtained in solution displayed some broadening and indication of multiple peaks. To help determine the nature of these spectra, running the sample in the solid state may provide useful information in elucidating any hyperfine coupling; if the additional signals are absent when run in the solid state, this would indicate that they are the result of isotropic hyperfine coupling. While most of the spectra appear to be generally broad, the

spectrum of the reaction product of genipin with **19** shows relatively well-resolved peaks, and thus would be best for comparison. Though noisier, the solid-state EPR spectrum of the spectrum of the reaction product of genipin with **19** retains numerous signals (**Figure 17**). This suggests that for the spectrum of the reaction product of genipin with **19**, the presence of multiple peaks is not the result of (or not *solely* the result of) hyperfine coupling but more likely to be multiple, separate signals with the same g-value. This is further supported by the previously mentioned NMR spectra, which are completely silent — we know that the dye product contains a mixture of monomers, dimers, and trimers, therefore if only some compounds contained an unpaired electron, the NMR spectrum would likely contain at least some noticeable signals.

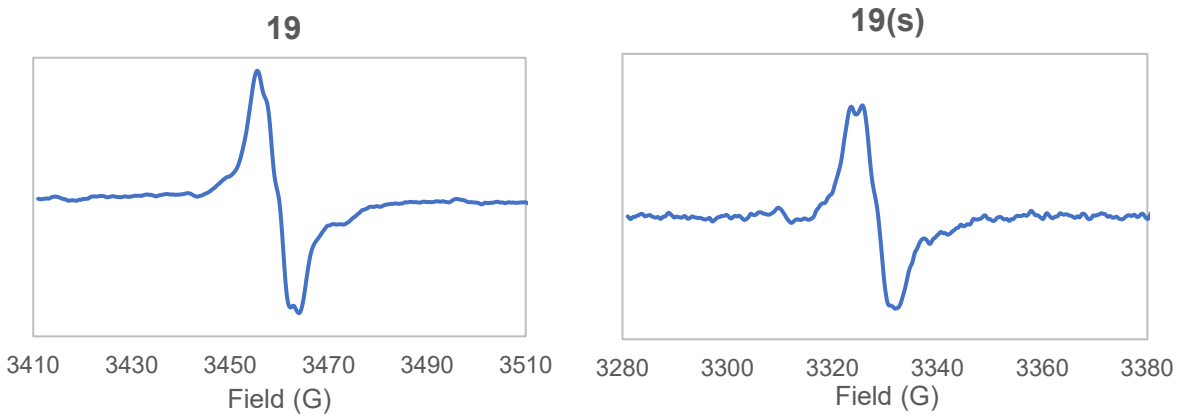

Figure 17. EPR spectra of **19** in DCM (left) and **19** in the solid state (right).

However, the lack of discernible splitting patterns makes determining the spin density of the radical somewhat difficult. Without a single and distinct structure, EPR simulations prove difficult and impractical to execute, since aside from the MS data, we have no further information to contribute to elucidating accurate molecular structures. Although, these data show that we do not have a predominantly nitrogen-centered radical, as a triplet is not observed in the EPR spectra. However, we do have a highly conjugated system with many carbon atoms; thus, the lack of splitting does not indicate whether the spin density is more evenly distributed across the molecule to the extent of a broadened, single signal, or if it resides on a single carbon atom.

Nevertheless, the presence of an unpaired electron is undeniable, and to further discern whether it was responsible for the blue/green, EPR spectroscopy on the red intermediate was undertaken in the absence of oxygen. This experiment would determine whether this type of species has an unpaired electron, indicating whether the single-electron oxidation event occurred during the reaction from starting materials to the red species, or the red species to the blue species. Due to limited solubility of **27** in suitable solvents, the reddish-brown intermediate of **28** was used to test this. This intermediate (**29**) showed no EPR signal (**Figure 18**), and thus confirms that the product does not adopt an open-shell configuration until after exposure to oxygen. It is therefore extremely probable that the deep blue/green colour is the product of the radical.

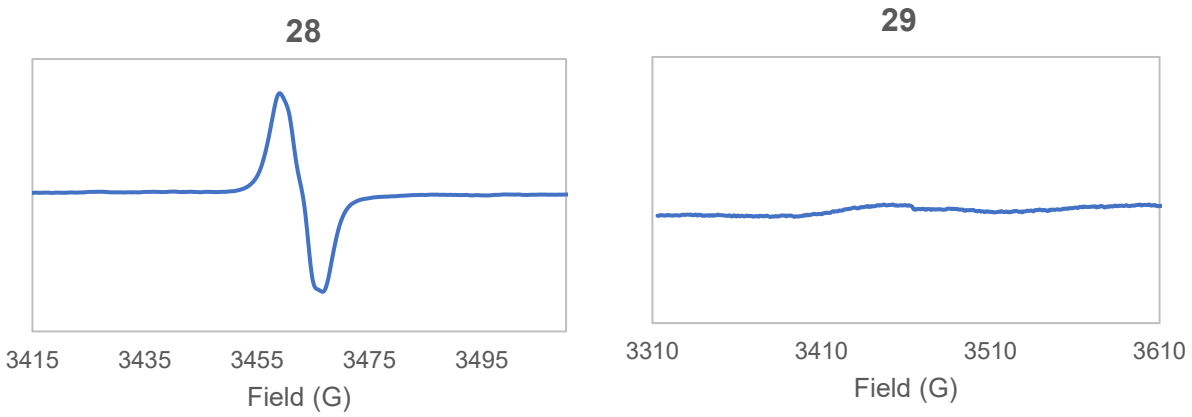

Figure 18. EPR spectra of **28** and **29**

Therefore, spectroelectrochemical studies were undertaken to confirm that the red to blue colour change observed with genipin is in fact a redox process; if it is, we should be able to electrochemically reduce the blue dye back to its red intermediate. Cyclic Voltammetry (CV) was first undertaken to determine the reduction potential of **27** and **28** in acetonitrile containing 0.1 M $TABPF_6$. The cyclic voltammograms shows very broad curves, likely due to the presence of many different genipin-amine products in the mixture. Nevertheless, quasi-reversible reduction events at -1.4 V and -0.9 V were observed for **27** and **28**, respectively (vs. Ag/AgCl; **Figure 19**). Excitingly, the spectroelectrochemical experiments showed that upon approaching the respective

reduction potentials, the absorption feature in the UV-Vis spectra corresponding to the blue/green colour decreases (λ = 592 nm for **27** and λ = 626 nm for **28**), indicating the disappearance of the blue colour as the compound is reduced (**Figure 20** and **Figure 21**).

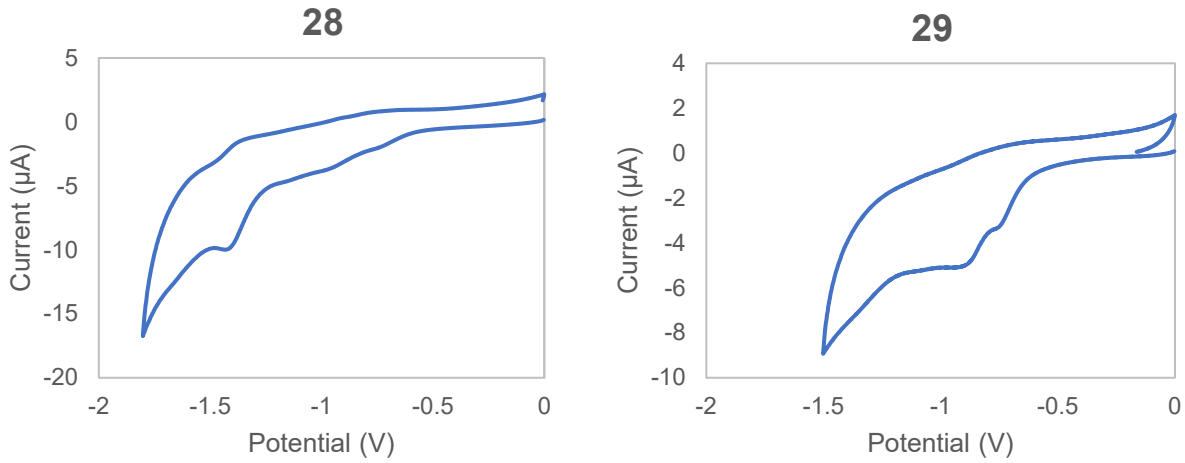

Figure 19. Cyclic Voltammograms of **28** and **29** in 0.1 M $TABPF_6$ in acetonitrile.

For **27**, the disappearance of the λ = 592 nm absorbance is accompanied by the decrease in the absorbance at λ = 237 nm and the appearance of a new peak at λ = 278 nm (**Figure 20**). This 278 nm peak contains a shoulder that extends into the visible light region (λ = ~400 nm), which is expectedly where we would observe an absorption feature for the red dye. This spillover from the UV region is similar to what is observed in the UV-vis spectra of aromatic amine dyes derived from **18**–**24**, and contributes to the possibility that the green colour is not necessarily the sole result of redshifting the λ = ~590 nm peak.

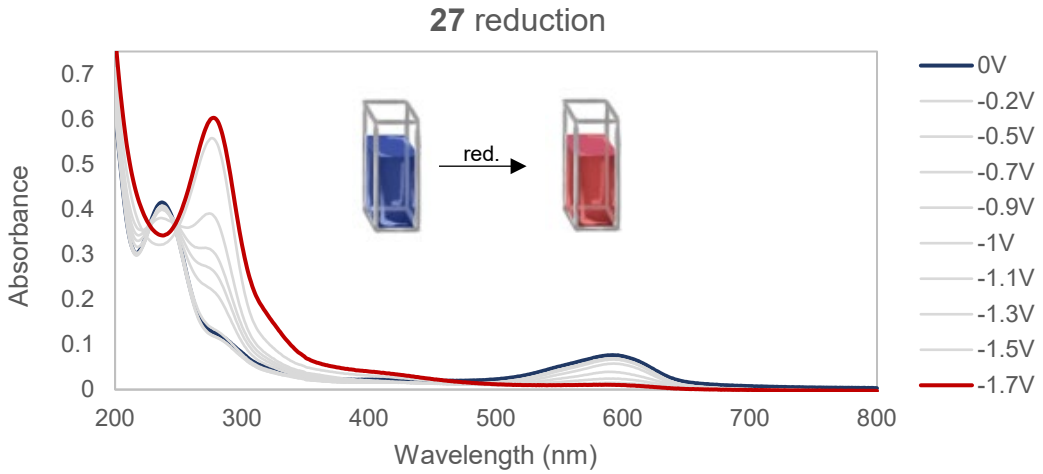

Figure 20. UV-Vis spectrum from the spectroelectrochemical experiments of **27** reduction.

For **28**, we see a very similar trend where the green absorption feature at λ = 626 nm decreases when approaching the reduction potential, with an increase in an absorption band in the higher wavelength UV region (λ = 305 nm; **Figure 21**). Similarly, this absorption band contains a shoulder that peeks into the visible light region, which would be observed as a red dye. This further supports the blue dye being the result of an unpaired electron, as when it is reduced and the radical is presumably quenched, the colour reverts to the red intermediate.

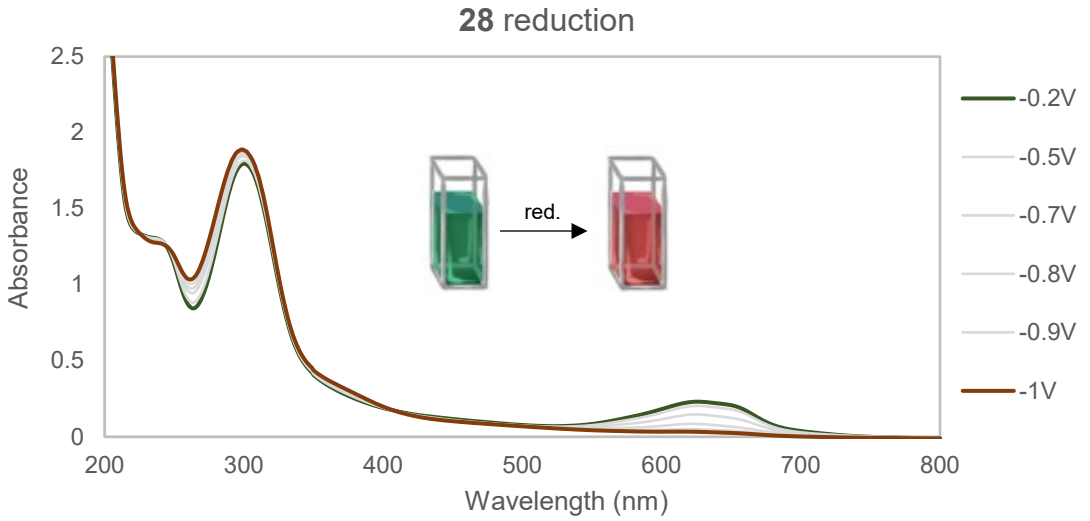

Figure 21. UV-Vis spectra from the spectroelectrochemical experiments of **28** reduction.

To confirm that the UV-Vis spectrum of the reduced **28** corresponds to the dye formed in the absence of oxygen, the UV-Vis spectrum of the intermediate dye **29** was compared to assess whether the reduced **28** was in fact the hypothesized parent red dye. As shown in **Figure 22a**, the spectra seem to overlap closely, with the exception of the reduced species derived from **28** exhibiting slightly broader features. This broadness does disguise some of the more subtle peaks that appear in the spectrum of **29**, such as the small peak at λ = 375 nm. However, the emergence of said peak can be seen when looking more closely at the spectroelectochemical data.

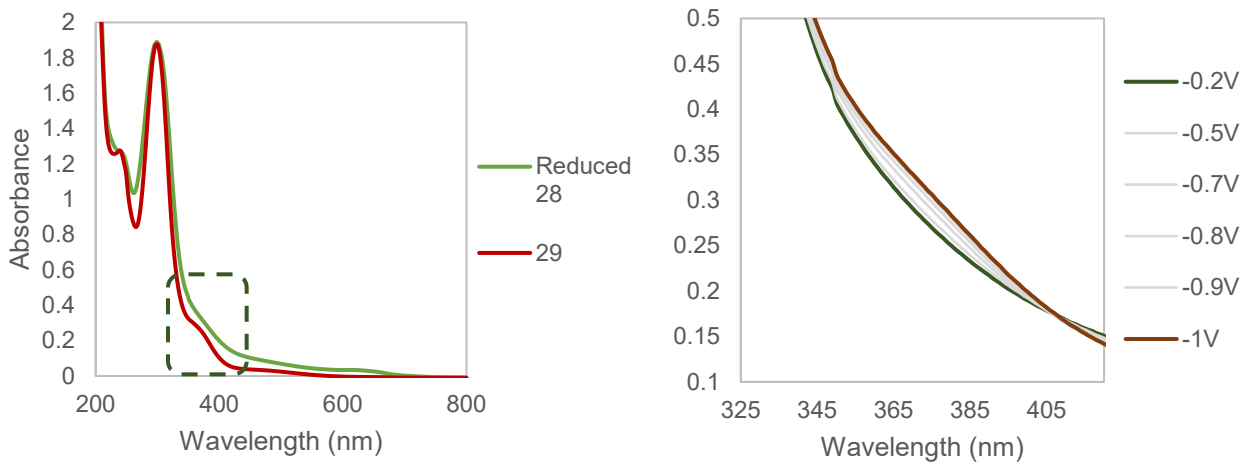

Figure 22. a) UV-Vis spectra of the reduced **28** and intermediate **29** b) zoomed in region of **28** reduction at 375 nm

The magnified region of the spectroelectrochemical spectrum in **Figure 22b** shows that when reduced back to the proposed red intermediate, we see a peak, albeit small, at λ = 375 nm emerging. Thus despite the broadness of the spectroelectrochemical spectrum, we do see the development of the characteristic features in **29**'s absorption spectrum. It can therefore be presumed that upon reduction of **27** and **28**, we can revert the blue/green colour back to the initial, red intermediate; which supports the theory that genipin forms blue dyes by adopting an open-shell configuration.

Overall, investigations into the colours of genipin dyes resulted in many unanticipated findings. Our first finding, however, was consistent with the expected results in demonstrating that extending the π system of the primary amine results in redshifting of the UV-Vis absorption spectrum of the genipin-aromatic amine dye, producing green dyes instead of blue. However, analysis of the polymer length led to the surprising discovery that genipin dyes are not polymeric, as previously thought. Instead, we found that upon oxygen exposure, the genipin-amine red intermediates adopt an open shell configuration, which was shown to be the source of the blue colour of genipin dyes, as opposed to the polymers as previously proposed in literature.

Chapter 2.4 Investigating the Effect of Synthetic Modifications of Genipin on Dye Colour

In addition to studying the impacts of amine substitution on genipin dye formation, we sought to explore what impacts that simple synthetic modifications to the parent genipin molecule would have on the resulting dyes. Based on the oligomeric structures elucidated by Touyama and coworkers, dimerization/oligomerization appears to occur most commonly at the cyclopentene moiety, thus modification of the alkene was a good starting point. Modifications of the genipin core have been researched on various occasions and include oxidation of the primary or secondary alcohols to their respective ketone or aldehyde counterparts, reductive aminations, alkylations and many others.[46–48] These are used for a variety of purposes, such as synthesis of other iridoids like cerbinal[46]; use as antiviral, insecticidal and fungicidal agents[47]; and even for investigating antitumor activity[48]. Yet, despite the extensive modifications and even demonstrating reactivity with primary amines, none appear to comment on the colours produced by these modified genipin compounds when reacted with primary amines. Thus, our goal was to investigate the resulting colours of these products, and we hypothesized that oxidation of the cyclopentene ring may alter the resulting genipin-amine dye.

The initial aim was to oxidize the alkene to the epoxide using standard reaction conditions. This was first attempted through epoxidation of geniposide with *m*CPBA to form **30**, and then cleavage of the glucose with β-glucosidase to obtain the epoxidized genipin, **30a** (**Scheme 7**). Epoxidation was conducted on geniposide as opposed to genipin in order to prevent unwanted side reactions from the ring opening of the hemiacetal ring. Epoxidation of geniposide to **30** was successful, as indicated by the disappearance of the olefinic C-H resonance at 5.82 ppm in the ^{1}H NMR spectrum and the appearance of a new resonance for H7 at 3.52 ppm. All other resonances aligned with the proposed product (see Appendix Figures A17-A21). Subsequently, the cleavage of glucose from **30** also yielded a single product. Curiously, ^{1}H NMR analysis of this product indicated proton H7 shifted from 3.52 ppm in **30** to 4.34 ppm in **30a** which is considerably

downfield for an epoxide proton, whose typical chemical shift is between 2.5–3.5 ppm[49]. Considering that the transformation was cleavage of a glucose molecule from the C1 position, drastic changes to H7 was very surprising, however this was insufficient evidence to determine that **30a** was not the isolated product. Cleavage of the glucose from the geniposide was carried out using the enzyme β-glucosidase, which functions optimally at 50ºC and at pH = 5.6. Thus, as the reaction was heated in aqueous, acidic conditions, it is possible that the epoxide can ring open to form the diol (**30b**, **Figure 23**). However, the ESI-MS did not correspond to the ring-opened epoxide **30b** but rather to **30a** ([M+Na]$^+$ – 266.0715 m/z, indicating a molecular weight of 242.08 g/mol). It seemed increasingly evident that the product isolated was **30a**, and thus further NMR studies in d-DMSO were undertaken to observe the hydroxyl resonances.

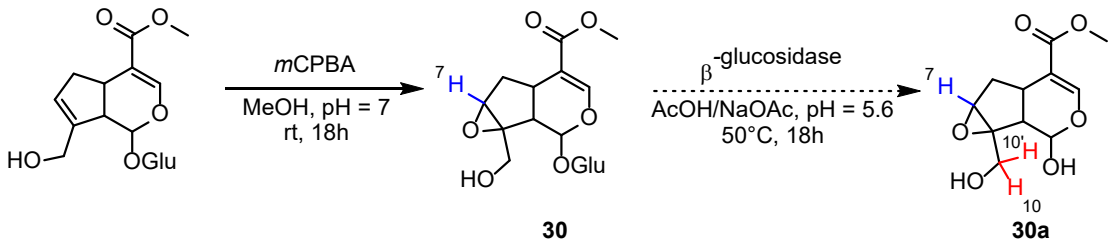

Scheme 7. Synthetic route of **30** and **30a** from geniposide.

Supporting the ESI-MS data, only two protons did not show a correlation in the ^{1}H-^{13}C HSQC spectrum, which would be for the existing C1 and C10 hydroxy groups (H14 and H15, respectively, **Figure 23**). Though despite this, proton **30a-**H15 only exhibited a singlet, where it should show a doublet of doublets from coupling to protons **30a**-H10 and -H10'. Likewise, the ^{1}H-^{1}H 2D COSY NMR spectrum did not show any correlations between **30a**-H15 and -H10/10', however **30a**-H14 did show coupling to **30a**-H1. Therefore, from the ESI-MS ([M+Na]$^+$ – 266.0715 m/z) we know we do not have **30b** (**Figure 23**) and NMR analysis shows that we do not have **30a** since we do not see the CH_2OH moiety of the 2,3-epoxy alcohol; however, since the ESI-MS matches **30a**, it led us to believe that we have a structural isomer instead.

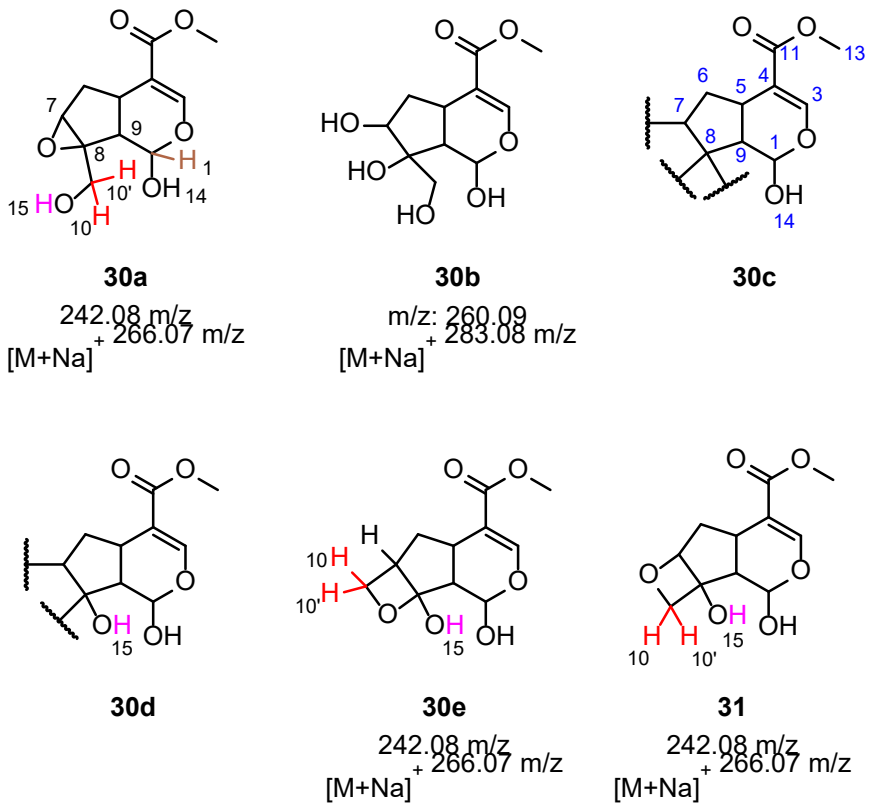

Figure 23. Structures of **30a**, **30b**, possible stereoisomers of **30a** (**30c-30g**) and **31**

Considering that all protons on both the pyran, cyclopentane ring, methyl ester (H13) and C1 hydroxy group (H14) are consistent with the expected chemical shifts and correlations, the remaining connectivity to be elucidated lies on carbons C7 and C8 (**30c**, **Figure 23**). From the NMR data concerning the second hydroxy group, the OH proton (H15) does not show any coupling and likewise, any COSY correlations, indicating that the location must be on a quaternary carbon. The outstanding moieties as determined by the ESI-MS are a CH_2-group and an ether functionality, thereby eliminating those the remaining assignments as possible connections to OH-15. Thus, **30d** is the plausible structure in terms of placement of OH-15. C8 is a quaternary carbon, and therefore we know that C7 and C8 each have one more bond to another atom and the only remaining atoms are still a -CH_2- and an -O-. While a cyclic ether on C7 and C8 was the initial goal with the epoxidation, the only possibility with the remaining -CH_2-O- is the oxetane. Two possibilities exist for its connectivity as shown in **Figure 23** (**30e** and **31**). As shown, the

proposed structure **30e** places oxetane O on **30e**-C8 and **30e**-H10/10' adjacent to **30e**-H7 and should therefore demonstrate splitting and at the very least, COSY correlations from the vicinal coupling. However, **30e**-H10 and -H10' show no COSY correlations aside from to each other and lack any further splitting patterns aside from their respective doublets from geminal coupling.

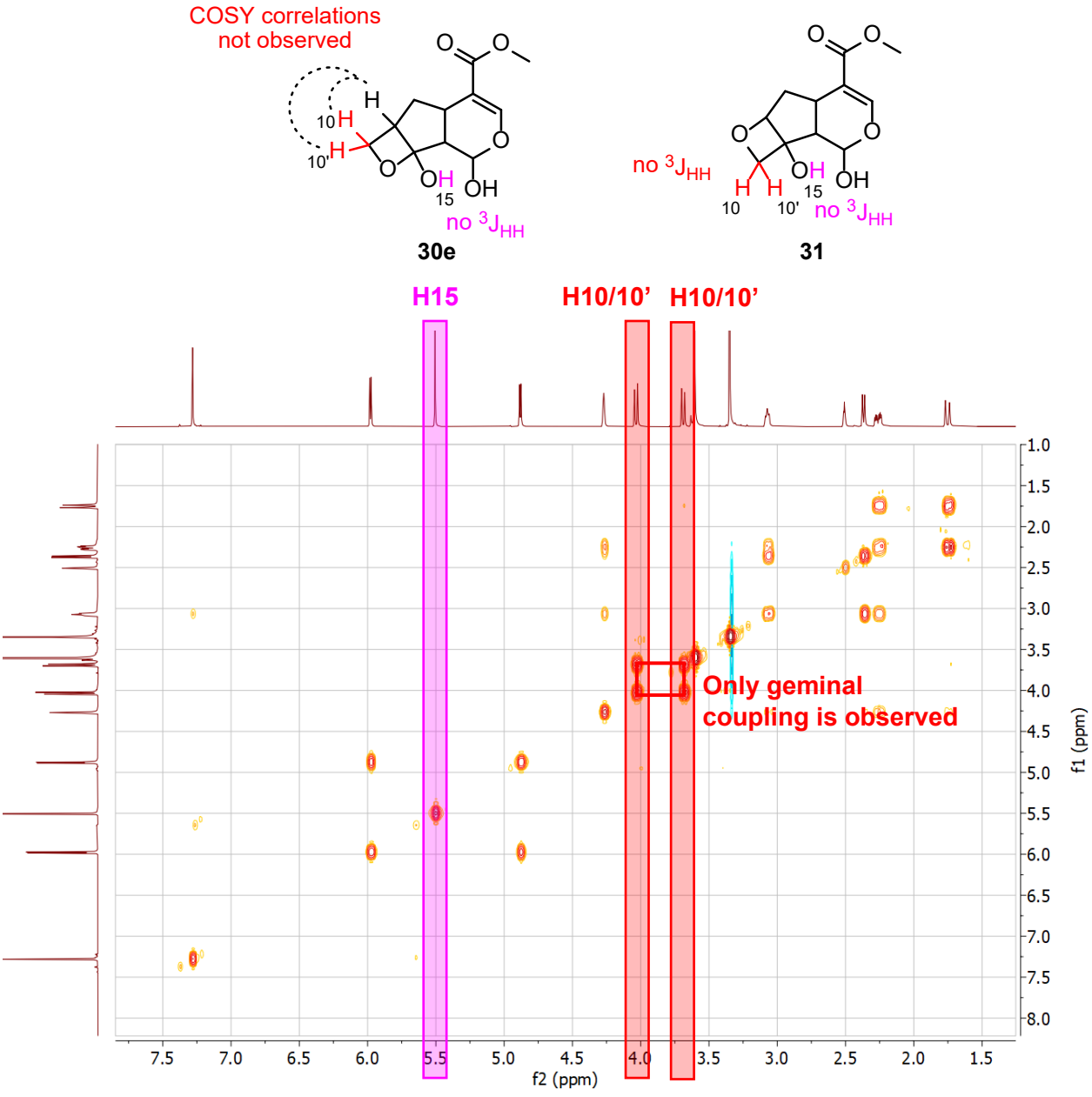

Figure 24. ^{1}H-^{1}H 2D COSY of the oxetane product **31**.

Thus, this leaves the structure of **31**, which exhibits all the correct NMR correlations (**Figure 24**) and matches the m/z ($[M+Na]^+$ – 266.0715 m/z). This also further explains the downfield shift of H7, as the ring strain of the epoxide usually results in more shielded protons than those of other ethers. The oxetane structure was unexpected, as oxetane formation does not typically occur with acid catalysis of 2,3-epoxy alcohols. Nevertheless, it provided an equally interesting molecule for our purposes.

The other synthetic route attempted was to epoxidize genipin directly (**Scheme 8**). The alkene of the allylic alcohol was successfully epoxidized to yield **30a**, as determined by the disappearance of the olefinic C-H resonanace at 5.85 ppm and the appearance of a new resonance corresponding to the epoxide proton at 3.43 ppm. To remove any excess *m*CPBA and its benzoic acid by-product, 5% aqueous K_2CO_3 was added until effervescence was no longer observed. Surprisingly, this also led to complete conversion to **31**. Thus, to remove by-products, purification via column chromatography was attempted, however this also proved difficult, as the attempted purification of **30a** using silica gel or alumina also resulted in conversion to **31**. The tendency of **30a** to form the oxetane remains a curious occurrence, as they are typically not easily made. In fact, oxetane synthesis is a lucrative area of research, as oxetane-containing molecules hold important significance in medicinal chemistry due to their increased metabolic stability compared to various functional groups (carbonyls, for example) and their ability to serve as substitutes for them in terms of their polarity and hydrogen-bonding characteristics.[50]

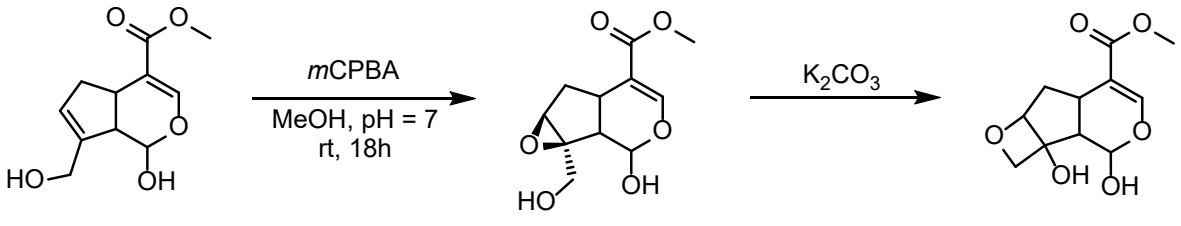

Scheme 8. Synthetic route of **30a** and **31** from genipin

While the exact mechanism that the reaction proceeds through is unclear, it is evident that it is catalyzed by both acidic and basic conditions. Rearrangements of 2,3-epoxyalcohols in basic conditions typically undergo the Payne rearrangement, which is the conversion of 2,3-epoxy alcohols to their corresponding 2,3-epoxy alcohol isomer (**Figure 25a**).[51,52]. Theoretically, the most stable isomer from this 2,3-epoxy alcohol rearrangement is actually that of the oxetane formed from attack of the alcohol on the 3-position instead of the 2-position, however the calculated activation barrier to achieve this structure is so high (144 kJ/mol) that it is generally unattainable and has only been seen in high energy conditions, such as during mass spectrometry.[53,54] Comparatively, the activation energy required to undergo the rearrangements between the two epoxide isomers of the simple 2,3-epoxypropoxide is calculated to be a mere 45 kJ/mol. Interestingly, our case appears to exhibit the type of reactivity that favours formation of the more stable oxetane. This is unexpected, as it appears to form in relatively mild conditions. Although 2,3-epoxy alcohols can be used to synthesize oxetanes using other methods, this requires first the reduction of the epoxide, monotosylation to generate the leaving group and then ring closure catalyzed by a strong base, such as *t*-butoxide or sodium hydride (**Figure 25b**).[55,56] In our case, while we do employ a base, there is no reducing agent present and no good leaving group; ring opening with OH^- would result in an extra OH group that is not present in the final product and would not be a sufficient leaving group to generate **31** (**Figure 25c**). Though neither examples of 2,3-epoxy alcohol base-catalyzed rearrangements to oxetanes are favourable, we hypothesize that if the geometric arrangement of genipin's fused ring structure could lower the activation energy barrier for the rearrangement, the more stable oxetane structure would be thermodynamically favourable and thus, preferentially formed by the Payne rearrangement (**Figure 25d**).

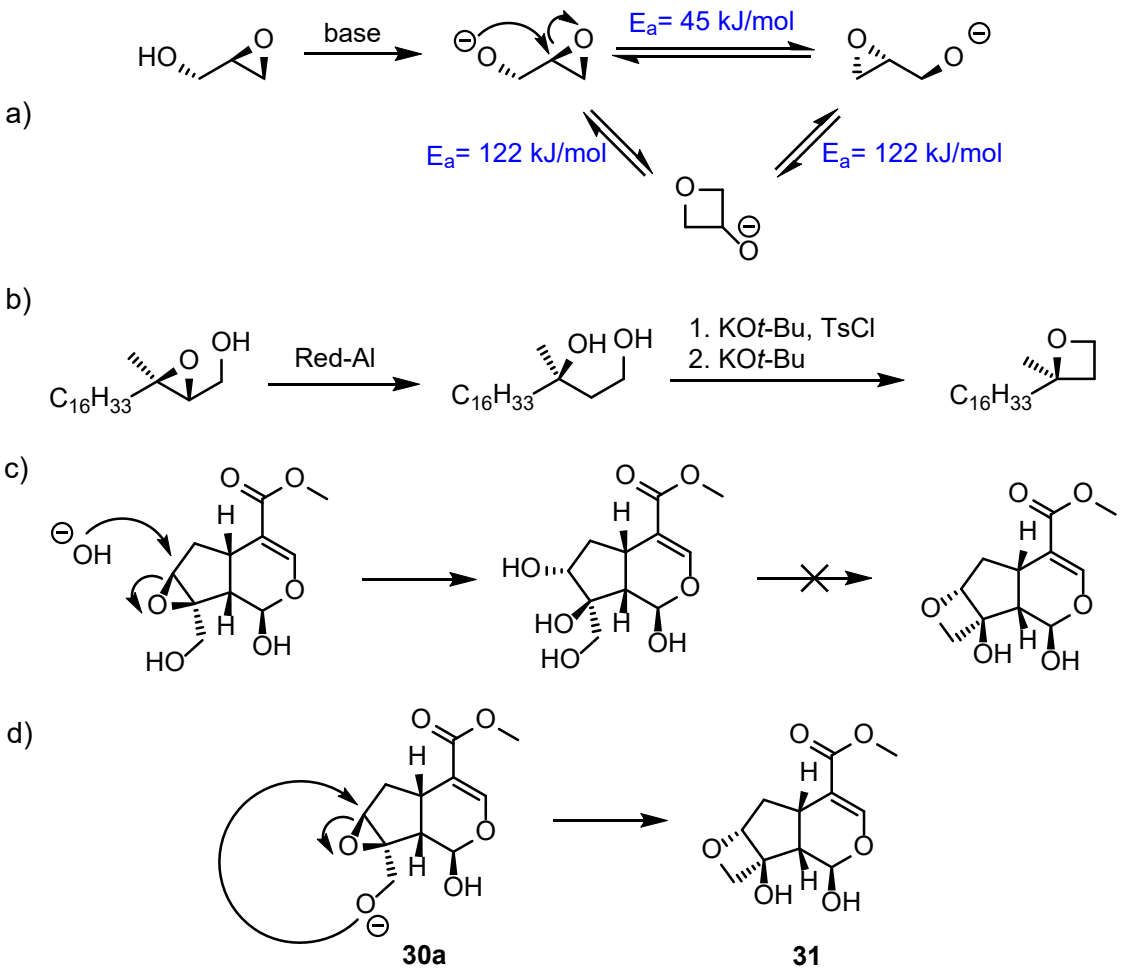

Figure 25. a) Mechanism of the Payne rearrangement of 2,3-epoxy alcohols **b)** Oxetane synthesis from 2,3-epoxy alcohols reported by Dussault and coworkers[56] **c)** base-catalyzed ring opening of **30a d)** base catalyzed Payne-type rearrangement for oxetane formation

As previously mentioned, the reaction also appears to be acid catalyzed during the cleavage of the glucose. Unlike the conversion of the epoxide to the oxetane through the diol in **Figure 25b**, the Payne rearrangement can (though much less common) be catalyzed by acidic conditions, as shown by Castle and coworkers.[57] This, however, is not necessarily analogous to our conditions as it is Lewis acid promoted as opposed to Brønsted acid promoted. Despite this, the Payne-type rearrangement exhibited in their work involves the migration of a trityl group as opposed to a hydrogen atom, as shown in **Figure 26a**. They theorize that this trityl migration is catalyzed by coordination of the copper or magnesium that is present in the reaction mixture; in

our case, the Brønsted acid can sufficiently catalyze the proton transfer. The analogous mechanism for **30a** to **31** is shown in **Figure 26b**. With the apparent stability of **31** based on the favourability to form the oxetane from both acidic and alkaline reaction conditions, the formation of the secondary carbocation in **Figure 26b** might be more favourable thermodynamically than the generically more stable tertiary carbocation. While the stereochemistry of the product has not yet been elucidated, both mechanisms imply that the oxetane ring forms on the opposing face of the epoxide.

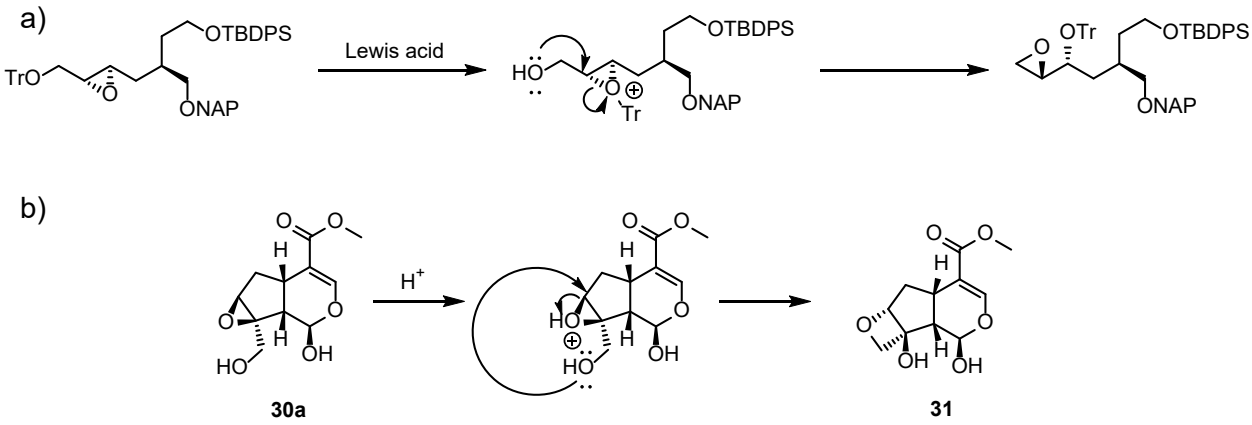

Figure 26. Proposed pathways of acid catalyzed formation of **31**. **a)** Unlikely pathway with carbocation formation on C7 **b)** more likely pathway with more stable carbocation on C8.

To investigate the effects of this synthetically modified genipin derivative on dye formation, **31** was reacted with the amino acid lysine. Unlike genipin, the dye formed was not the typical dark blue, despite being exposed to oxygen. Instead, a yellow/orange colour was observed similar to the intermediate red from aforementioned genipin-amine reactions, suggesting that unlike genipin, its oxetane counterpart does not adopt an open-shell configuration when reacted with amines. The UV-Vis spectrum of the product (**32**) clearly shows a λ_{max}= 432 nm in the visible light region, which closely relates to the absorption region of the genipin intermediate dyes (**Figure 27**). The product could not be purified using silica gel or alumina column chromatography due to

strongly adhering to the column and thus preventing elution. ESI-MS revealed that the product did not retain the oxetane functionality, which ring opened to form the diol once the reaction with the amine had occurred (**32**, $[M+H]^+$ = 371.18079 m/z, **Figure 27**).

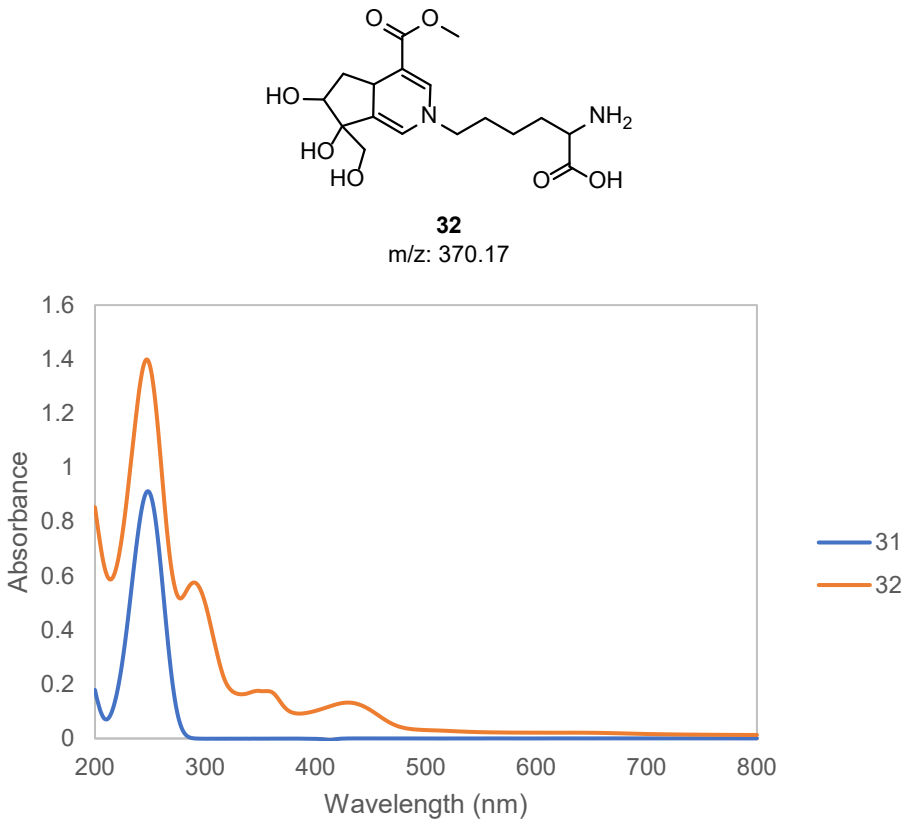

Figure 27. Proposed structure and UV-Vis spectra of **31** and **32.**

Therefore, **31** is not only able to form genipin-amine dyes, but also appears to do so without the one-electron oxidation. Thus, one major and beneficial implication this has is that if the dye product truly does not form a radical, it can then be studied via NMR spectroscopy. The reaction between **31** and lysine was tracked with ^{1}H NMR spectroscopy over a period of 20 hours. The stacked NMR spectra can be seen in **Figure 28**, and the integrations of the relevant protons normalized to 1 over time are displayed in **Figure 29**. The integrations show that as **31** reacts to form **32**, we see direct correlations between the decrease in **31**-H1 and increase in **32**-H1; decrease in **31**-H3 and increase in **32**-H3; and a decrease in **31**-H9. This demonstrates that **31**-

H1 and **31**-H9 still undergo the expected dehydration, with the decrease in **31**-H9 and downfield shift from **31**-H1 to **32**-H1. **31**-H3 also undergoes a slight shift to **32**-H3 as expected, supporting the proposed structure of **32** from the ESI-MS.

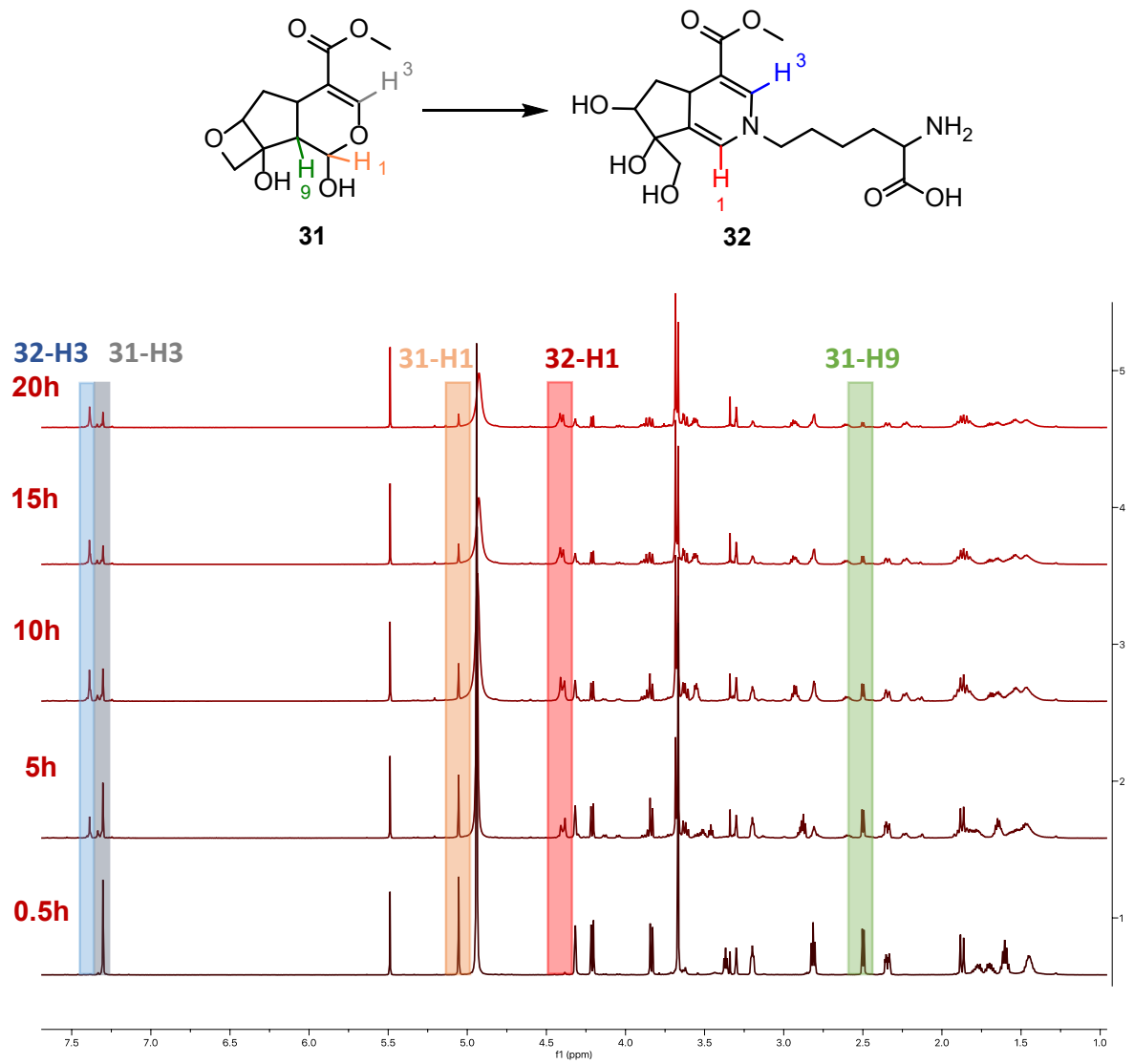

Figure 28. Stacked ^{1}H NMR spectra of the reaction of 31 with lysine in 5-hour intervals in methanol-d4.

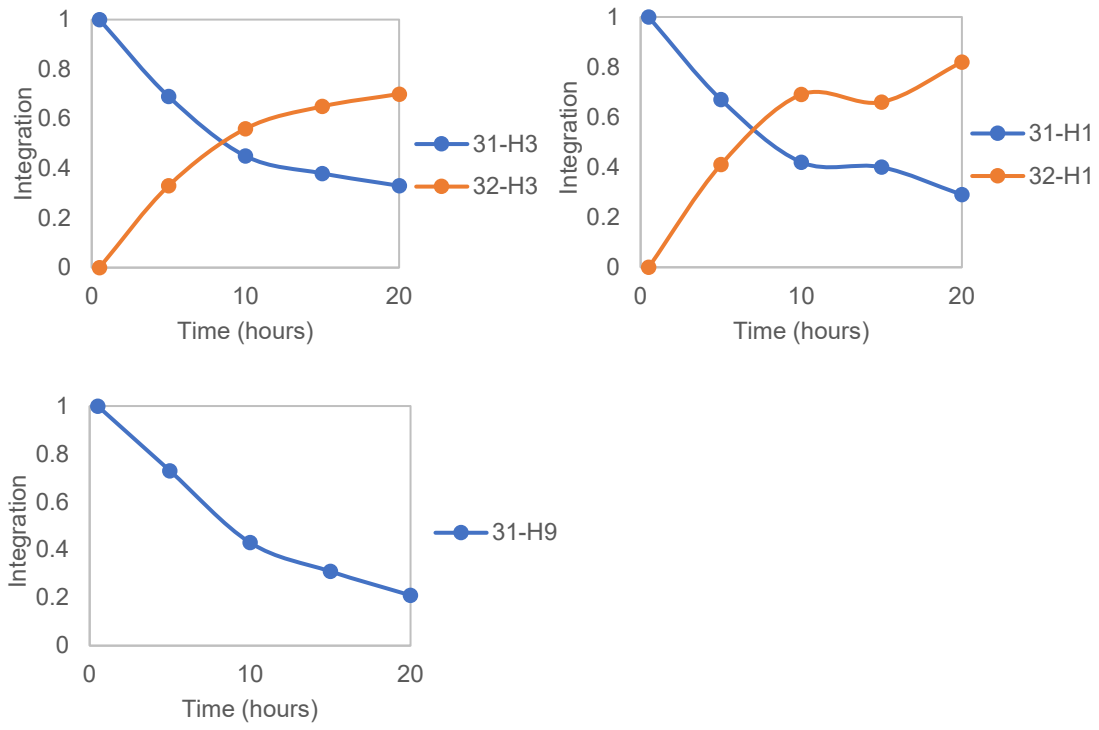

Figure 29. Relative integrations of protons a) 31-H3 and 32-H3, b) 31-H1 and 32-H1 and c) 31-H9 over 20 hours of the reaction between **31** and lysine

Further NMR studies were conducted to verify the proposed product. Since lysine contains two primary amine groups, **31** could potentially react with either one. Thus, a ^{1}H-^{13}C 2D HMBC experiment and a ^{1}H-^{15}N HMBC experiment were conducted to validate that the reactive amine in **33** was that of the side chain. The ^{1}H-^{13}C 2D HMBC shows that **32**-C3 only correlates to two protons; one of which is **32**-H1, as expected (**Figure 30**). The other correlation is to **32**-H14 on the lysine, the H adjacent to the side chain amine.

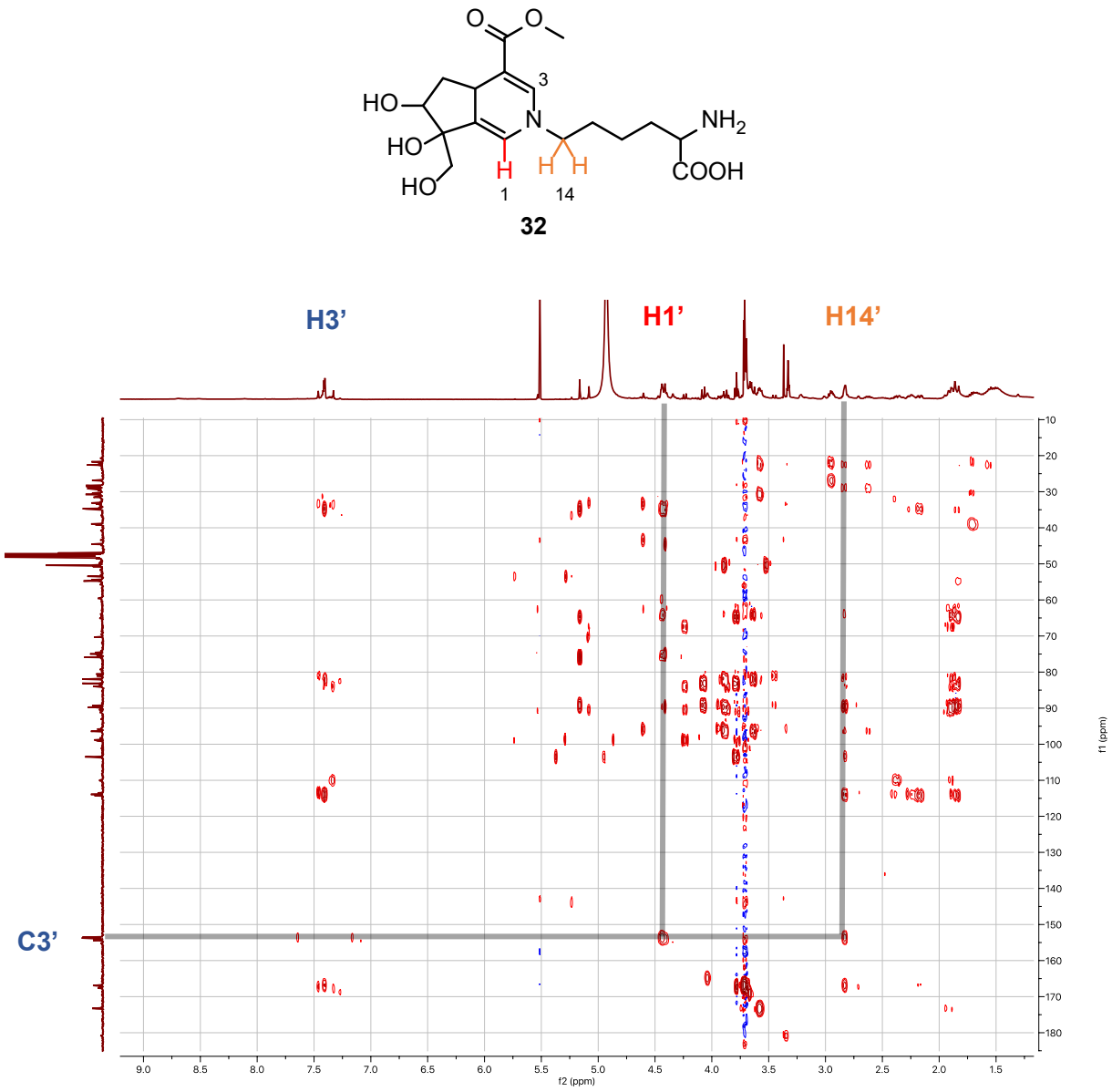

Figure 30. ^{1}H-^{13}C 2D HMBC of **32**, showing correlations between the H1 proton on the 6-membered ring and the protons adjacent to the side chain amine of L-lysine.

Furthermore, the ^{1}H-^{15}N 2D HMBC spectrum confirms that the N atom that correlates to **32**-H1 also shows scalar coupling to the protons **32**-H15 on the side chain, reaffirming the side chain amine as the reactive amine (**Figure 31**). No other ^{15}N signals seem to indicate that there

is an amine group bonded to both lysine and genipin. This was expected, as it correlates to m/z obtained from the ESI-MS. Additionally, this suggests that the lysine is not opening the oxetane.

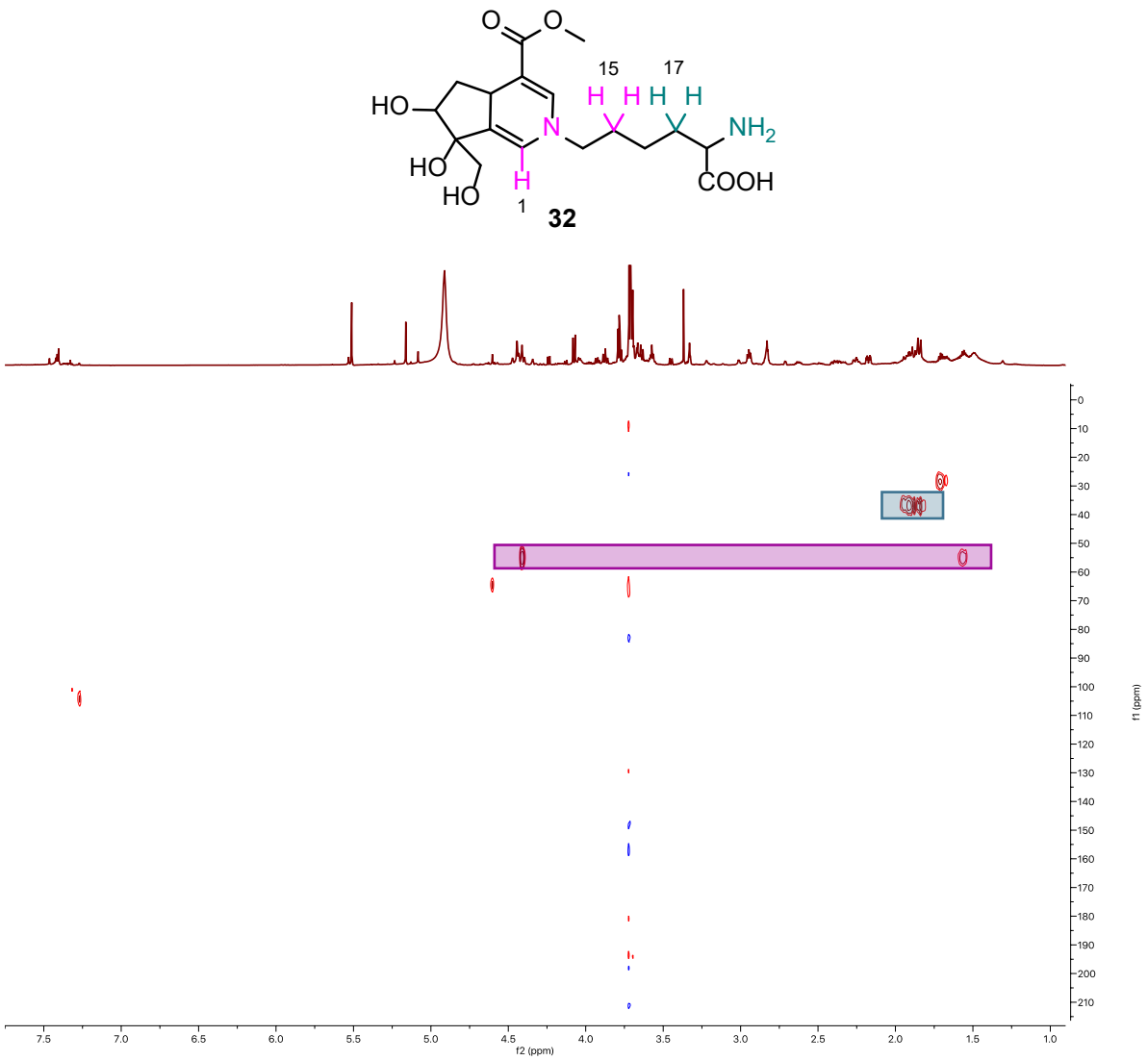

Figure 31. ^{1}H-^{15}N 2D HMBC of **32**.

Of course, it is important to note that there were other products formed in the reaction, however since the monomer was the most abundant and ^{15}N NMR is highly insensitive, correlations of the other less abundant products are not easily observed. Nevertheless, this provides valuable information as to the similarities between **31** and genipin and their reactivity

with amines, demonstrating the same reactivity with the pyran ring, yet differing in its reactivity with the cyclopentane ring, where the persistent radical forms with genipin reactions.

While it appears that this modification in particular was successful in preventing the formation of a blue dye, simply altering the cyclopentene ring is not always a reliable method for "stabilizing" this intermediate form. This can be demonstrated with loganin, an iridoid very similar to geniposide. Hydrolysis of the glucose results in the corresponding loganin aglycone (LA), which is in turn very similar to genipin (**Figure 32**). LA has also been shown to generate a dark blue dye — loganin blue, much like genipin — and it is possible that this too, forms a radical which results in its blue colour.[58] However, despite the similarities to genipin, it also contains some characteristics similar to **31**, in that carbon C7 is bonded to an oxygen atom, and the alkene between C7 and C8 is absent. Thus, simply modifying the cyclopentene moiety of genipin does not guarantee a significant change in the redox potential of the dye product that would be enough to prevent radical formation. Nonetheless, doing so is clearly possible, and it opens the door to achieving other coloured dyes by modifying the absorptive properties of the molecule without concern for the unpaired electron.

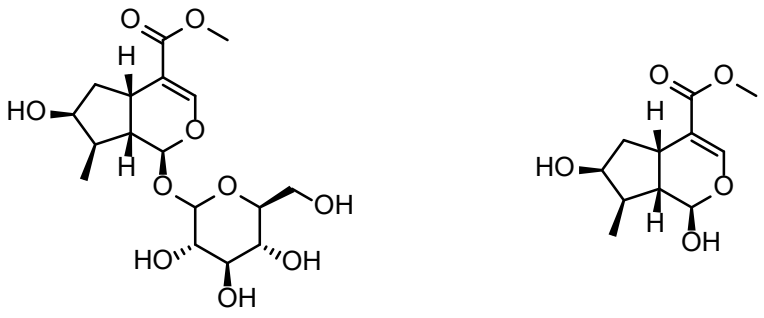

loganin loganin aglycone

Figure 32. Molecular structures of loganin and LA.

Chapter 3. Conclusions and Future Work

In conclusion, the chemistry of genipin reactivity and products turned out to be considerably different than previously thought. To our knowledge this is the first instance that the nature of genipin blue has been extensively explored, and the first to demonstrate that the literature accounts may not have been entirely accurate. As genipin has previously been reacted with only aliphatic amines, genipin was shown to react readily with some aromatic amines. These dye products show redshifted absorption peaks in the UV-Vis spectra, as expected from extension of the π system. The difference in colour was visually observable, where the dyes generated from genipin and the aromatic amines were green in colour as opposed to blue. However, reactivity was shown to be somewhat limited, as highly electron deficient amines of the aromatic amine and significant steric bulk around the amine group were shown to slow down or completely inhibit reactivity. While previous reports did suggest that oxygen exposure induces some radical reaction with the red dye, it was reportedly a polymerization event and did not contain an unpaired electron in the final structure. We have now shown that the oxygen-induced radical reaction does not result in polymers, but instead leads to a mixture of small molecules which was confirmed to contain a persistent radical by EPR spectroscopy. It was also shown that it is the open-shell configuration that is responsible for the blue dye; with the disappearance of the blue absorptive feature in the UV-Vis spectrum when reduced electrochemically via spectroelectrochemistry. In addition, we have successfully altered the genipin core to seemingly prevent the persistent radical, resulting in an orange dye. This entailed epoxidation of the allylic alcohol on genipin, which turned out that under relatively mild conditions, formed the oxetane isomer. Thus, we have gained further insight into the process in which genipin-amine products form, and the source of their deeply coloured dyes.

Future work for this project entails computational analysis on some of the presumed structures of the blue and green dyes. As EPR spectroscopy does not provide sufficient

information to infer the location of the radical on the blue coloured compounds, computational analysis will be an important next step in elucidating the electronic structure and reactivity of these blue dyes. Experimental data would also be useful in supporting the computational data. However, while the blue dye can be separated from the red compounds, the mixture of compounds that compose the blue dye cannot be separated via column chromatography. Thus, other approaches to purification will be a necessary step in future work. This may entail other purification methods, or purification on the unoxidized compounds. Furthermore, UV-Vis spectroscopy is not always indicative of the differences in colour of the various dyes, other colorimetric methods can be explored to more accurately describe the dye colours.

In addition, as the oxetane formation proceeds with unprecedented ease, further analysis into this method of oxetane synthesis with similar compounds can help provide insight into this reactivity. While it is suggested by the colour that the oxetane-lysine product does not form a radical species, EPR spectroscopy is necessary to confirm this, and additional modified genipin species can be synthesized for studying potential radical-free genipin dyes.

Chapter 4. Experimental

Chapter 4.1 General Considerations

All chemical reagents or solvents were purchased from Fisher Scientific or Millipore Sigma and used as received unless otherwise indicated. Genipin was kindly donated by Inkbox Ink and purity verified independently by ^{1}H NMR analysis. All manipulations were performed under ambient conditions unless otherwise stated. An MBraun LABstar Glove Box Workstation under N_2 atmosphere or employing Schlenk techniques were utilized for reactions requiring oxygen gas exclusion. *NMR Spectroscopy.* Experiments monitored by NMR spectroscopy were conducted in NMR tubes (8” x 5 mm) sealed with standard plastic caps. ^{1}H NMR and ^{13}C{^{1}H} NMR spectra were obtained on a 400 MHz Bruker spectrometer in Methanol-d_4 or DMSO. Chemical shifts are

reported relative to $SiMe_4$ and referenced to the residual solvent signal (^1H, $^{13}C\{^1H\}$). NMR spectra were analyzed using either TopSpin 4.0.1 or MestReNova 6.0.2-5475 software. Chemical shifts are reported in ppm and coupling constants as scalar values in Hz. Absorption measurements were recorded with a Cary 5000 UV-Vis-NIR Spectrophotometer from Agilent Technologies. Recordings were obtained at 25 °C and taken with the instrument operating in dual beam mode and referenced to methanol. All absorption experiments were conducted in quartz cuvettes (1cm x 1cm) equipped with a Teflon seal. *Electron Paramagnetic Resonance (EPR) Spectroscopy.* EPR samples measured in solution were prepared by dissolving the dye product in dichloromethane and placing in a PYREX® 90 mm Capillary Melting Point Tubes inside a quartz EPR tube. The samples run in the solid state were placed directly in a quartz EPR tube. X-band continuous-wave (CW) EPR spectra were collected using a Bruker X-band CW EMX EPR spectrometer equipped with a 6" electromagnet. *Mass Spectrometry.* Mass spectrometry was conducted with either a Bruker Autoflex Speed spectrometer with an α-cyano-4-hydroxycinnamic acid (CHCA) matrix, or an Agilent 6538 UHD spectrometer in positive mode. *Cyclic Voltammetry and Spectroelectrochemistry*. Cyclic Voltammetry was performed with an Autolab PGSTAT204 potentiostat on 10 mg/ml solutions in dry acetonitrile containing 0.1M $TABPF_6$. A typical three-electrode cell was used with a Pt wire counter electrode, an Ag/AgCl reference electrode and glassy carbon working electrode. Spectroelectrochemistry was performed with an Autolab PGSTAT204 potentiostat and a Cary 5000 UV-Vis-NIR Spectrophotometer from Agilent Technologies on 2 mg/mL solutions in dry acetonitrile containing 0.1 M $TABPF_6$.

Chapter 4.2 Experimental Procedures

Chapter 4.2.1 Preparation of dye products

General procedure of genipin-amine products (17-26)

Genipin and amine (0.5 mmol) were dissolved in 10 ml of methanol and stirred at room temperature for 48 hours in a 20 mL scintillation vial and diluted with methanol to 0.025 mM solutions (with respect to initial genipin concentration) for UV-Vis spectroscopy.

Preparation of Genipin-methylamine product (27)

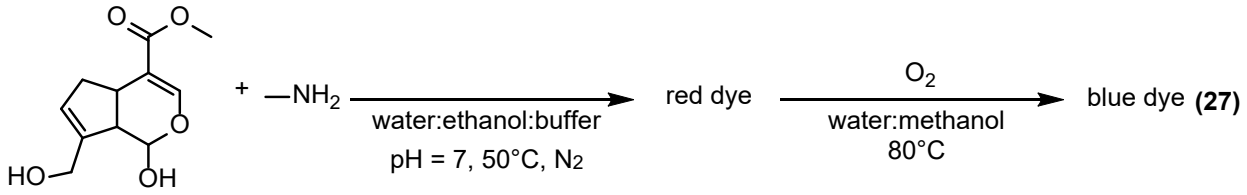

Methylamine (40% in water) (34.3 mg, 1.1 mmol), was added to 15 mL of a 1:1:1 distilled water:ethanol:phosphate buffer (pH=7) mixture in a 100mL 3-neck flask and sparged with nitrogen. Genipin (250 mg, 1.1 mmol) was added to the reaction mixture and stirred for 2.5 hours at 50˚C under an N_2 atmosphere. The product was extracted with DCM and dried *in vacuo*, yielding a dark red solid. The red product was dissolved in a 1:1 water:methanol mixture and stirred at 80˚C while bubbling with air for 6 hours. The dark purple/blue product was washed with DCM. ESI-MS: *m/z*: 831.35 (tetramer) $[M-H]^+$. UV-vis (methanol) λ_{max} 279, 590 nm.

Preparation of genipin-p-toluidine product (28)

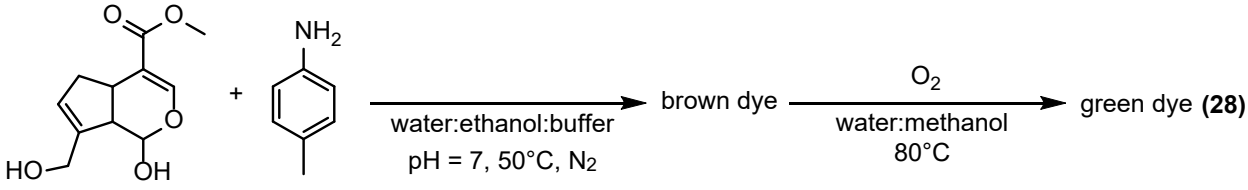

p-toluidine (117.9 mg, 1.1 mmol), was added to 15 mL of a 1:1:1 distilled water:ethanol:phosphate buffer (pH=7) mixture in a 100mL 3-neck flask and sparged with

nitrogen. Genipin (250 mg, 1.1 mmol) was added to the reaction mixture and stirred for 2.5 hours at 50˚C under an N_2 atmosphere. The product was extracted with DCM and dried *in vacuo*, yielding a brown solid. The brown product was dissolved in a 1:1 water:methanol mixture and stirred at 80˚C while bubbling with air for 6 hours, yielding a dark green product ESI-MS: *m/z*: 832.33 (trimer) $[M-H]^+$. UV-vis (methanol) λ_{max} 302, 621 nm.

Preparation of unoxidized genipin-p-toluidine dye (29)

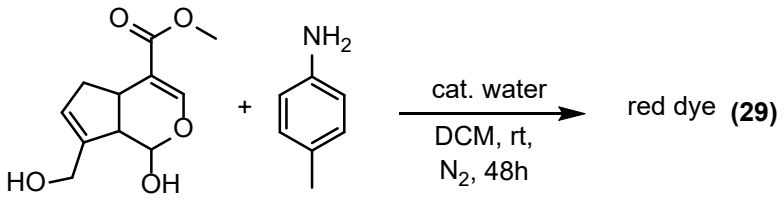

In a Schlenk flask under an N_2 atmosphere, 0.1 mL of degassed, distilled water was added to a degassed solution of genipin (250 mg, 1.1 mmol) in DCM. 117.9 mg of p-toluidine was added to the flask and stirred at room temperature in for 48 hours under an N_2 atmosphere. The solvent was removed *in vacuo* to yield a deep red solid, which was transferred into the glovebox and redissolved in either dry DCM for EPR spectroscopy or 0.1M acetonitrile for UV-Vis spectroscopy.

Chapter 4.2.2 Preparation of oxidized genipin species

Synthesis of epoxygeniposide (30)

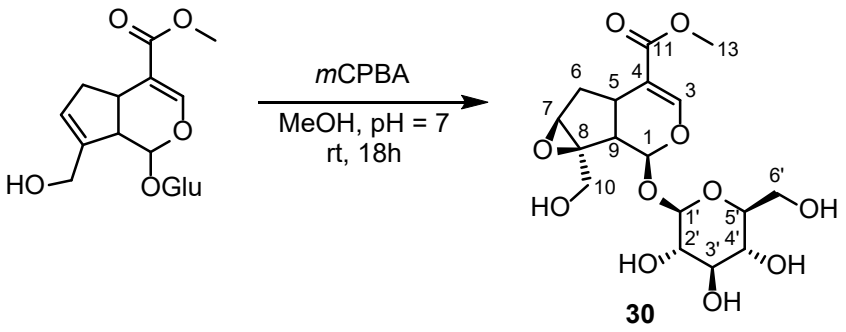

Geniposide (1.94 g, 5 mmol) and *m*CPBA (1.29 g, 7.5 mmol) were dissolved in 20 mL methanol. 2 drops of pH=7 phosphate buffer was added to the solution and the reaction mixture was stirred at room temperature overnight. The reaction mixture was poured directly into water, the methanol was removed under reduced pressure and precipitate filtered off. The water was removed *in vacuo* yielding a whitish-yellow solid. (1.76 g, 87%) ^{1}H NMR (400 MHz, MeOD) δ 7.49 (s, 1H, H3), 5.27 (d, *J* = 9.6 Hz, 1H, H1), 4.84 (s, 1H, Glu-H1'), 4.24 (d, *J* = 13.0 Hz, 1H, H10), 3.93 (d, *J* = 11.5 Hz, 1H, Glu-H6'), 3.83 (d, *J* = 13.0 Hz, 1H, H10'), 3.71 (s, 3H, H13), 3.67 (m, 1H, Glu-H6''), 3.51 (s, 1H, H7), 3.44 – 3.33 (m, 4H, Glu-H2', -H3', -H4', -H5'), 2.76 (q, *J* = 7.9 Hz, 1H, H5), 2.56 (dd, *J* = 13.9, 7.6 Hz, 1H, H6), 2.47 (dd, *J* = 9.3, 7.5 Hz, 1H, H9), 1.47 (dd, *J* = 13.6, 10.5 Hz, 1H, H6'). ^{13}C NMR (100 MHz, MeOD) δ 168.03 (C11), 152.79 (C3), 108.67 (C4), 99.70 (Glu-C1'), 95.61 (C1), 78.30 (Glu-C2'), 77.24 (Glu-C5'), 74.43-71.31 (Glu-C3', -4'), 68.23 (C8), 62.54 (Glu-6'), 61.29 (C10), 60.13 (C7), 51.67 (C13), 41.93 (C9), 34.70 (C6), 31.23 (C5). Expected m/z: 404.13. Found m/z: $[M+Na]^{+}$ = 427.12106 m/z

Synthesis of genipin oxetane (31) from 30

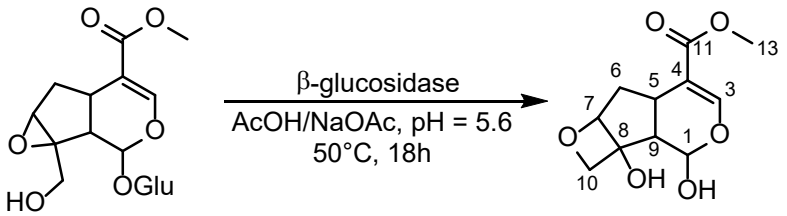

30 **31**

Epoxidized geniposide **28** (1.76 g, 4.4 mmol) and β-glucosidase (300 mg) were dissolved in 30 mL of pH = 5.6 acetate buffer and stirred at 50°C overnight. The product was extracted with ethyl acetate. These fractions were combined and the solvent removed *in vacuo* yielding a white solid (0.82 g, 77%) ^{1}H NMR (400 MHz, MeOD) δ 7.32 (s, 1H, H3), 5.07 (s, 1H, H1), 4.34 (s, 1H, H7), 4.24 (d, *J* = 9.3 Hz, 1H, H6), 3.86 (d, *J* = 9.3 Hz, 1H, H6'), 3.68 (s, 3H, H13), 3.21 (t, *J* = 5.0 Hz, 1H, H5), 2.52 (d, *J* = 6.6 Hz, 1H, H9), 2.34 (ddd, *J* = 12.2, 4.3, 2.9 Hz, 1H, H6), 1.90 (d, *J* = 12.2 Hz, 1H, H6'). ^{13}C NMR (100 MHz, MeOD) δ 168.96 (C11), 155.76 (C3), 111.94 (C4), 100.11 (C1), 91.78 (C8), 85.22 (C7), 71.59 (C10), 69.07 (C9), 51.83 (C13), 34.47 (C5), 32.87 (C6). Expected m/z: 242.08. Found m/z: $[M+Na]^{+}$ = 265.07165 m/z

Synthesis of 31 from genipin

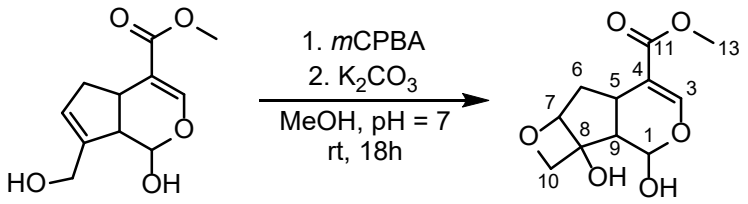

31

Genipin (1 g, 4.4 mmol) and *m*CPBA (0.91 g, 5.3mmol) were dissolved in 30 mL of MeOH with a drop of pH = 7 phosphate buffer and stirred at room temperature overnight. The reaction mixture was quenched with 5% K_2CO_3 until effervescence stopped. The product was extracted with EtOAc, dried over magnesium sulfate and solvent was removed *in vacuo*. The product was purified via column chromatography (3:1 DCM:EtOAc) yielding white needles (0.89 g, 70 %). ^{1}H NMR (400 MHz, MeOD) δ 7.32 (s, 1H, H3), 5.07 (s, 1H, H1), 4.34 (s, 1H, H7), 4.24 (d, *J* = 9.3 Hz, 1H, H6), 3.86 (d, *J* = 9.3 Hz, 1H, H6'), 3.68 (s, 3H, H13), 3.21 (t, *J* = 5.0 Hz, 1H, H5), 2.52 (d, *J* = 6.6 Hz, 1H, H9), 2.34 (ddd, *J* = 12.2, 4.3, 2.9 Hz, 1H, H6), 1.90 (d, *J* = 12.2 Hz, 1H, H6'). ^{13}C NMR (100 MHz, MeOD) δ 168.96 (C11), 155.76 (C3), 111.94 (C4), 100.11 (C1), 91.78 (C8), 85.22 (C7), 71.59 (C10), 69.07 (C9), 51.83 (C13), 34.47 (C5), 32.87 (C6). Expected m/z: 242.08. Found m/z: $[M+Na]^+$ = 265.07165 m/z

References

(1) Nassau, K. The Fifteen Causes of Color: The Physics and Chemistry of Color. *Color Res. Appl.* **1987**, *12* (1), 4–26.

(2) Croft, H.; Chen, J. M. Leaf Pigment Content. In *Comprehensive Remote Sensing*, Vol. 3; Liang, S., Chen Jing M., Eds.; Elsevier, 2017; pp 117–142.

(3) Sun, J.; Bhushan, B.; Tong, J. Structural Coloration in Nature. *RSC. Adv*. **2013**, *3*, 14862–14889.

(4) Newsome, A. G.; Culver, C. A.; van Breemen, R. B. Nature's Palette: The Search for Natural Blue Colorants. *J. Agric. Food Chem*. **2014**, *62* (28), 6498–6511.

(5) Basílio, N.; Pina, F. Chemistry and Photochemistry of Anthocyanins and Related Compounds: A Thermodynamic and Kinetic Approach. *Molecules*, **2016**, *21* (11), 1502.

(6) Takeda, K. Blue Metal Complex Pigments Involved in Blue Flower Color. *Proc. Jpn. Acad. Ser. B*. **2006**, *82*, 142–154.

(7) Paik, Y.-S.; Lee, C.-M.; Cho, M.-H.; Hahn, T.-R. Physical Stability of the Blue Pigments Formed from Geniposide of Gardenia Fruits: Effects of PH, Temperature, and Light. *J. Agric. Food Chem*. **2001**, *49*, 430–432.

(8) Jespersen, L.; Lene, ·; Strømdahl, D.; Olsen, K.; Skibsted, L. H. Heat and Light Stability of Three Natural Blue Colorants for Use in Confectionery and Beverages. *Eur. Food Res. Technol*. **2005**, *220*, 261–266.

(9) Kim, B. C.; Kim, H. G.; Lee, S. A.; Lim, S.; Park, E. H.; Kim, S. J.; Lim, C. J. Genipin-Induced Apoptosis in Hepatoma Cells Is Mediated by Reactive Oxygen Species/c-Jun NH2-Terminal Kinase-Dependent Activation of Mitochondrial Pathway. *Biochem. Pharmacol*. **2005**, *70* (9), 1398–1407.

(10) Kojima, K.; Shimada, T.; Nagareda, Y.; Watanabe, M.; Ishizaki, J.; Sai, Y.; Miyamoto, K.-I.; Aburada, M. Preventive Effect of Geniposide on Metabolic Disease Status in Spontaneously Obese Type 2 Diabetic Mice and Free Fatty Acid-Treated HepG2 Cells. *Biol. Pharm. Bull*. **2011**, *34* (10), 1613–1618.

(11) Akao, T.; Kobashi, K.; Aburada, M. Enzymatic Studies on the Animal and Intestinal Bacterial Metabolism of Geniposide. *Bio. Pharm. Bull*. **1994**, *17* (12), 1573–1576.

(12) Tsai, C.-C.; Huang, R.-N.; Sung, H.-W.; Liang, H. C. In Vitro Evaluation of the Genotoxicity of a Naturally Occurring Crosslinking Agent (Genipin) for Biologic Tissue Fixation. *J. Biomed. Mater. Res*. **2000**, *52* (1), 58–65.

(13) Yamamoto, M.; Miura, N.; Ohtake, N.; Amagaya, S.; Ishige, A.; Sasaki, H.; Komatsu, Y.; Fukuda, K.; Ito, T.; Terasawa, K. Genipin, a Metabolite Derived From the Herbal Medicine Inchin-Ko-to, and Suppression of Fas-Induced Lethal Liver Apoptosis in Mice. *Gastroenterology* **2000**, *118*, 380–389.

(14) Zhang, C. Y.; Parton, L. E.; Ye, C. P.; Krauss, S.; Shen, R.; Lin, C. T.; Porco, J. A.; Lowell, B. B. Genipin Inhibits UCP2-Mediated Proton Leak and Acutely Reverses Obesity- and High

Glucose-Induced β Cell Dysfunction in Isolated Pancreatic Islets. *Cell Metab*. **2006**, *3* (6), 417–427.

(15) Qiu, W.; Zhou, Y.; Jiang, L.; Fang, L.; Chen, L.; Su, W.; Tan, R.; Zhang, C. yu; Han, X.; Yang, J. Genipin Inhibits Mitochondrial Uncoupling Protein 2 Expression and Ameliorates Podocyte Injury in Diabetic Mice. *PLoS One* **2012**, *7* (7), 41391.

(16) Shanmugam, M. K.; Shen, H.; Tang, F. R.; Arfuso, F.; Rajesh, M.; Wang, L.; Kumar, A. P.; Bian, J.; Goh, B. C.; Bishayee, A.; Sethi, G. Potential Role of Genipin in Cancer Therapy. *Pharmacol. Res.* **2018**, *133*, 195–200.

(17) Moura, M. J.; Margarida Figueiredo, M.; Gil, M. H. Rheological Study of Genipin Cross-Linked Chitosan Hydrogels. *Biomacromolecules* **2007**, *8*, 3823–3829.

(18) Ninh, C.; Iftikhar, A.; Cramer, M.; Bettinger, C. J. Diffusion-Reaction Models of Genipin Incorporation into Fibrin Networks. *J. Mater. Chem. B* **2015**, *3* (22), 4607–4615.

(19) Touyama, R.; Takeda, Y.; Inoue, K.; Kawamura, Ik.; Yatsuzuka, M.; Ikumoto, T.; Shingu, T.; Yokoi, T.; Inouye, H. Studies on the Blue Pigments Produced from Genipin and Methylamine. I. Structures of the Brownish-Red Pigments, Intermediates Leading to the Blue Pigments. *Chem. Pharm. Bull.* **1994**, *42* (3), 668–673.

(20) Touyama, R.; Inoue, K.; Takeda, Y.; Yatsuzuka, M.; Ikumoto, T.; Moritome, N.; Shingu, T.; Yokoi, T.; Inouye, H. Studies on the Blue Pigments Produced from Genipin and Methylamine. II. On the Formation Mechanisms of Brownish-Red Intermediates Leading to the Blue Pigment Formation. *Chem. Pharm. Bull*. **1994**, *42* (8), 1571–1578.

(21) Handley, T. J.; Handley, B.; Caputo, C. B.; Zrehen, A. M. Body Ink Compositions and Applicators. US20160367460A1, December 22, 2016.

(22) Cho, Y. J.; Kim, S. Y.; Kim, J.; Choe, E. K.; Kim, S. I.; Shin, H. J. One-Step Enzymatic Synthesis of Blue Pigments from Geniposide for Fabric Dyeing. *Biotechnol. Bioprocess Eng*. **2006**, *11* (3), 230–234.

(23) Fujikawa, S.; Fukui, Y.; Koga, K.; Iwashita, T.; Komura, H.; Nomoto, K. Structure of Genipocyanin G1, a Spontaneous Reaction Product between Genipin and Glycine. *Tetrahedron Lett.* **1987**, *28* (40), 4699–4700.

(24) Butler, M. F.; Ng, Y.-F.; Pudney, P. D. A. Mechanism and Kinetics of the Crosslinking Reaction between Biopolymers Containing Primary Amine Groups and Genipin. *J. Polym. Sci., Part A: Polym. Chem.* **2003**, *41*, 3941–3953.

(25) Zhu, Y.; Chan-Park, M. B. Density Quantification of Collagen Grafted on Biodegradable Polyester: Its Application to Esophageal Smooth Muscle Cell. *Anal. Biochem.* **2007**, *363* (1), 119–127.

(26) Park, J.-E.; Lee, J.-Y.; Kim, H.-G.; Hahn, T.-R.; Paik, Y.-S. Isolation and Characterization of Water-Soluble Intermediates of Blue Pigments Transformed from Geniposide of Gardenia Jasminoides. *J. Agric. Food Chem*. **2002**, *50* (22), 6511–6514.

(27) Di Tommaso, S.; David, P.; Picolet, K.; Gabant, M.; David, H.; Morançais, J.-L.; Gomar, J.; Leroy, F.; Adamo, C. Structure of Genipin in Solution: A Combined Experimental and Theoretical Study. *RSC Adv*. **2013**, *3* (33), 13764.

(28) Tommaso, S. Di; Hervé, D.; Gomar, J.; Leroy, F.; Adamo, C. From Iridoids to Dyes: A Theoretical Study on Genipin Reactivity. *RSC Adv*. **2014**, *4*, 11029–11038.

(29) Heeger, A. J. Semiconducting and Metallic Polymers: The Fourth Generation of Polymeric Materials. *J. Phys. Chem. B*, **2001**, *105* (36), 8475–8491.

(30) Nezakati, T.; Seifalian, A.; Tan, A.; Seifalian, A. M. Conductive Polymers: Opportunities and Challenges in Biomedical Applications. *Chem. Rev.* **2018**, *118*, 6766–6843

(31) Cherrington, R.; Liang, J. Materials and Deposition Processes for Multifunctionality. In *Design and Manufacture of Plastic Components for Multifunctionality: Structural Composites, Injection Molding, and 3D Printing*; Elsevier Inc., 2016; pp 19–51.

(32) Zuliani, C.; Curto, V. F.; Matzeu, G.; Fraser, K. J.; Diamond, D. Properties and Customization of Sensor Materials for Biomedical Applications. In *Comprehensive Materials Processing*, Vol 13; Elsevier Ltd, 2014; pp 221–243.

(33) Simya, O. K.; Radhakrishnan, P.; Ashok, A.; Kavitha, K.; Althaf, R. Engineered Nanomaterials for Energy Applications. In *Handbook of Nanomaterials for Industrial Applications*; Elsevier, 2018; pp 751–767.

(34) Schwarz, A.; Van Langenhove, L. Types and Processing of Electro-Conductive and Semiconducting Materials for Smart Textiles. In *Multidisciplinary Know-How for Smart-Textiles Developers*; Elsevier Ltd, 2013; pp 29–69.

(35) Tang, S.; Irgum, K.; Edman, L. Chemical Stabilization of Doping in Conjugated Polymers. *Org. Electron*. **2010**, *11* (6), 1079–1087.

(36) Letheby, H. On the Production of a Blue Substance by the Electrolysis of Sulphate of Aniline. *J. Chem. Soc*. **1862**, *15* (0), 161–163.

(37) Tarver, J.; Loo, Y.-L. Polyanilines. In *Conjugated Polymers: A Practical Guide to Synthesis*; Müllen, K., Reynolds, J. R., Masuda, T., Eds.; Polymer Chemistry Series; Royal Society of Chemistry: Cambridge, 2013; pp 248–264.

(38) MacDiarmid, A. G.; Chiang, J. C.; Richter, A. F.; Somasiri, N. L. D.; Epstein, A. J. Polyaniline: Synthesis and Characterization of the Emeraldine Oxidation State by Elemental Analysis. In *Conducting Polymers*; Springer Netherlands, 1987; pp 105–120.

(39) Bhadra, S.; Khastgir, D.; Singha, N. K.; Lee, J. H. Progress in Preparation, Processing and Applications of Polyaniline. *Prog. Polym. Sci*. **2009**, *34* (8), 783–810.

(40) Canales, M.; Torras, J.; Fabregat, G.; Meneguzzi, A.; Alemán, C. Polyaniline Emeraldine Salt in the Amorphous Solid State: Polaron versus Bipolaron. *J. Phys. Chem. B,* **2014**, *118* (39), 11552–11562.

(41) Huang, W. S.; Macdiarmid, A. G. Optical Properties of Polyaniline. *Polymer*, **1993**, *34* (9), 1833–1845.

(42) Karaoğlan, N.; Bindal, C. Synthesis and Optical Characterization of Benzene Sulfonic Acid Doped Polyaniline. *Eng. Sci. Technol. an Int. J*. **2018**, *21* (6), 1152–1158.

(43) Sweeney, T. E.; Beuchat, C. A. Limitations of Methods of Osmometry: Measuring the Osmolality of Biological Fluids. *Am. J. Physiol*. **1993**, *264* (3), R469–R480.

(44) Ge, Y.; Isoe, S. An Efficient Synthesis of Cerbinal, a 10 π Aromatic Iridoid. *Chem. Lett*. **1992**, *21*(1), 139–140.

(45) Xia, Q.; Dong, J.; Li, L.; Wang, Q.; Liu, Y.; Wang, Q. Discovery of Glycosylated Genipin Derivatives as Novel Antiviral, Insecticidal, and Fungicidal Agents. *J. Agric. Food Chem*. **2018**, *66* (6), 1341–1348.

(46) Fang, J.; Huang, T.; Xia, M.; Deng, L.; Hao, X.; Wang, Y.; Mu, S. Design and Synthesis of Novel Monoterpenoid Indole Alkaloid-like Analogues and Their Antitumour Activities in Vitro. Org. *Biomol. Chem* **2018**, *16*, 3026–3037.

(47) Tarzia, A.; Montanaro, J.; Casiello, M.; Annese, C.; Nacci, A.; Maffezzoli, A. Synthesis, Curing, and Properties of an Epoxy Resin Derived from Gallic Acid. *Bioresources* **2018**, *13* (1), 632–645.

(48) Bull, J. A.; Croft, R. A.; Davis, O. A.; Doran, R.; Morgan, K. F. Oxetanes: Recent Advances in Synthesis, Reactivity, and Medicinal Chemistry. *Chem. Rev.* **2016**, *116* (19), 12150–12233.

(49) Payne, G. B. Epoxide Migrations with a, ß-Epoxy Alcohols. *J. Org. Chem.* **1962**, *27*(11), 3719–3822.

(50) Hanson, R. M. Epoxide Migration (Payne Rearrangement) and Related Reactions. In *Organic Reactions*; John Wiley & Sons, Inc., 2002; pp 1–156.

(51) Dua, S.; Taylor, M. S.; Buntine, M. A.; Bowie, J. H. The Degenerate Payne Rearrangement of the 2,3-Epoxypropoxide Anion in the Gas Phase. A Joint Theoretical and Experimental Study. *J. Chem. Soc., Perkin Trans. 2*, **1997**, *11*, 1991–1997.

(52) Dua, S.; Bowie, J. H.; Taylor, M. S.; Buntine, M. A. The Gas Phase Payne Rearrangement. Part 2. Methyl Substitution: A Joint Ab Initio and Experimental Study. *Int. J. Mass Spectrom. Ion Process*. **1997**, *165–166*, 139–153.

(53) Picard, P.; Leclercq, D.; Bats, J. P.; Moulines, J. An Efficient One-Pot Synthesis of Oxetanes from 1,3-Diols. *Synth.* **1981**, *1981* (7), 550–551.

(54) Dussault, P. H.; Trullinger, T. K.; Noor-e-Ain, F. Opening of Substituted Oxetanes with H2O2 and Alkyl Hydroperoxides: Stereoselective Approach to 3-Peroxyalcohols and 1,2,4-Trioxepanes. *Org. Lett.* **2002**, *4* (26), 4591–4593.

(55) Loertscher, B. M.; Zhang, Y.; Castle, S. L. Exploration of an Epoxidation-Ring-Opening Strategy for the Synthesis of Lyconadin A and Discovery of an Unexpected Payne Rearrangement. Beilstein *J. Org. Chem.* **2013**, *9*, 1179–1184.

(56) Patil, S. P.; Pandit, P.; Laddha, K. S. Eco-Friendly Single Bath Dyeing and Ultraviolet Protective Finishing of Proteinous Fabric Using Loganin Derived Blue Dye. *J. Nat. Fibers*, **2019**, *17* (12), 1748–1756.

Appendix (Figures)

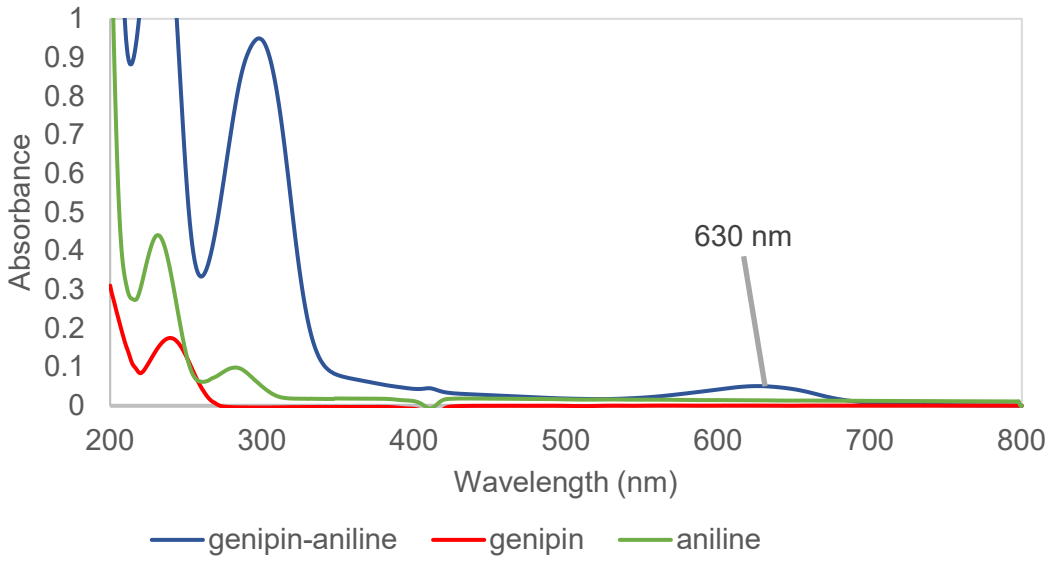

Figure A1. UV-Vis spectra of 0.025 mM genipin, aniline and **17**

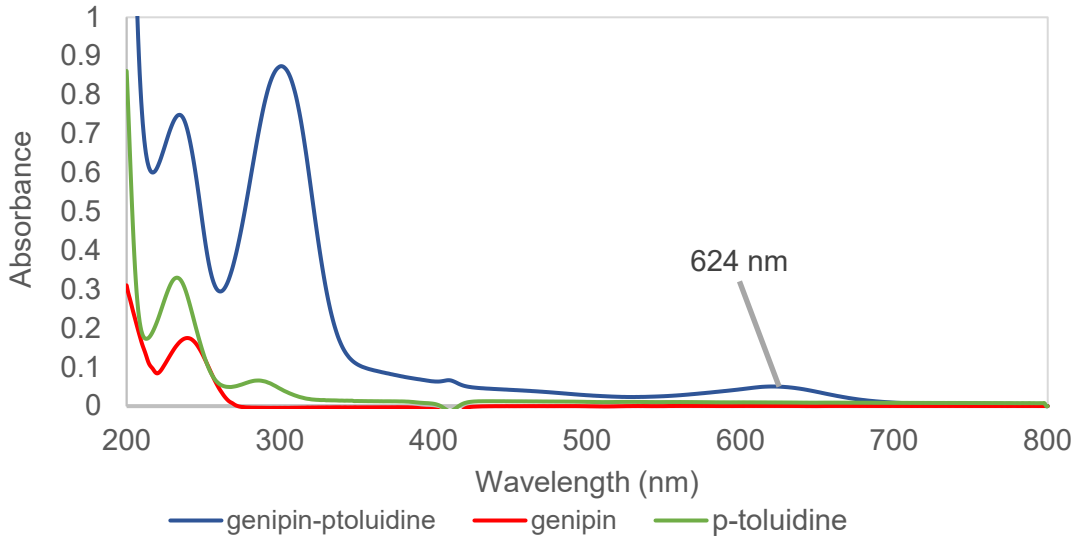

Figure A2. UV-Vis spectra of 0.025 mM genipin, p-toluidine and **18**

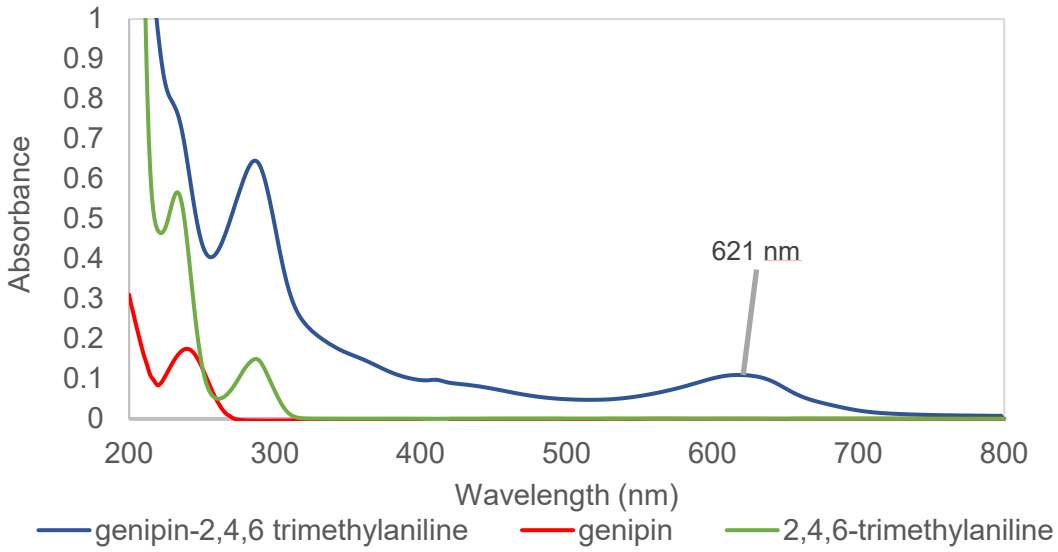

Figure A3. UV-Vis spectra of 0.025 mM genipin, 2,4,6-trimethylaniline and **19**

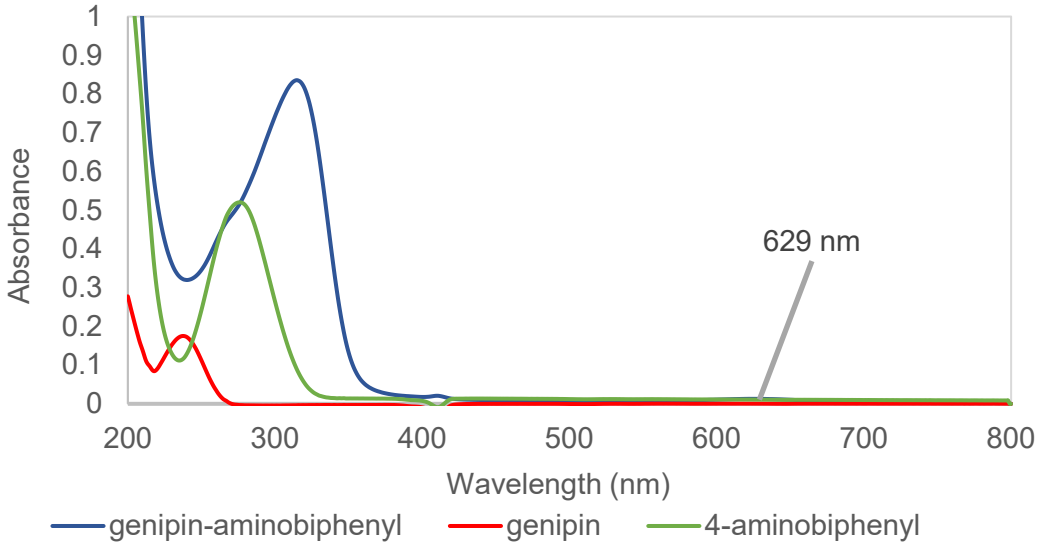

Figure A4. UV-Vis spectra of 0.025 mM genipin, 4-aminobiphenyl and **21**

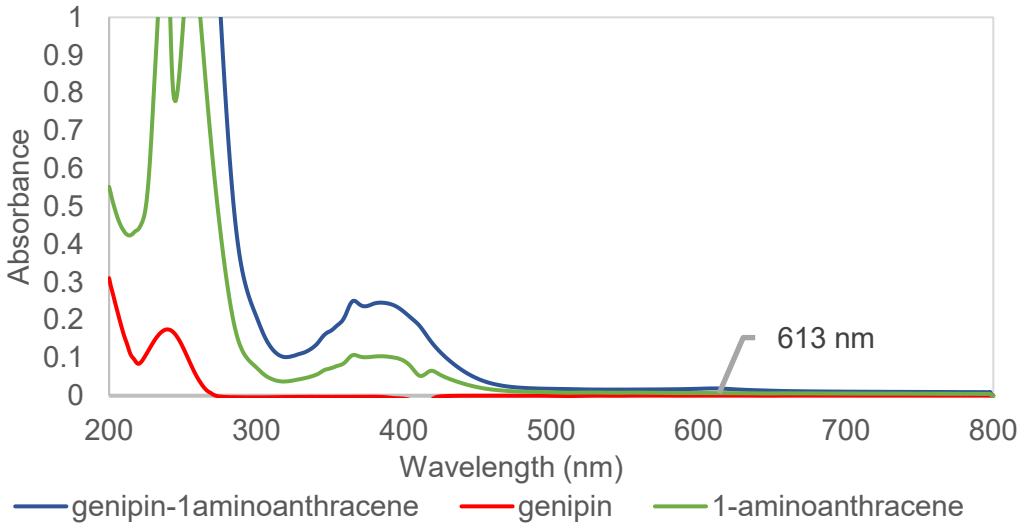

Figure A5. UV-Vis spectra of 0.025 mM genipin, 1-aminoanthracene and **22**

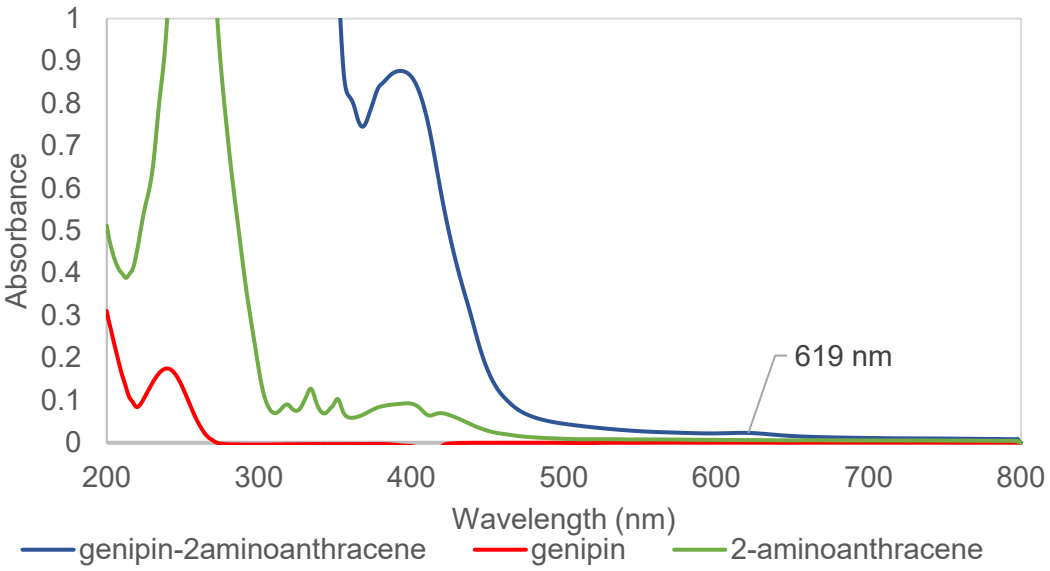

Figure A6. UV-Vis spectra of 0.025 mM genipin, 2-aminoanthracene and **23**

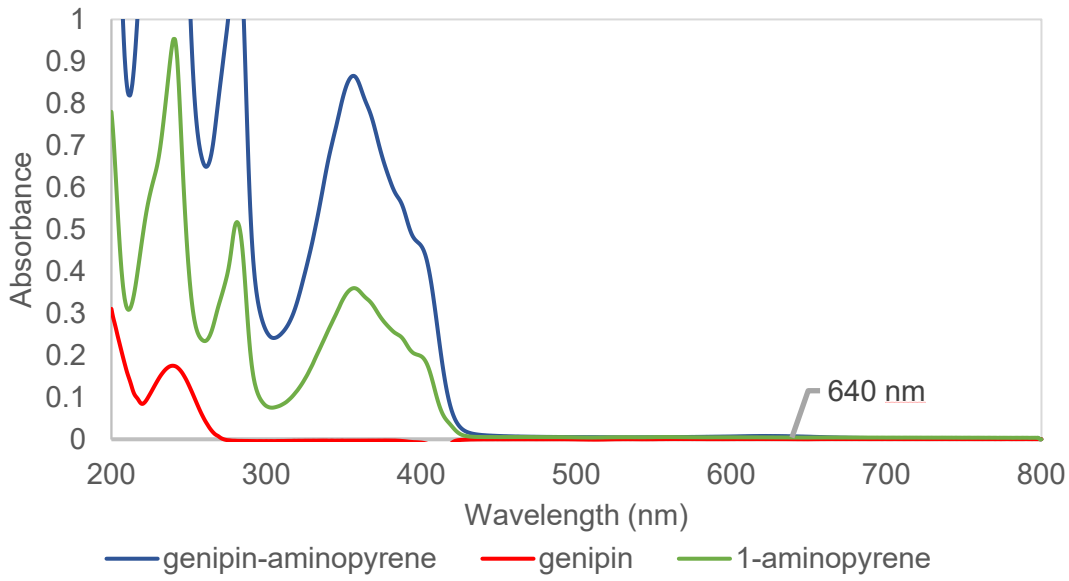

Figure A7. UV-Vis spectra of 0.025 mM genipin, 1-aminopyrene and **24**

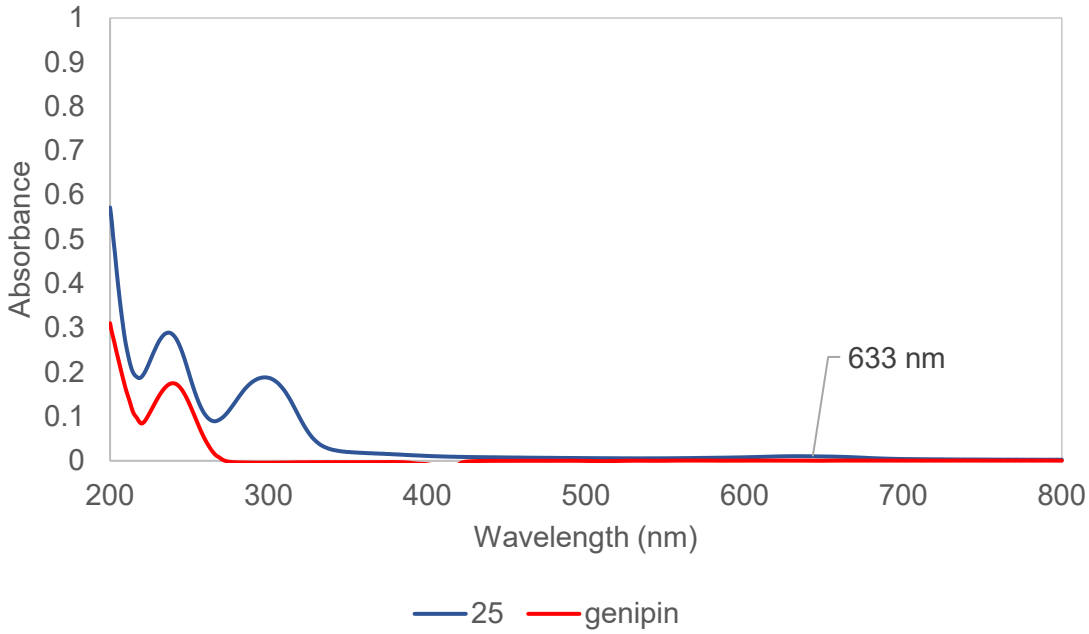

Figure A8. UV-Vis spectra of 0.025 mM genipin and **25**

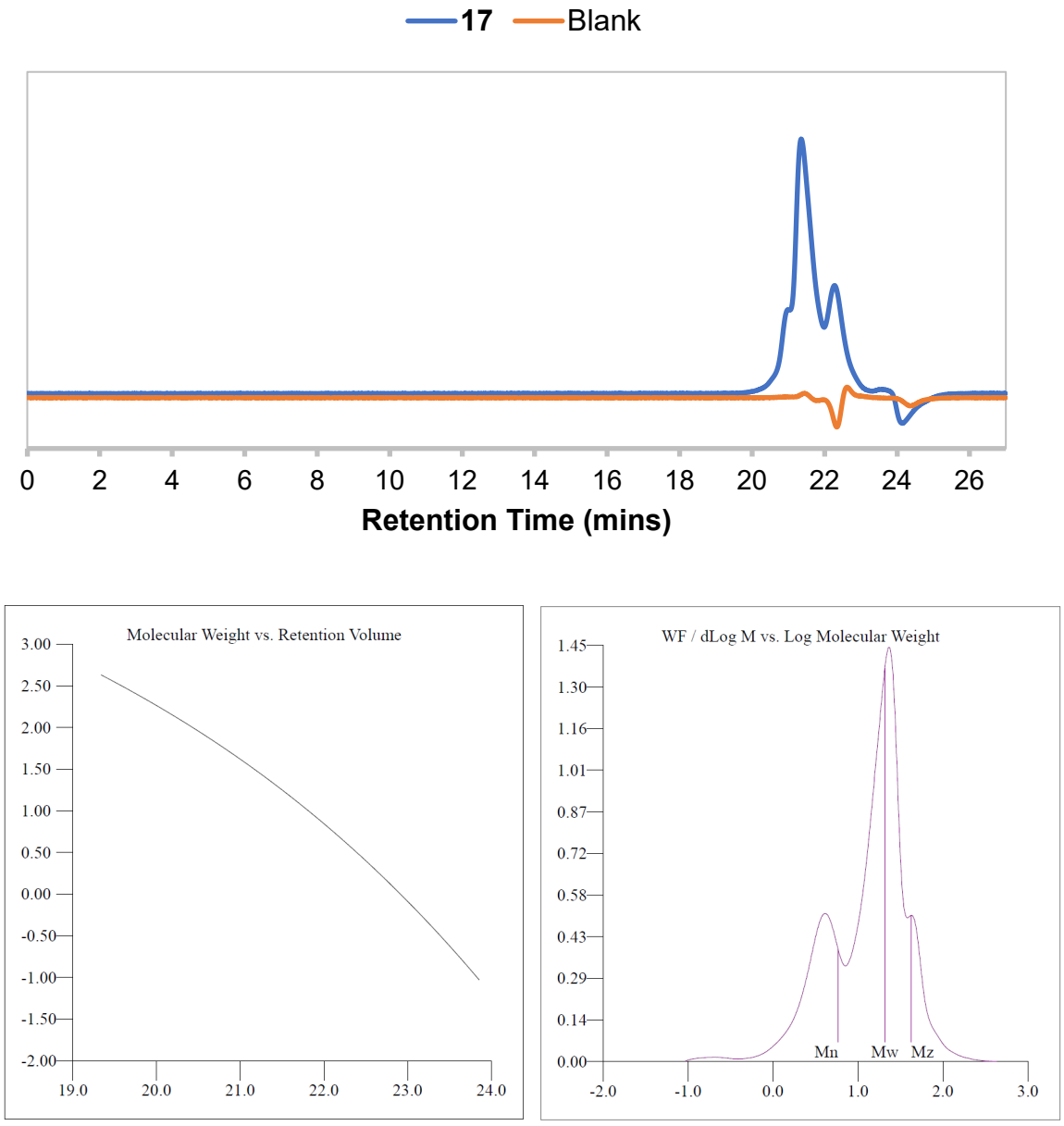

Figure A9. GPC data for **17**

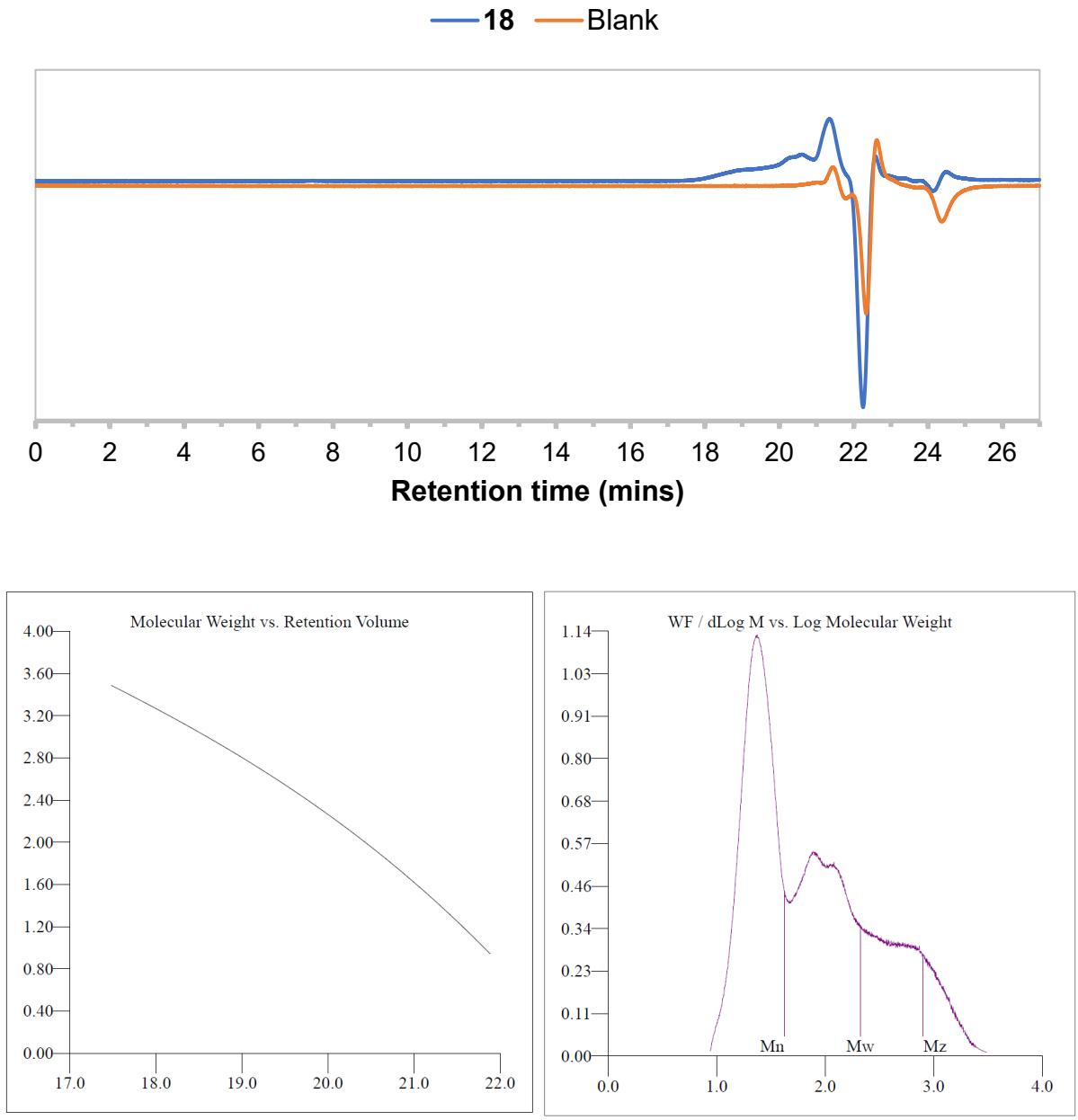

Figure A10. GPC data for **18**

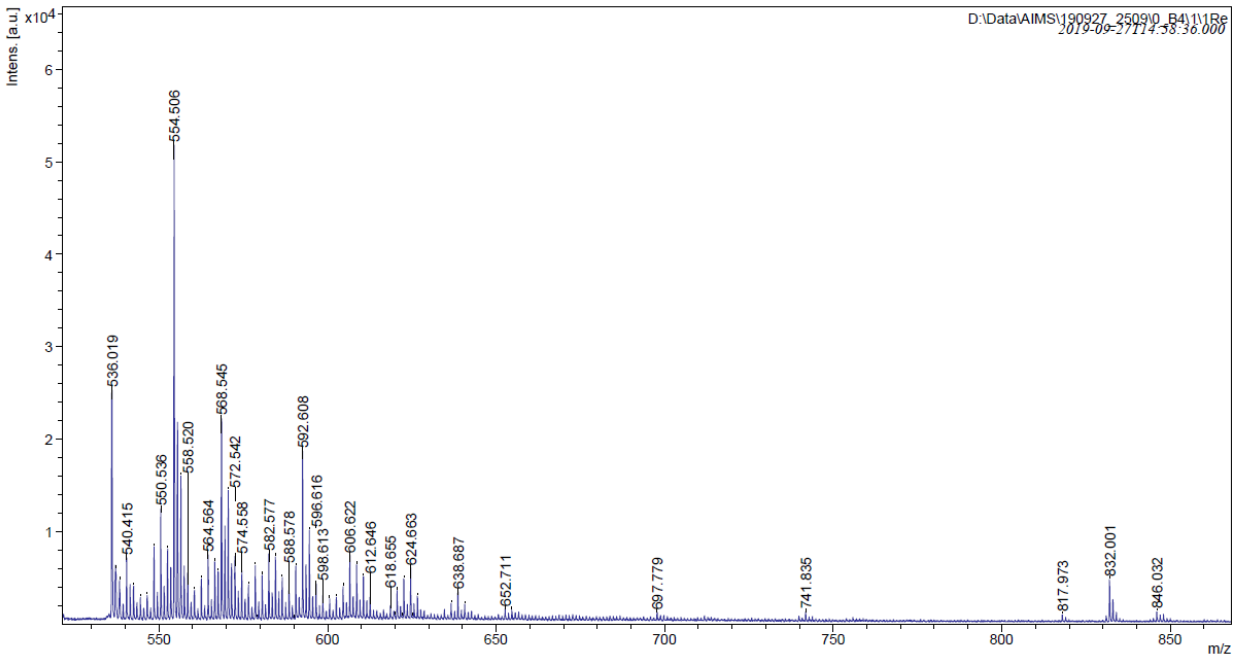

Figure A11. MALDI-TOF of 27. 832.001 m/z – **27** tetramer

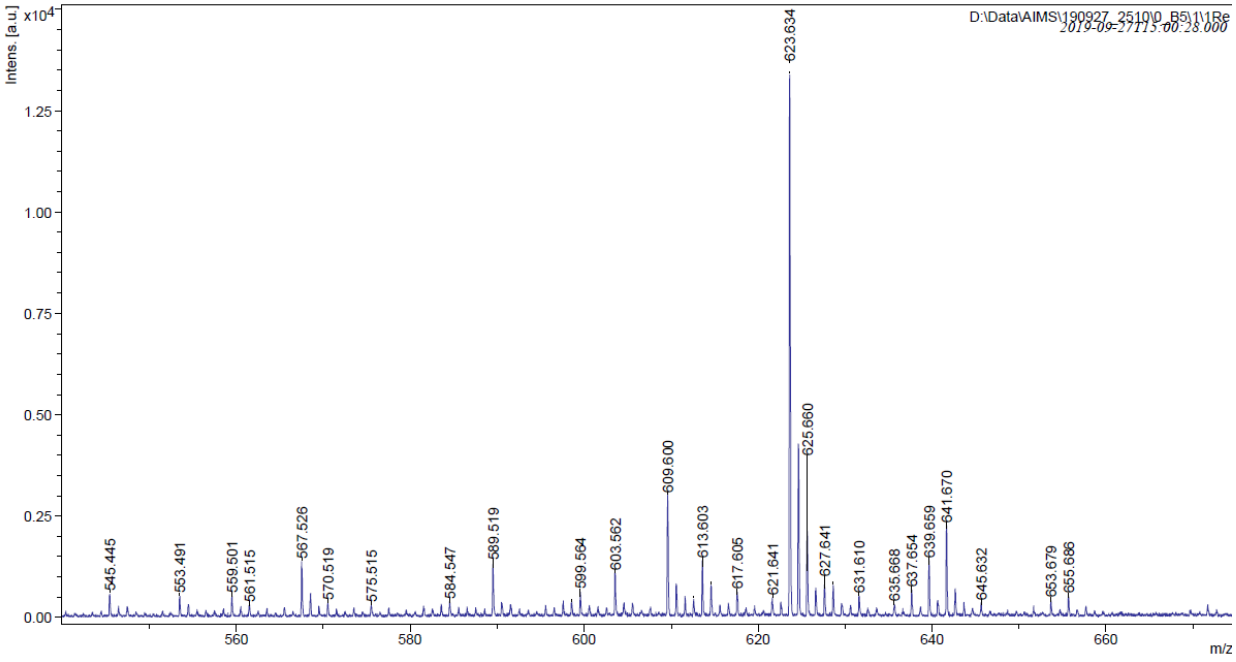

Figure A12. MALDI-TOF of **28**

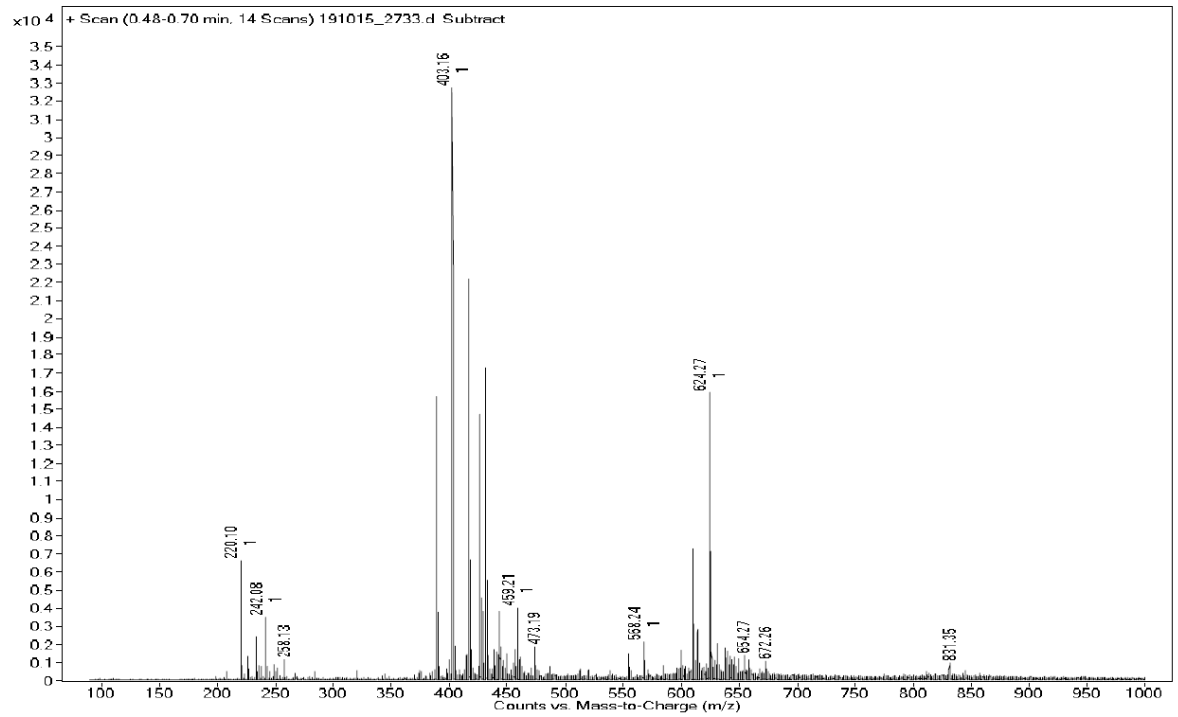

Figure A13. ESI-MS in positive mode of **27**. 831.35 m/z – **27** tetramer, 624.271 m/z –**27** trimer $[M+H]^+$, 403.161 m/z – **27** dimer $[M+H]^+$, 220.101 m/z – **27** monomer $[M+H]^+$.

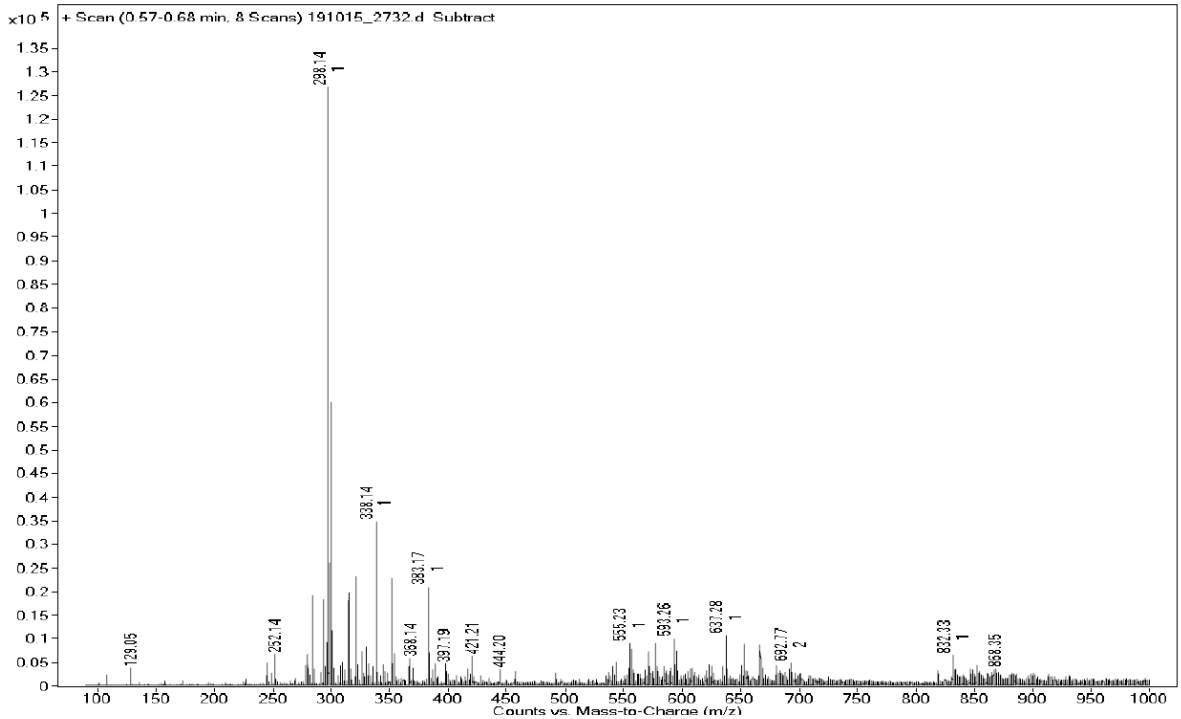

Figure A14. ESI-MS in positive mode of **28**. 832.331 m/z – **28** trimer $[M+H]^+$, 555.231 m/z – **28** dimer $[M+H]^+$, 298.141 m/z – **28** monomer $[M+H]^+$.

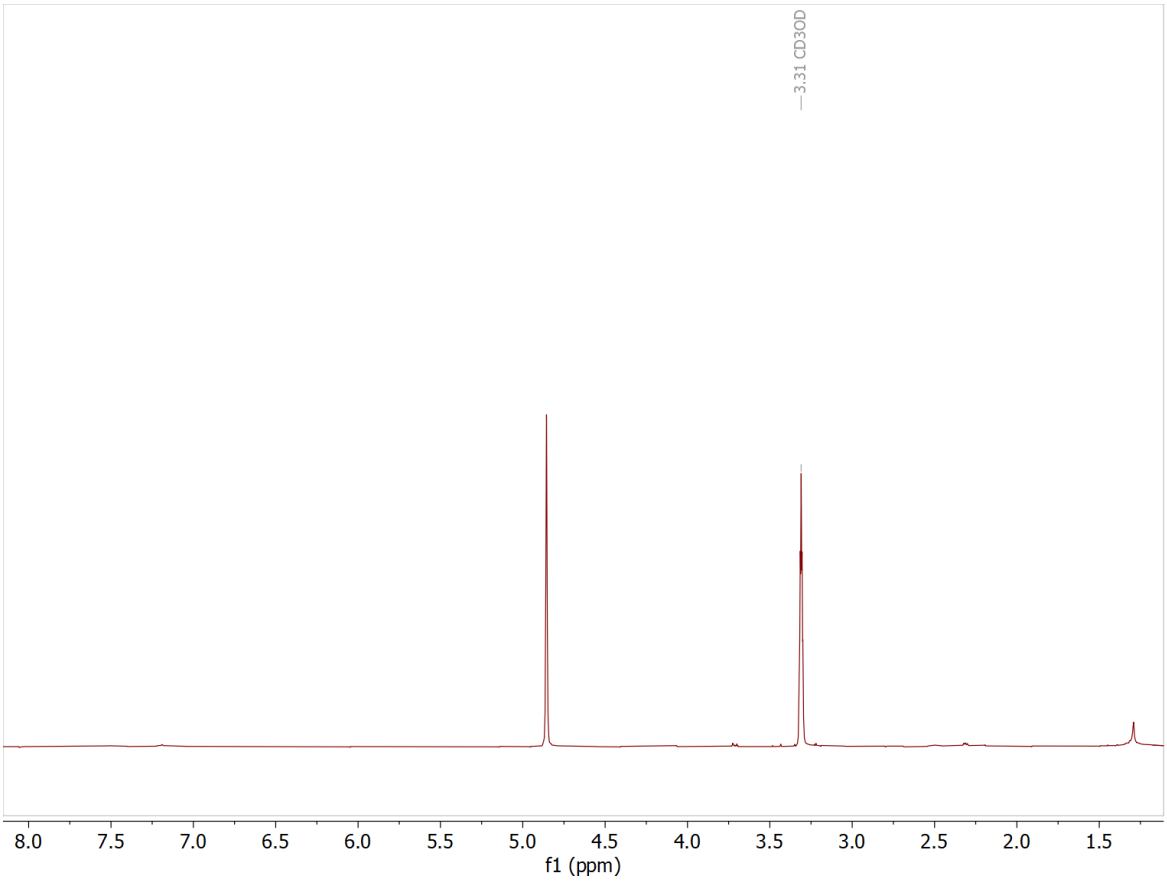

Figure A15. ^{1}H NMR spectrum of the purified green **28** in MeOD.

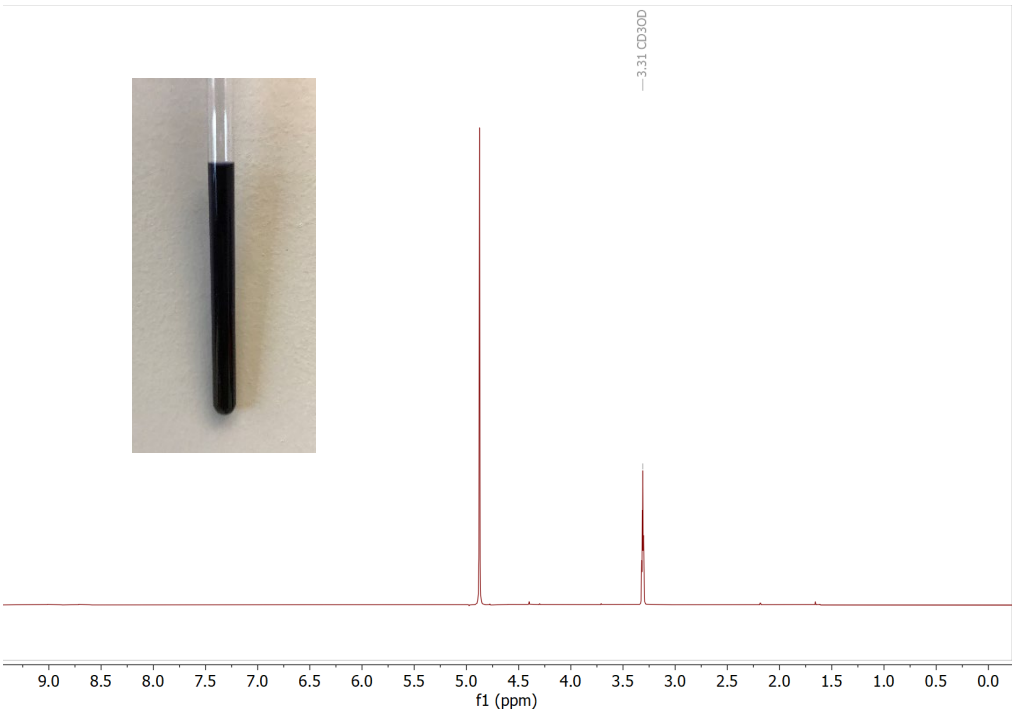

Figure A16. ^{1}H NMR spectrum of **27** from aqueous phase in MeOD. Inset: Sample in NMR tube

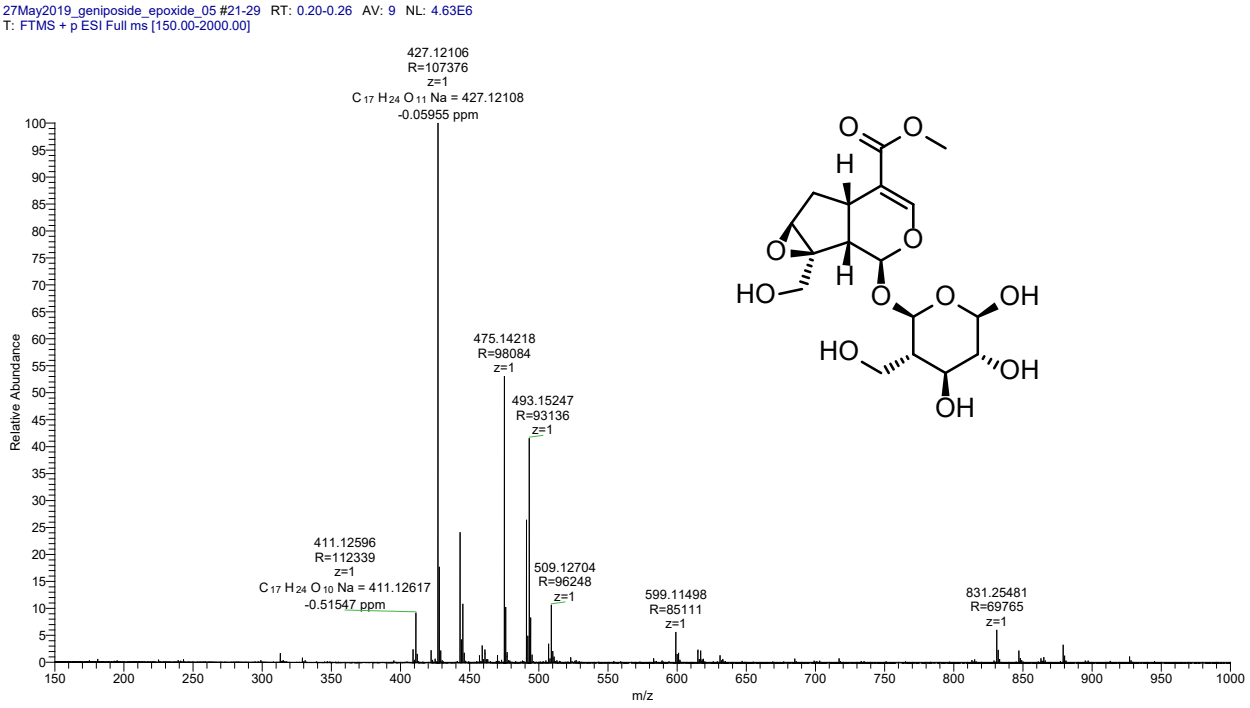

Figure A17. ESI-MS in positive mode of **30**. 427.1206 m/z – **30** $[M+Na]^{+}$

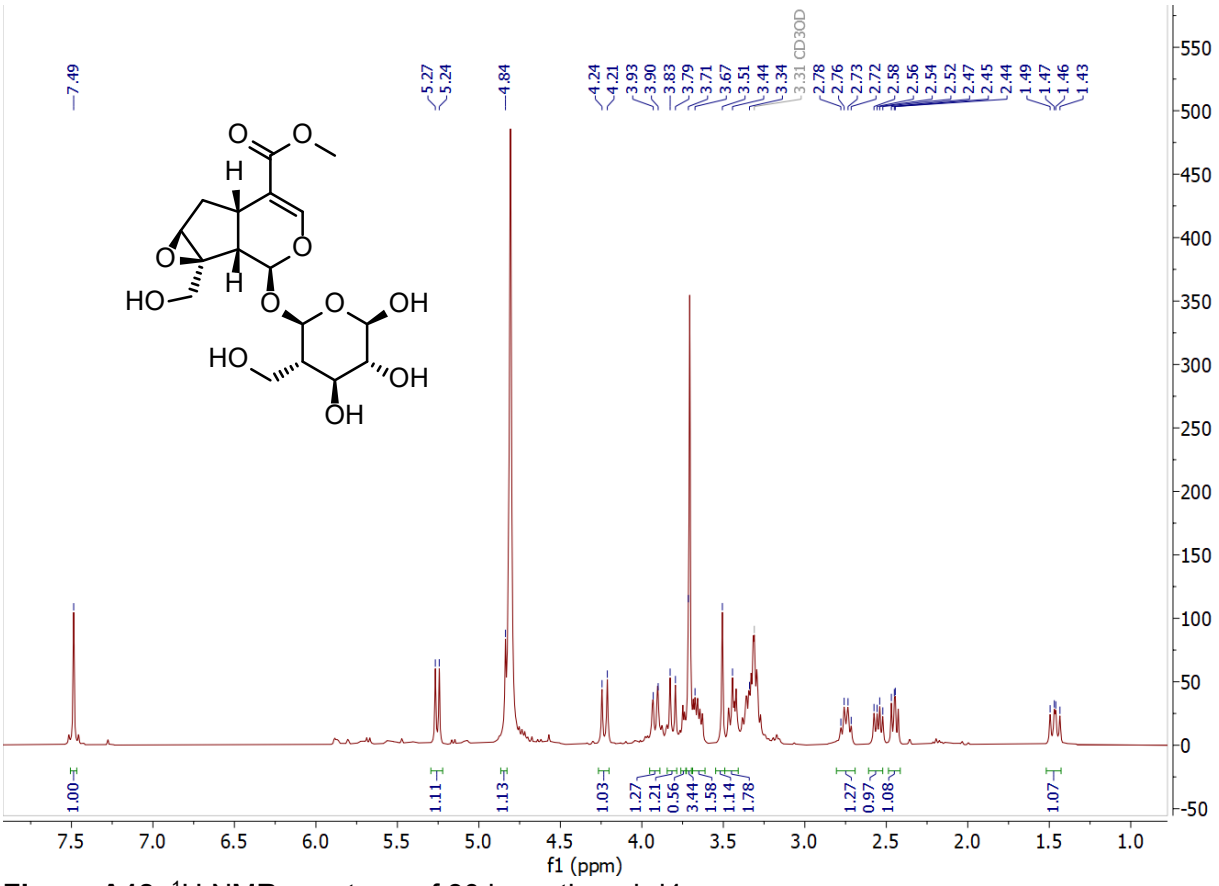

Figure A18. ^{1}H NMR spectrum of **30** in methanol-d4.

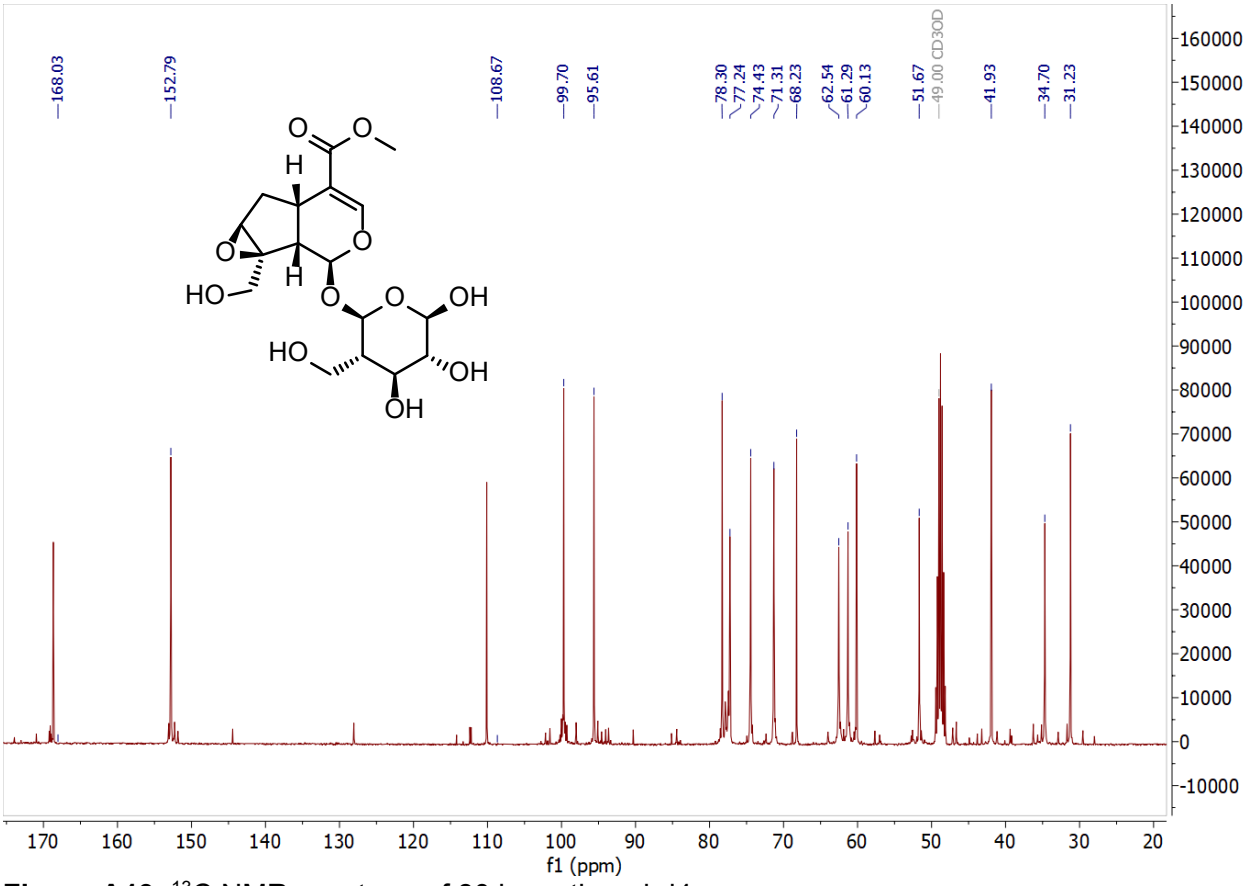

Figure A19. ^{13}C NMR spectrum of **30** in methanol-d4.

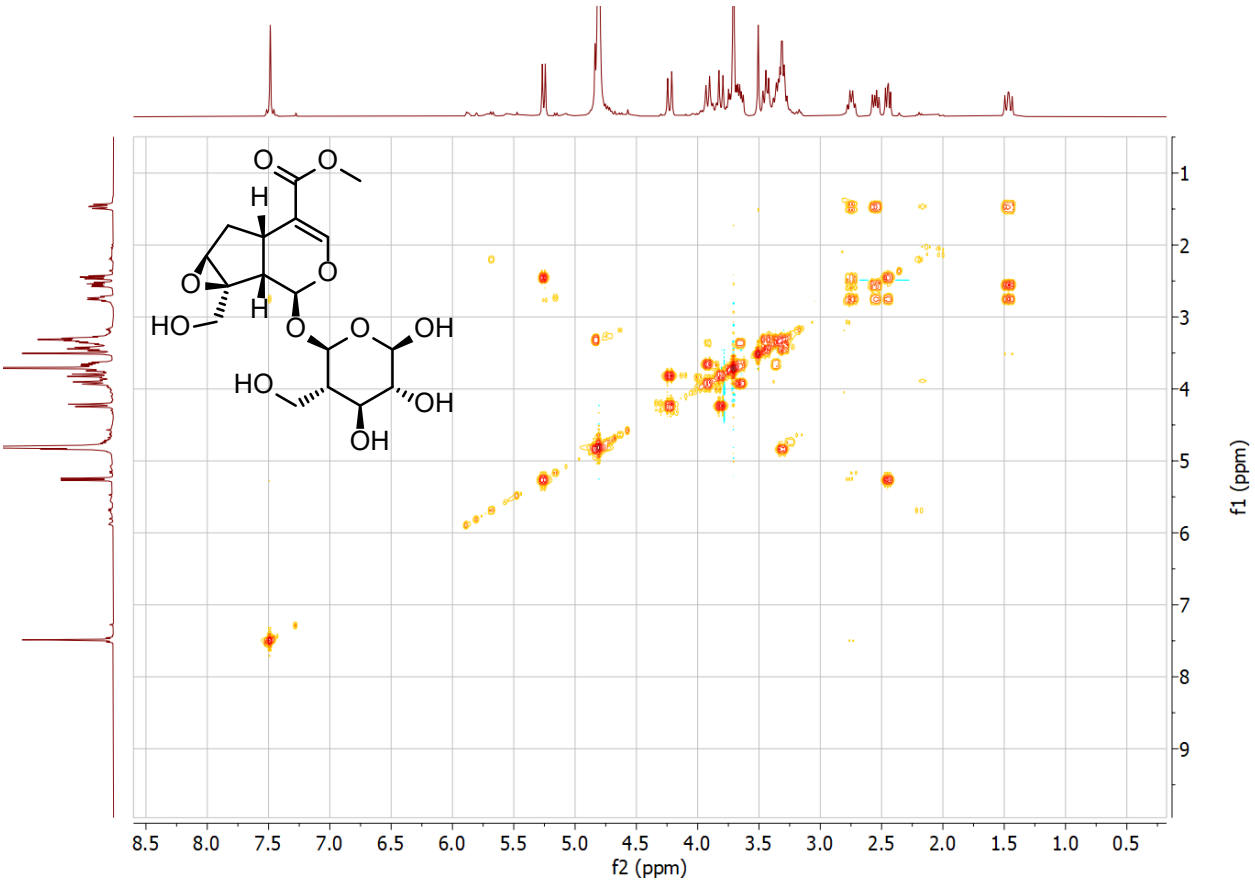

Figure A20. ^{1}H-^{1}H 2D COSY spectrum of **30** in methanol-d4.

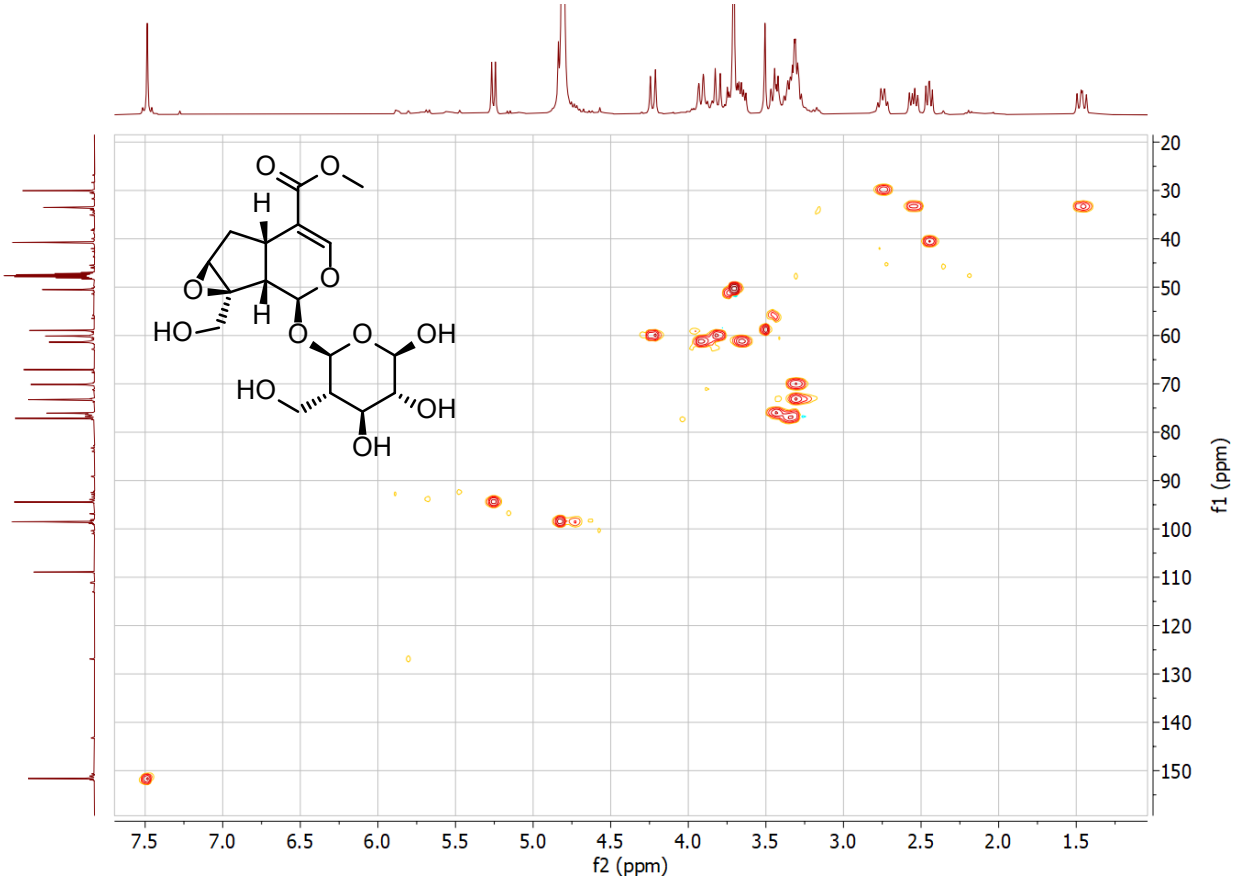

Figure A21. ^{1}H-^{13}C 2D HSQC spectrum of **30** in methanol-d4.

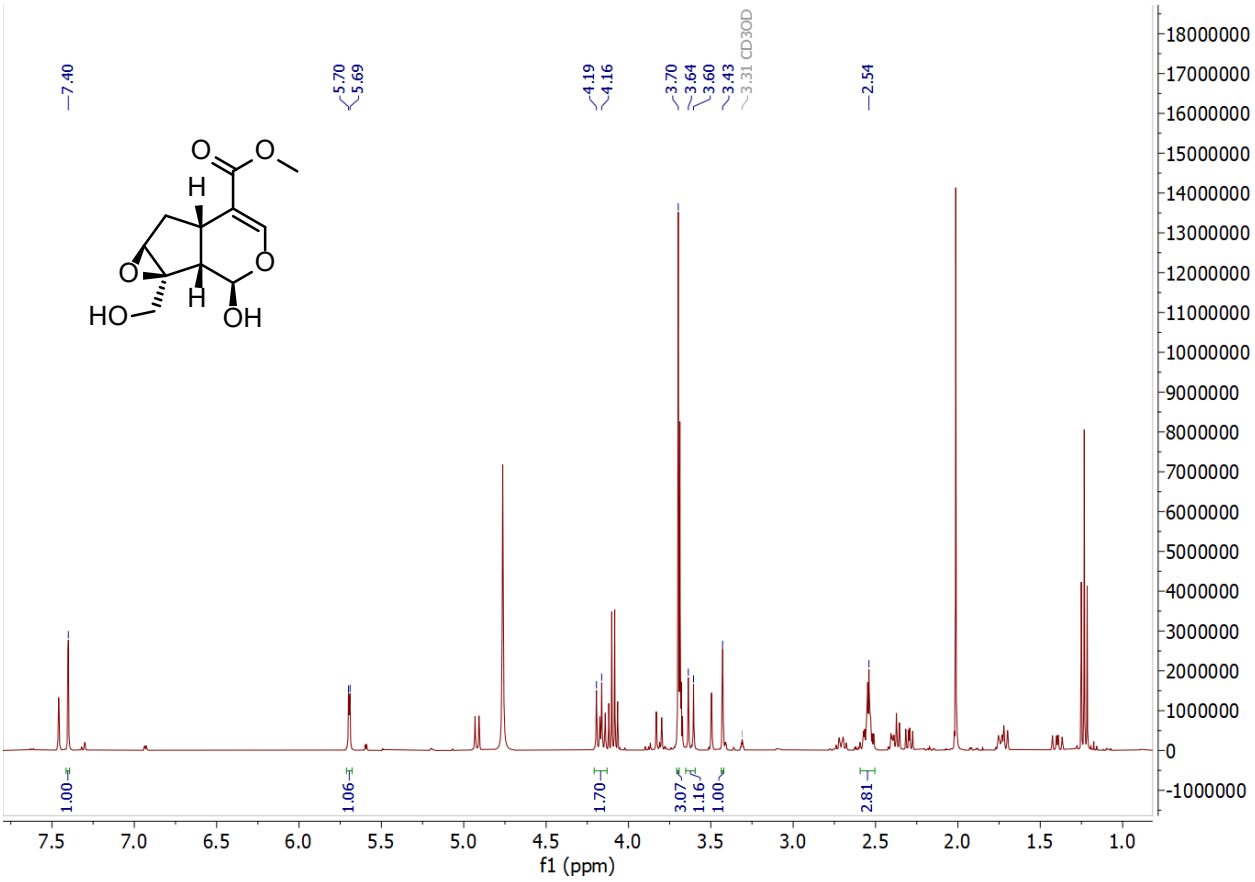

Figure A22. ^{1}H NMR spectrum of **30a** in methanol-d4.

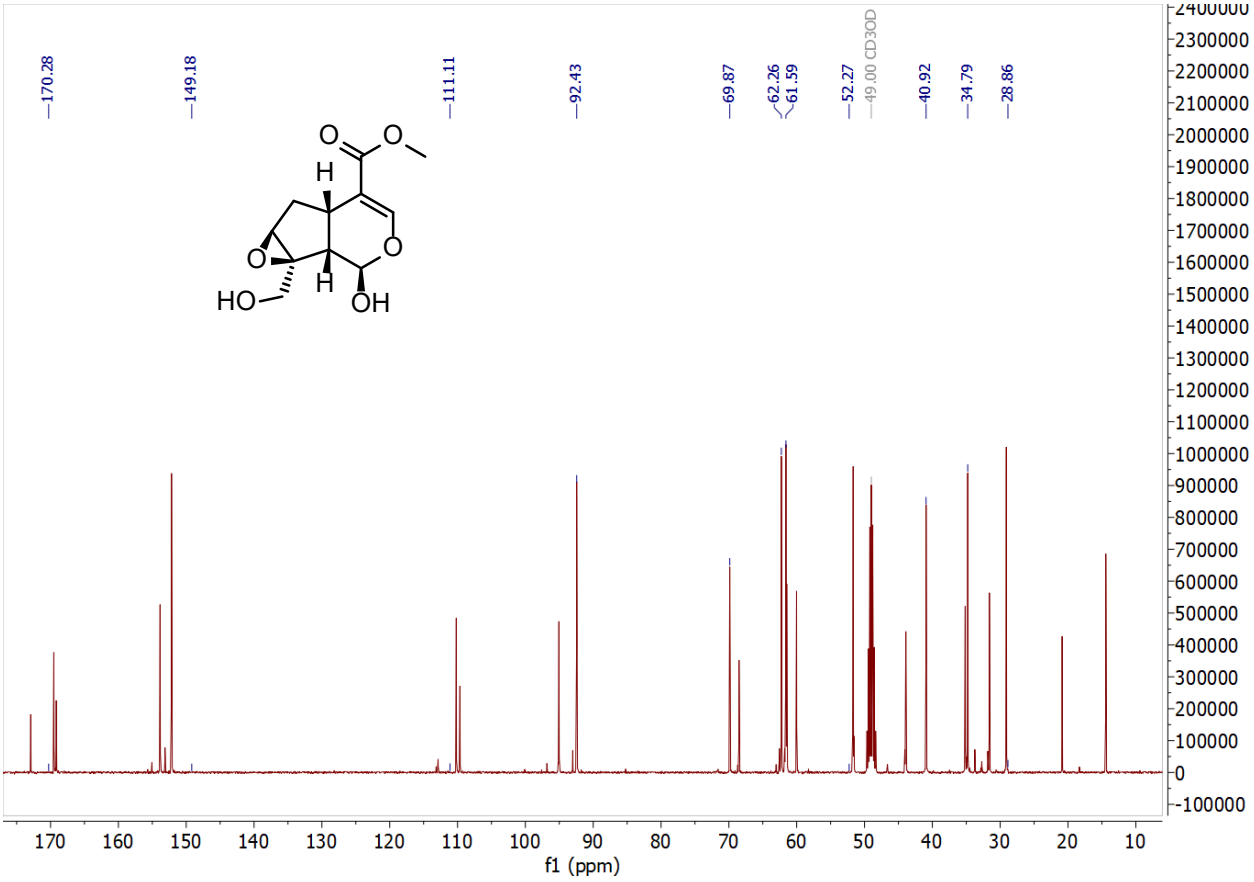

Figure A23. ^{13}C NMR spectrum of **30a** in methanol-d4.

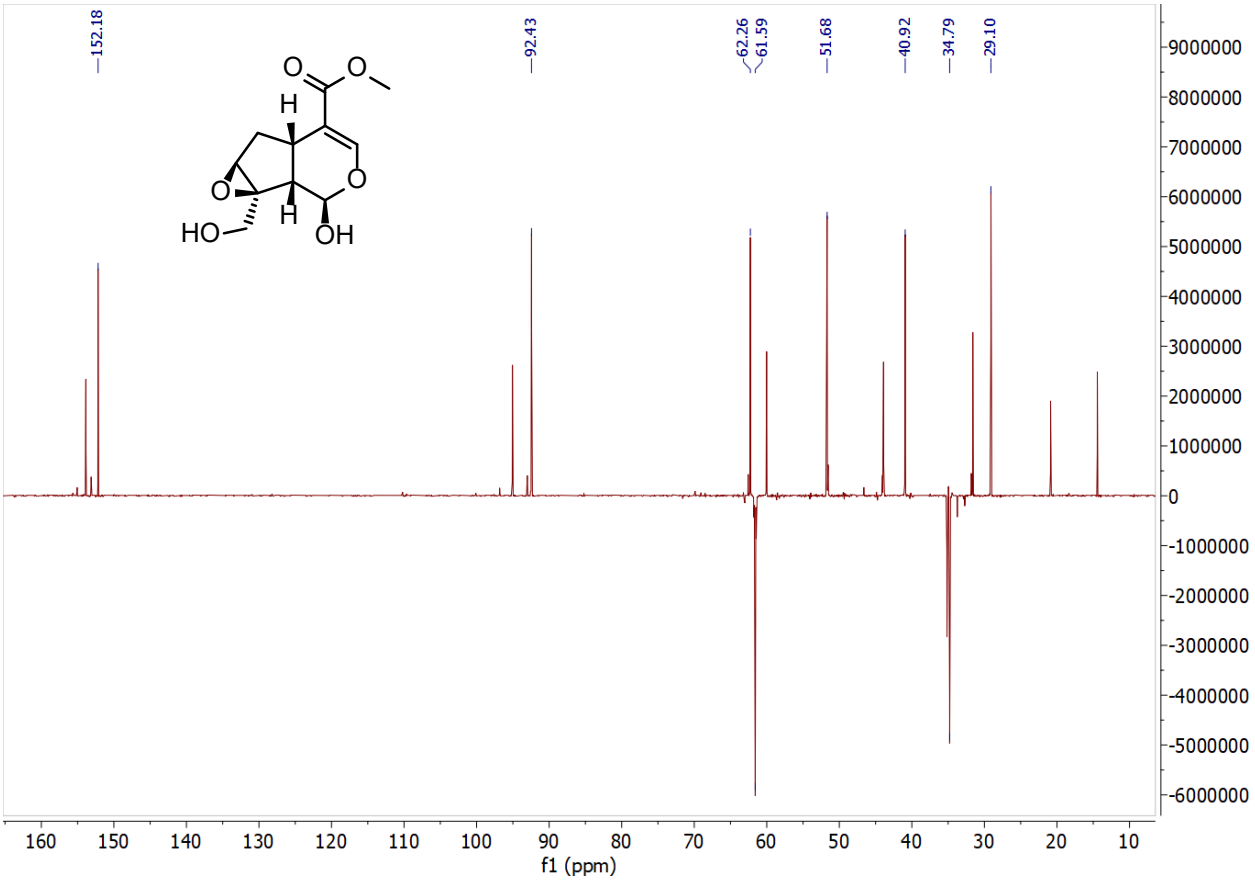

Figure A24. ^{13}C DEPT-135 NMR spectrum of **30a** in methanol-d4.

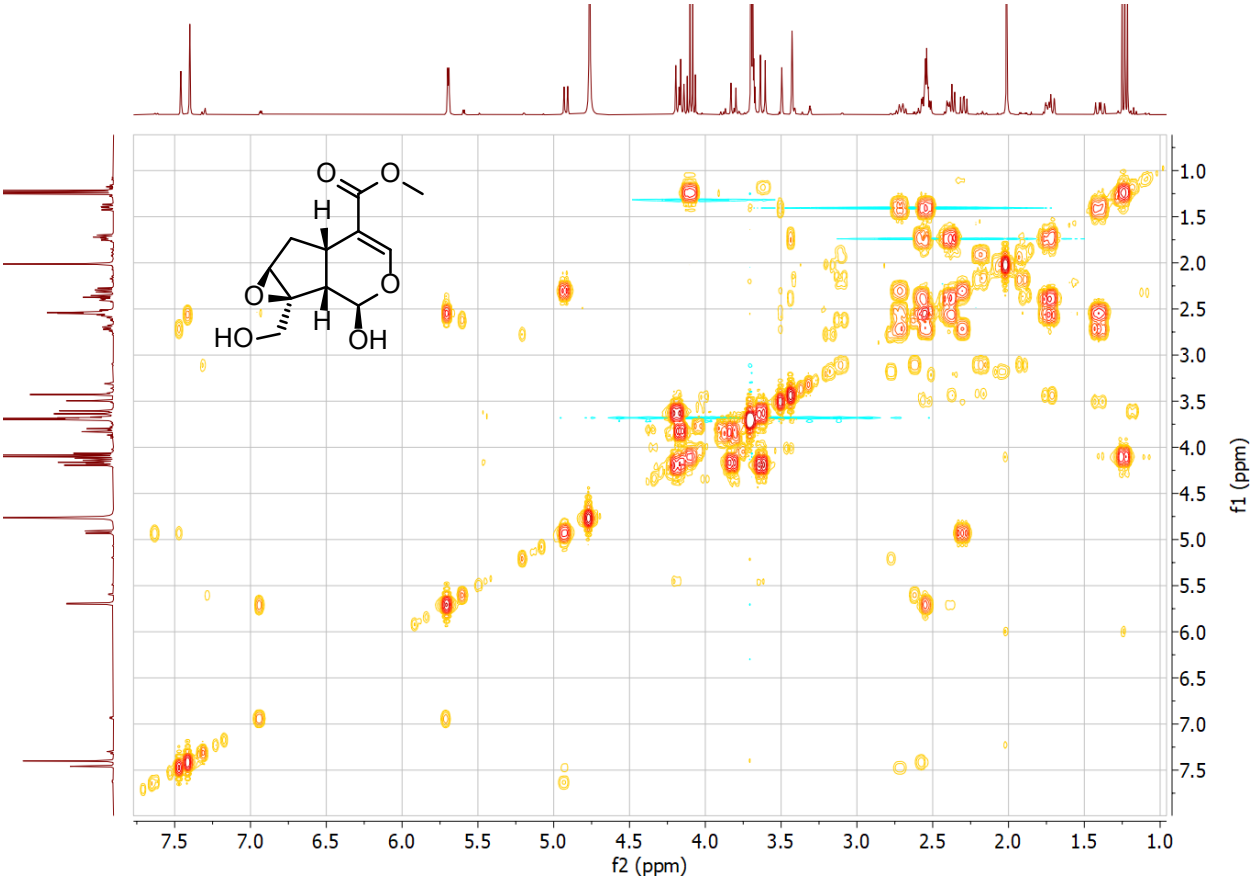

Figure A25. ^{1}H-^{1}H 2D COSY spectrum of **30a** in methanol-d4.

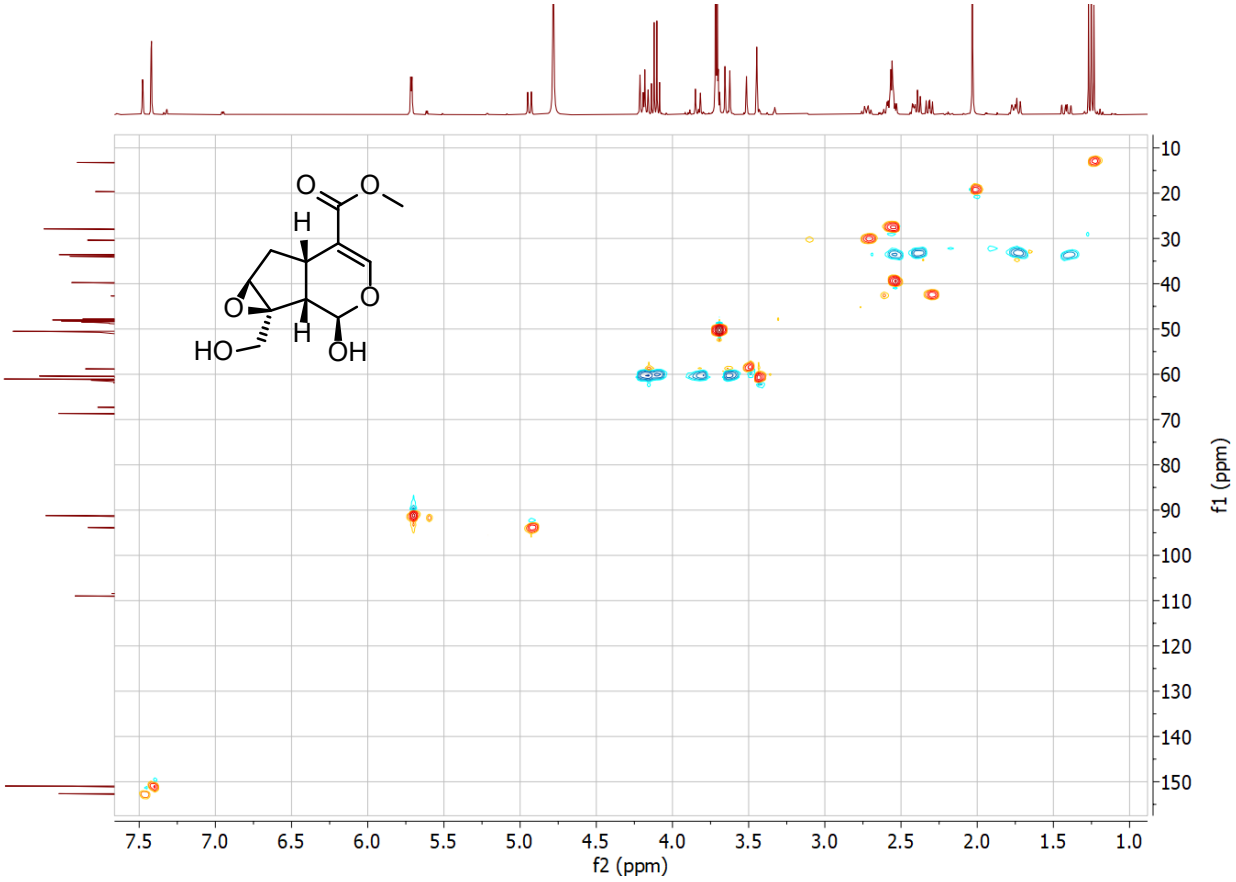

Figure A26. ^{1}H-^{13}C 2D HSQC DEPT-135 of **30a** in methanol-d4.

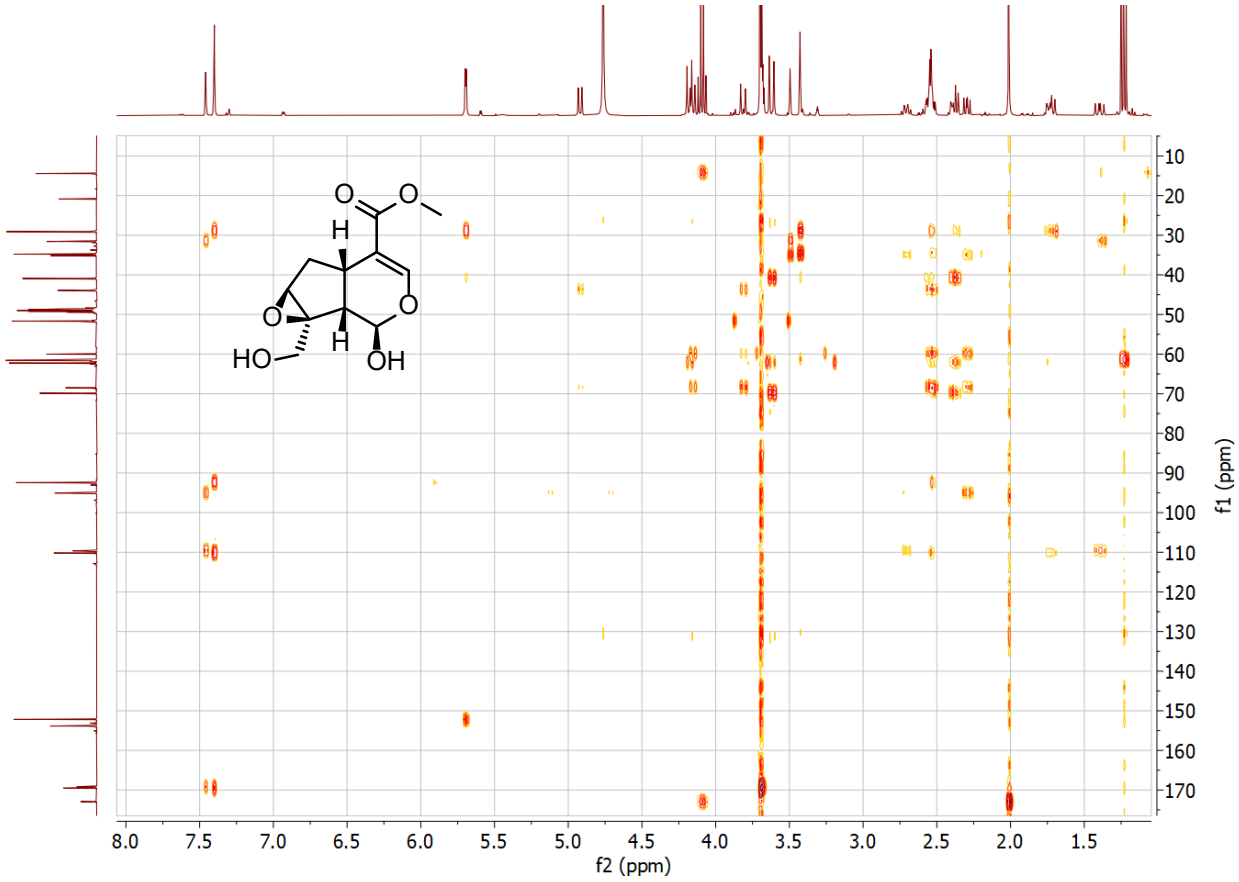

Figure A27. ^{1}H-^{13}C 2D HMBC spectrum of **30a** in methanol-d4.

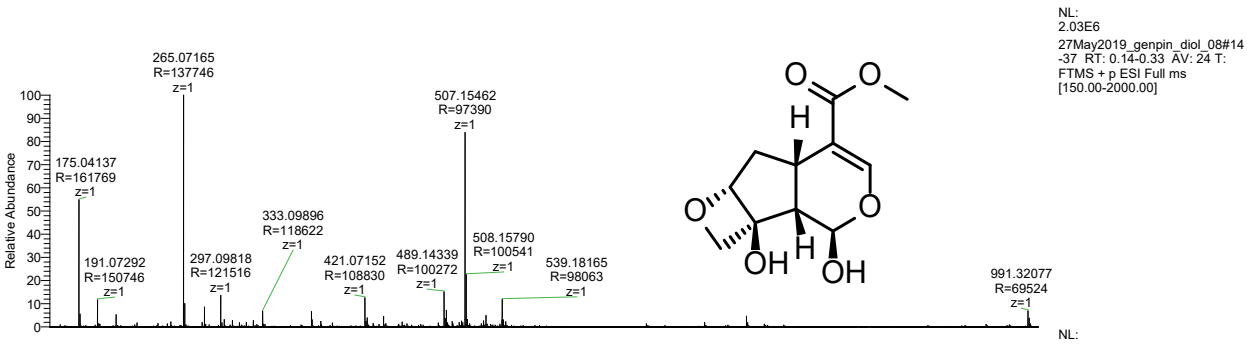

Figure A28. ESI-MS in positive mode of **31**. 266.0715 m/z – **31** $[M+Na]^{+}$

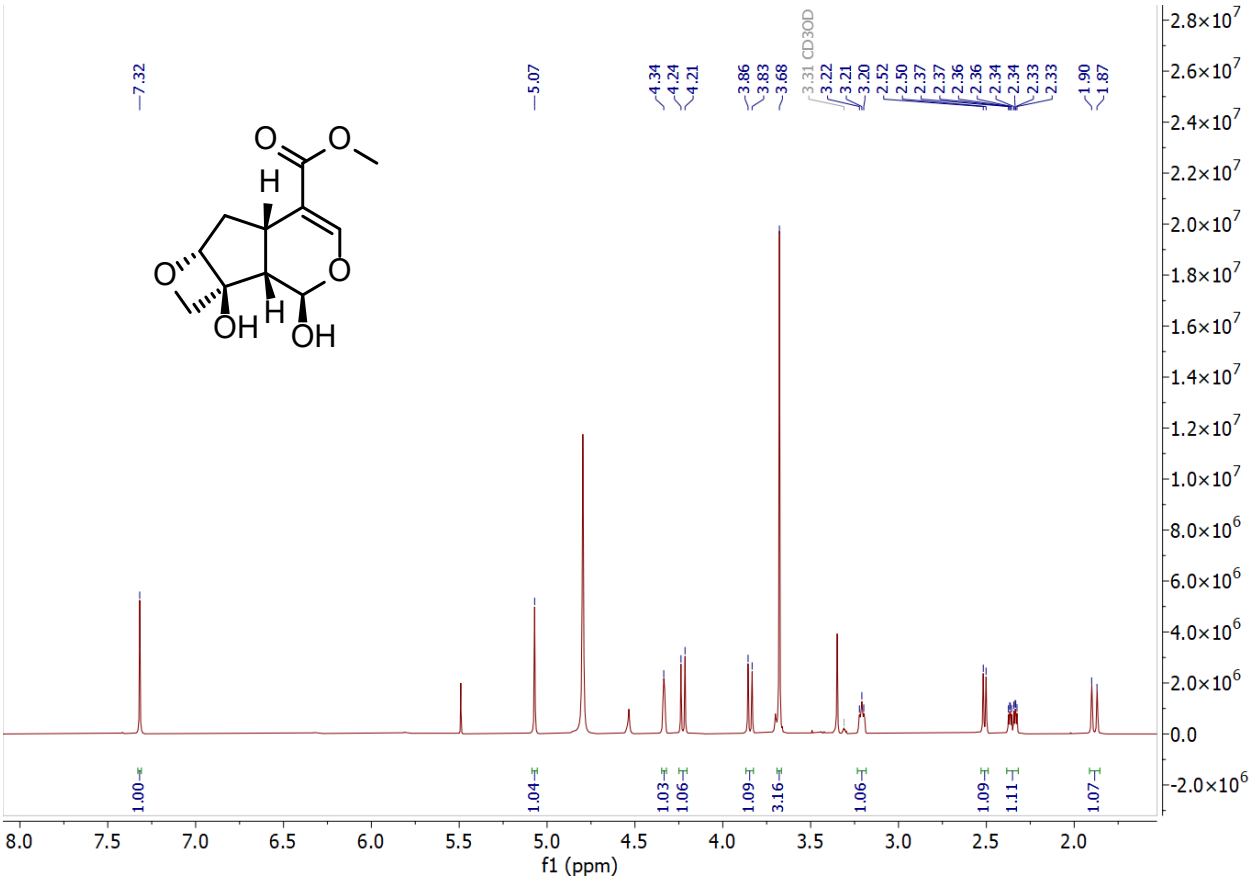

Figure A29. ^{1}H NMR spectrum of **31** in methanol-d4.

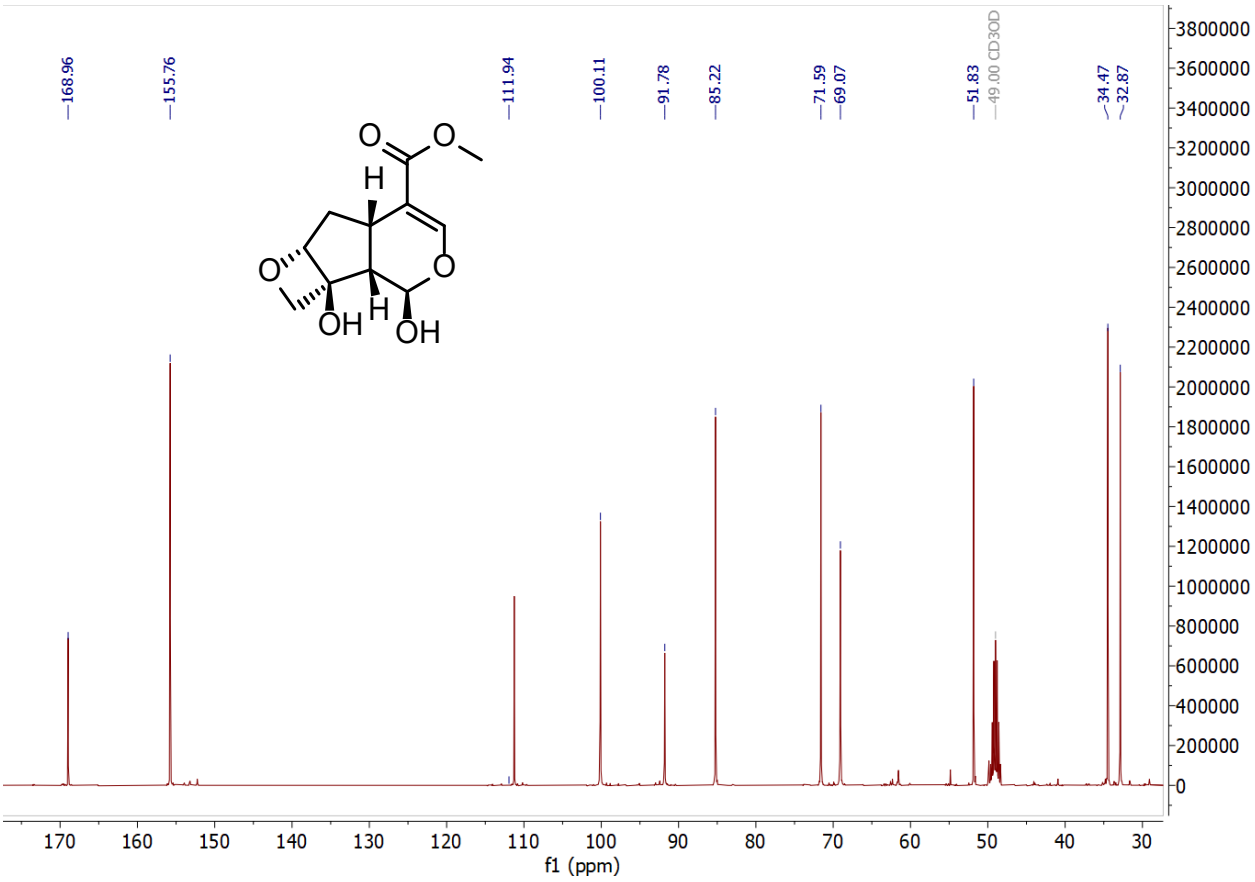

Figure A30. ^{13}C NMR spectrum of **31** in methanol-d4.

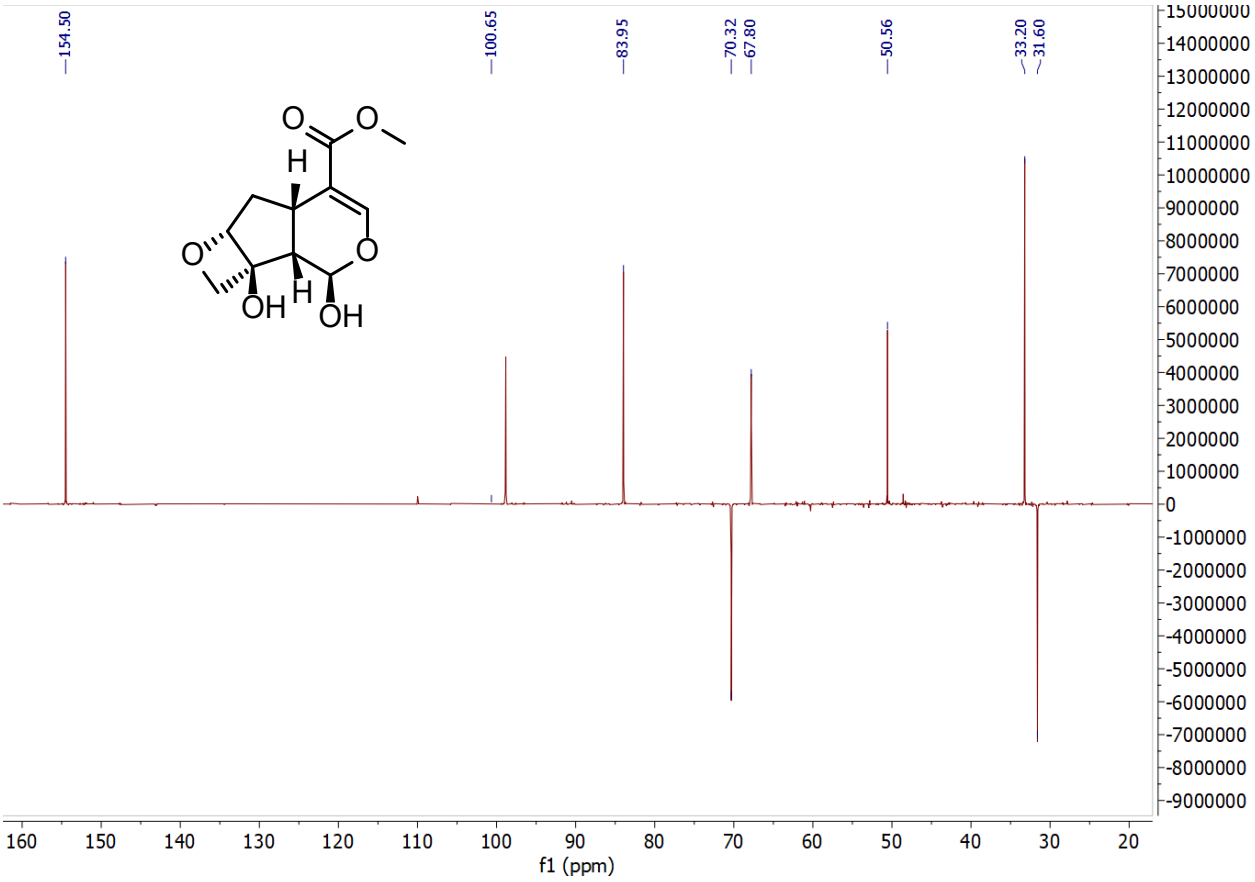

Figure A31. ^{13}C DEPT-135 NMR spectrum of **31** in methanold-4.

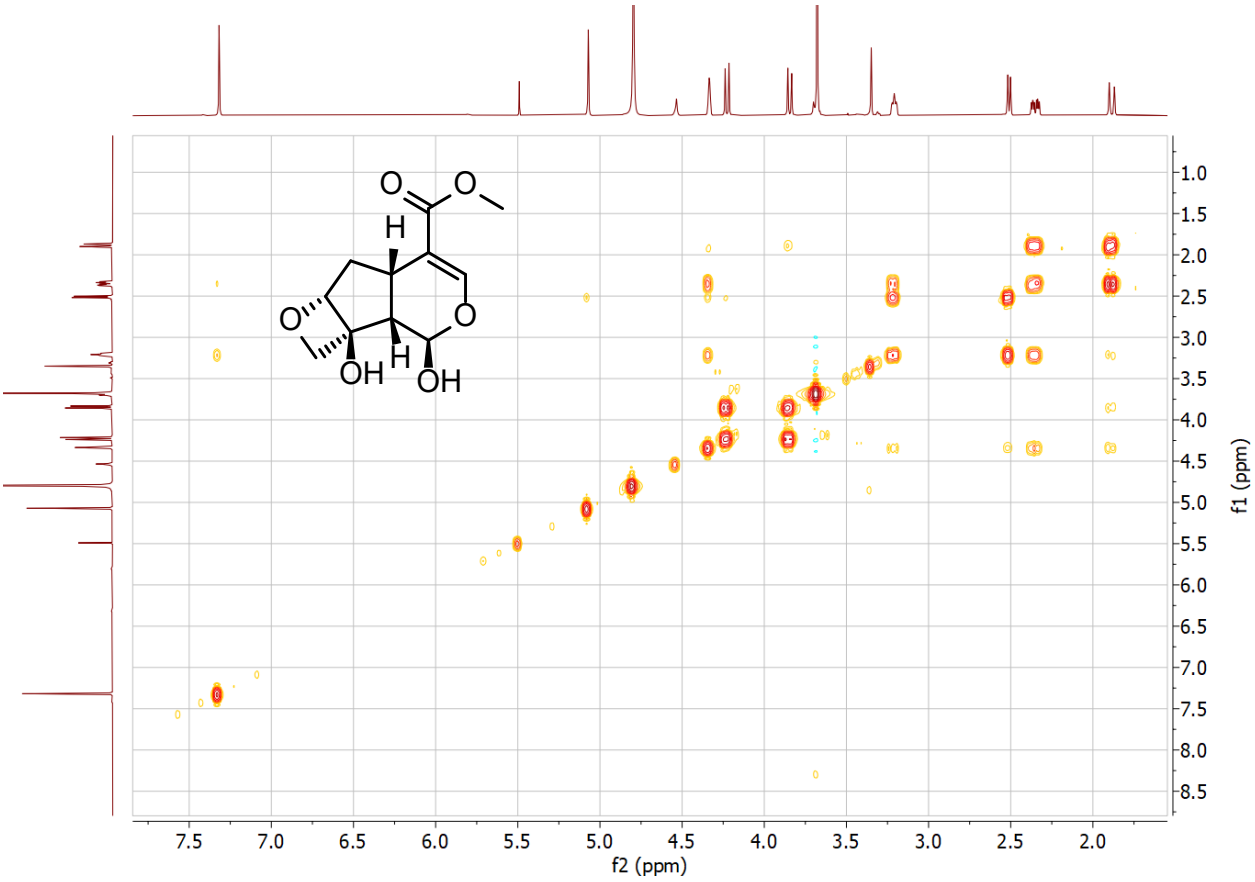

Figure A32. ^{1}H-^{1}H 2D COSY spectrum of **31** in methanol-d4.

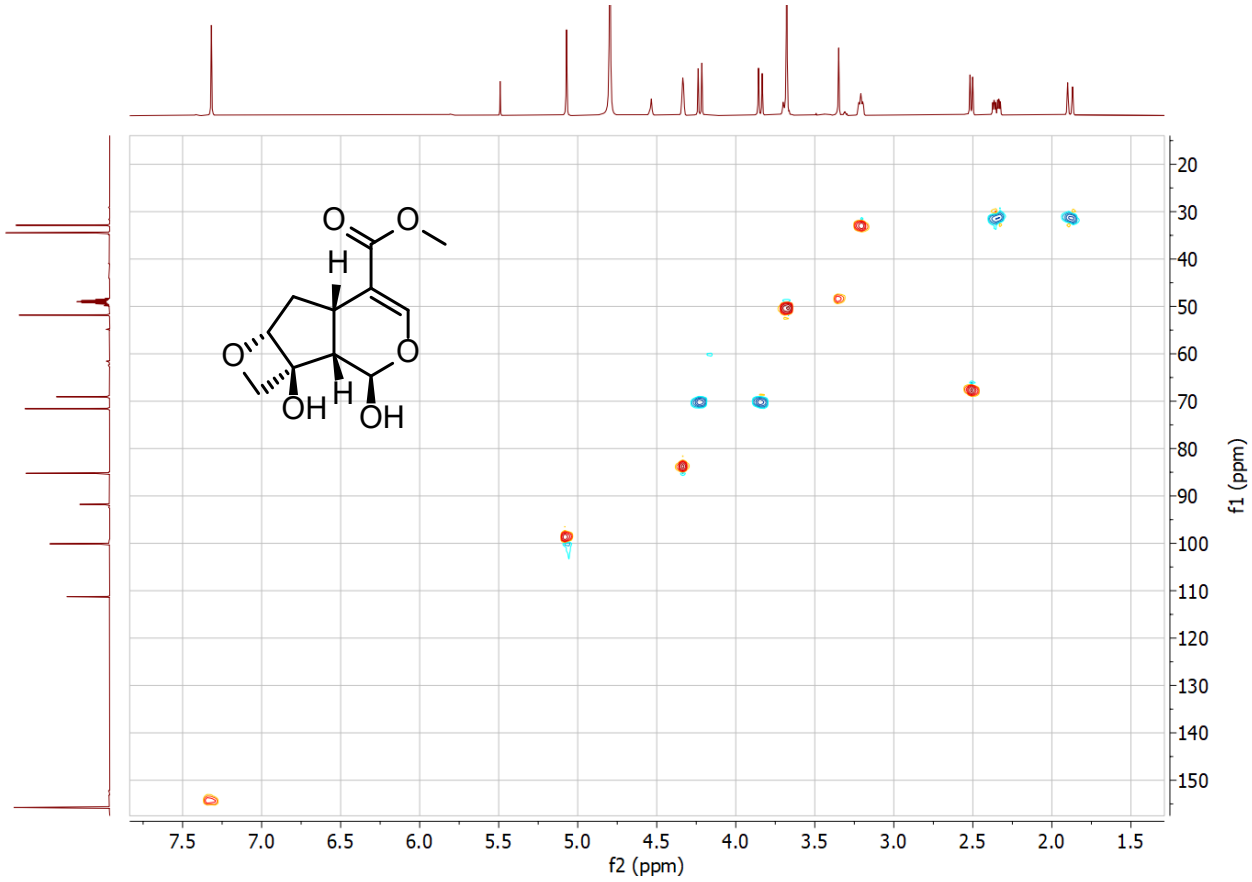

Figure A33. ^{1}H-^{13}C 2D HSQC DEPT-135 spectrum of **31** in methanol-d4.

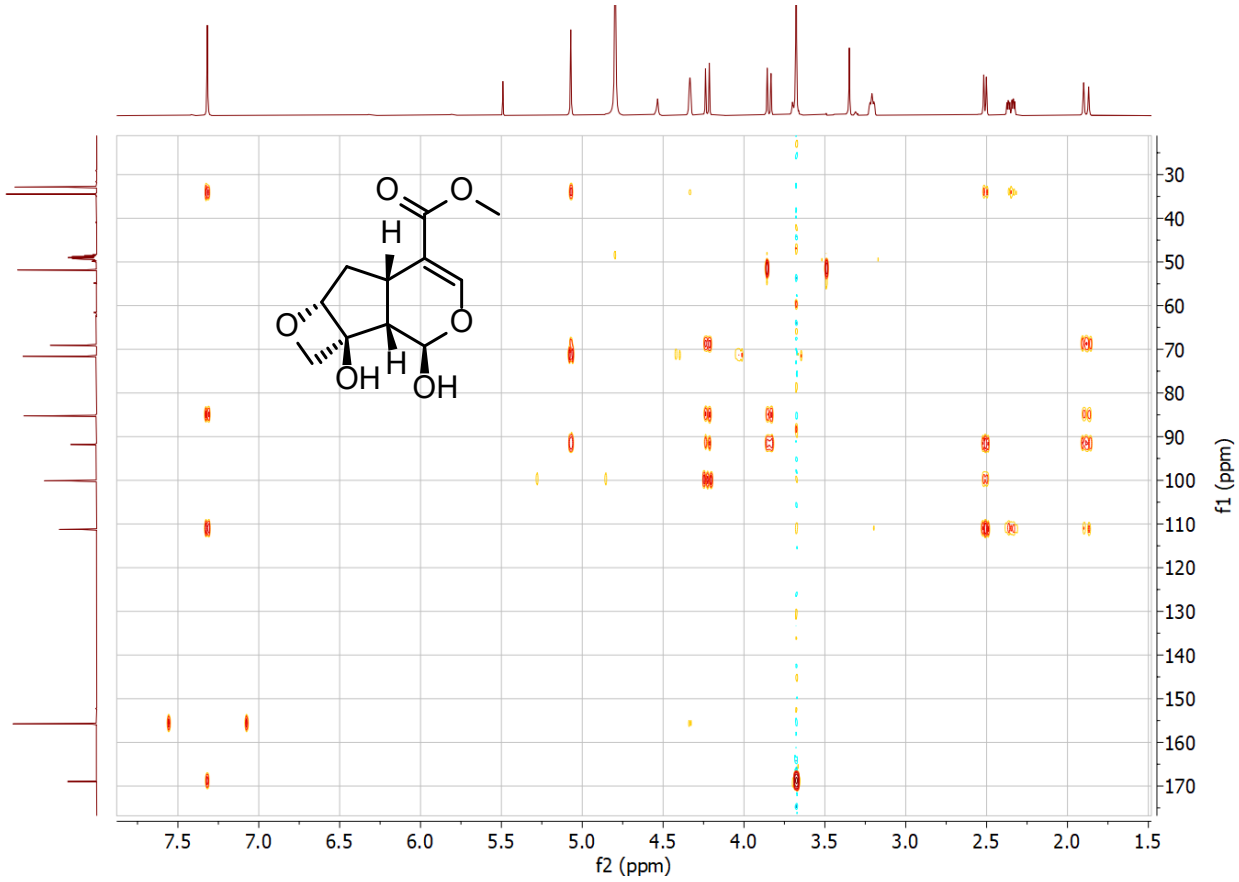

Figure A34. ^{1}H-^{13}C 2D HMBC spectrum of **31** in methanol-d4.

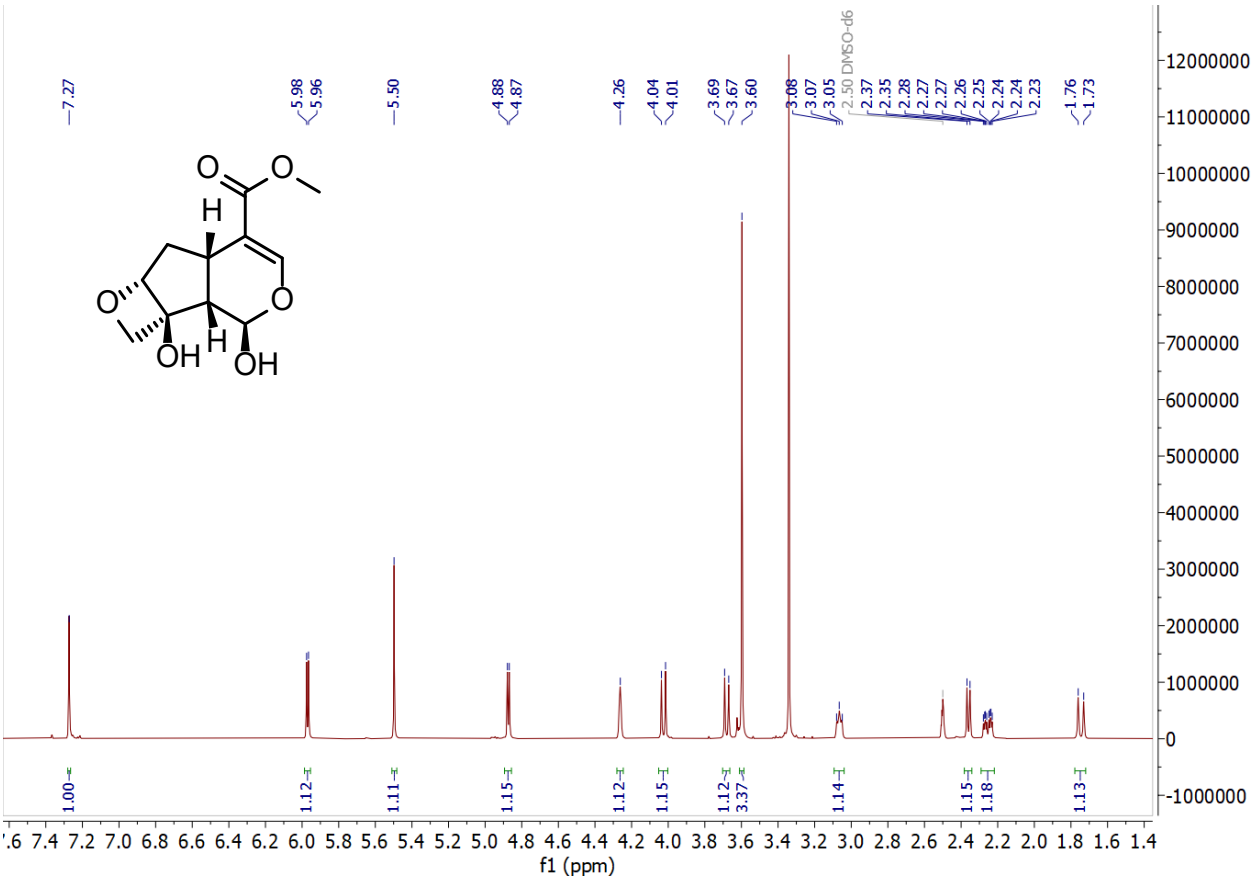

Figure A35. ^{1}H NMR spectrum of **31** in DMSO-d6.

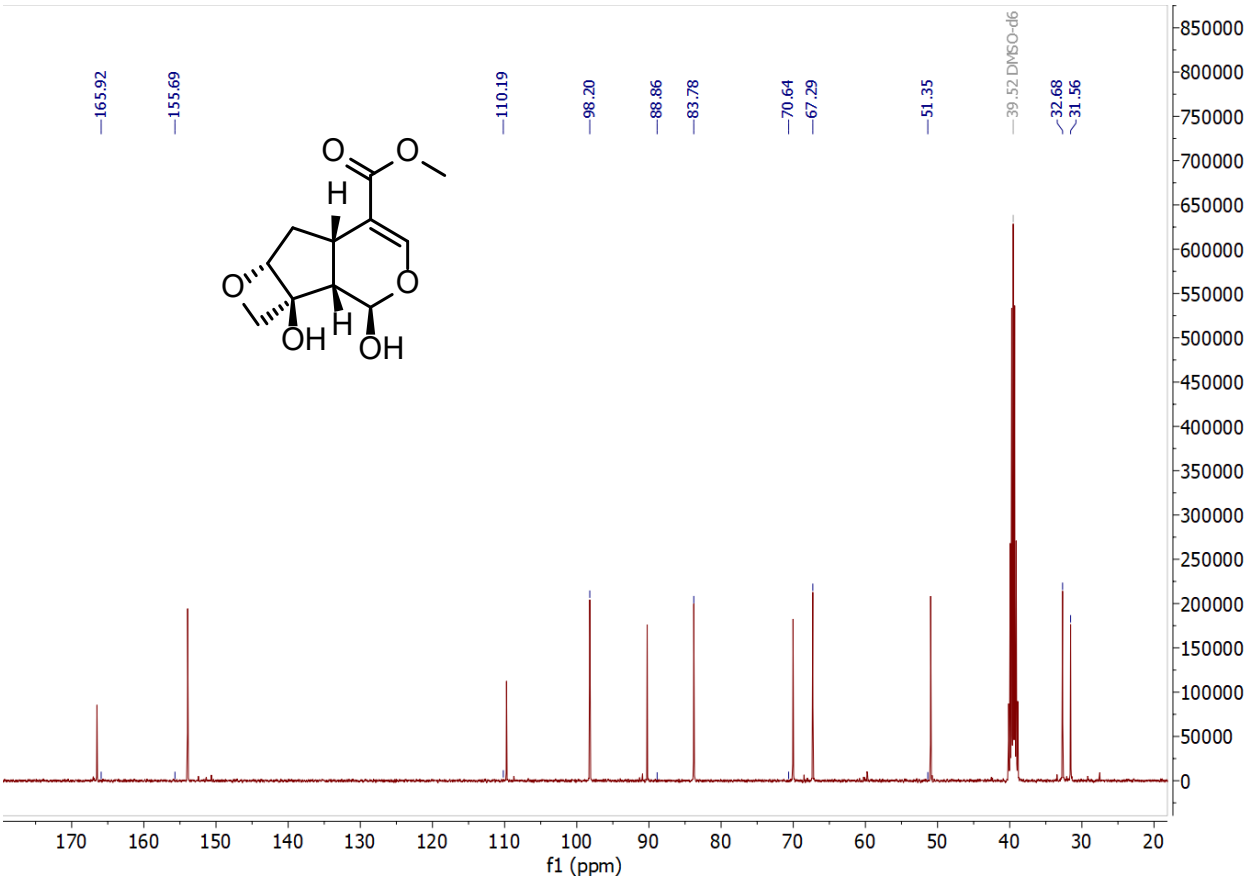

Figure A36. ^{1}H NMR spectrum of **31** in DMSO-d6.

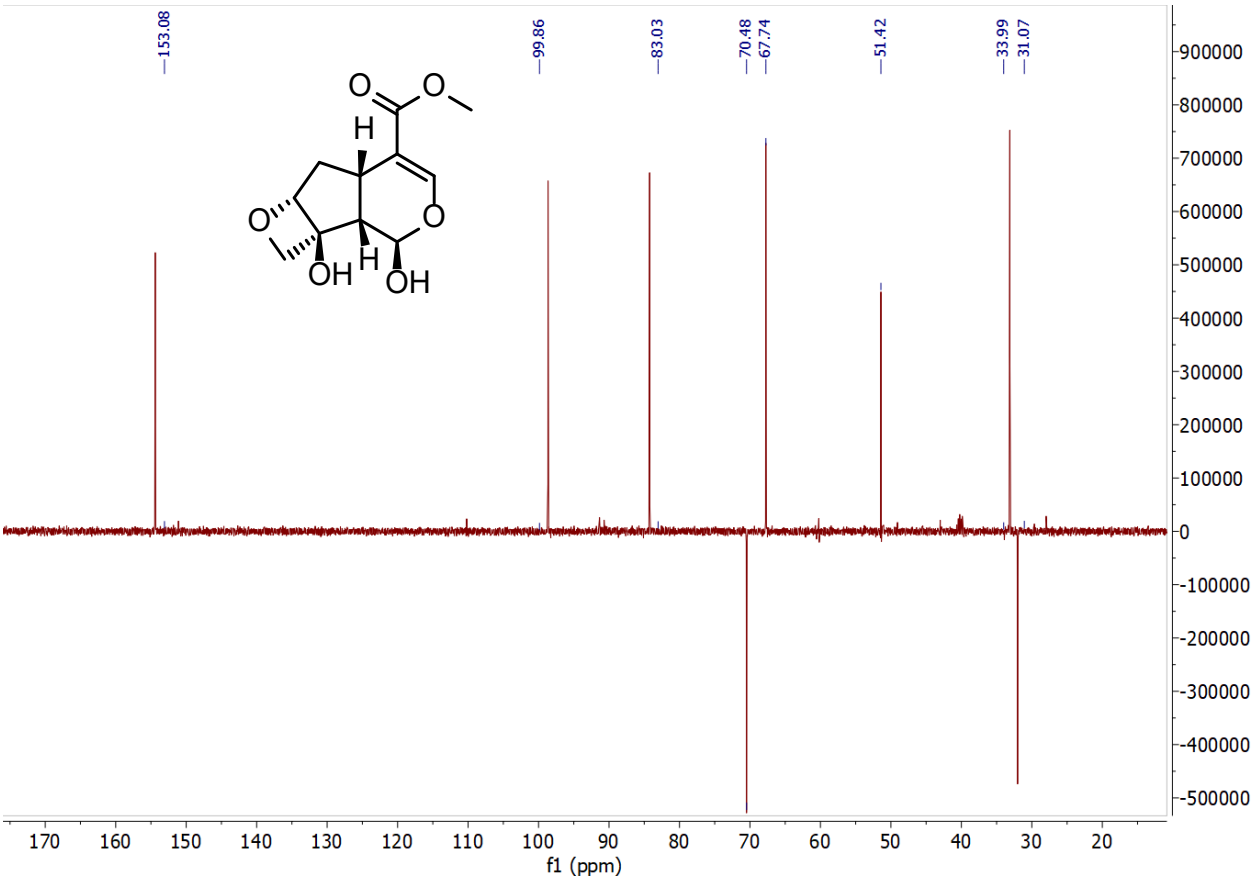

Figure A37. ^{13}C DEPT-135 NMR spectrum of **31** in DMSO-d6.

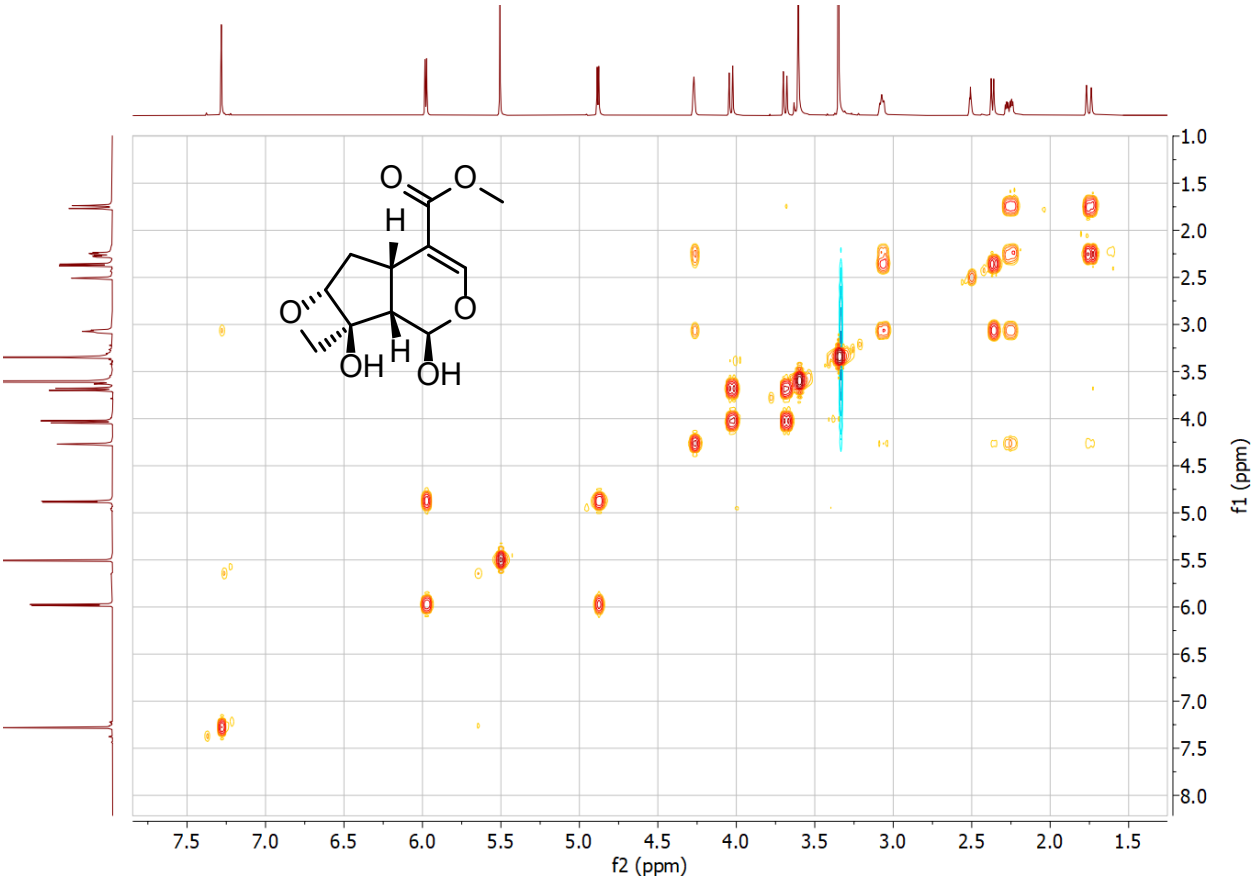

Figure A38. ^{1}H-^{1}H 2D COSY spectrum of **31** in DMSO-d6.

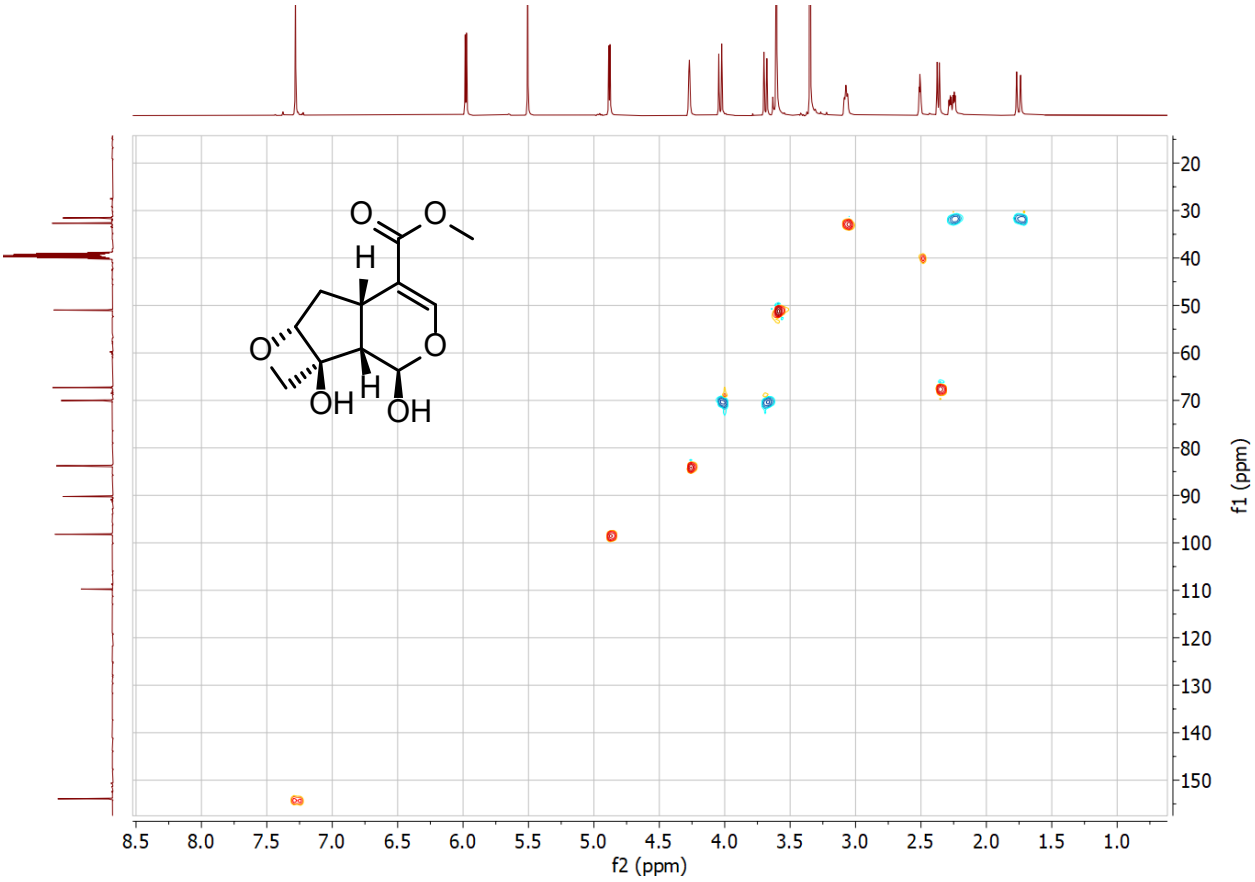

Figure A39. ^{1}H-^{13}C 2D HSQC DEPT-135 spectrum of **31** in DMSO-d6

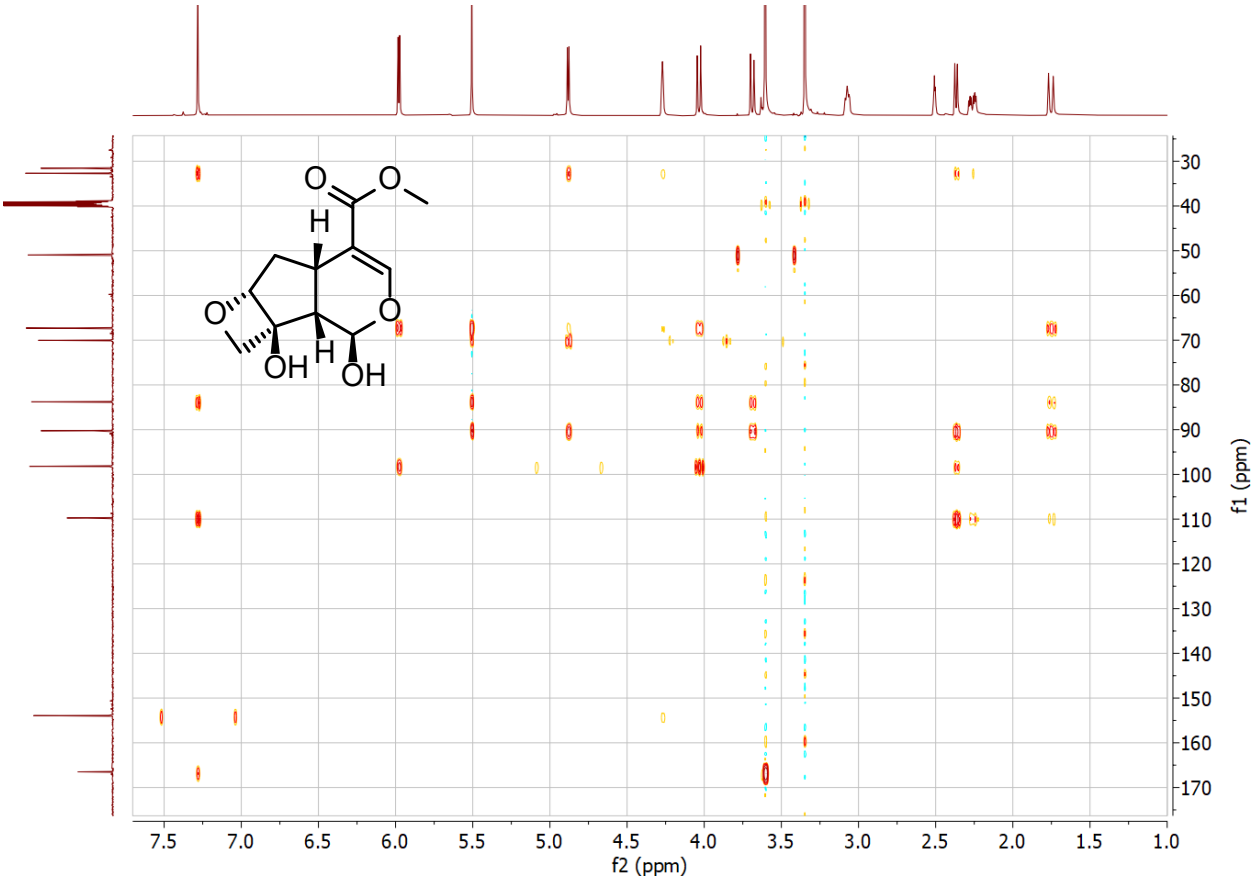

Figure A40. ^{1}H-^{13}C 2D HMBC spectrum of **31** in DMSO-d6.

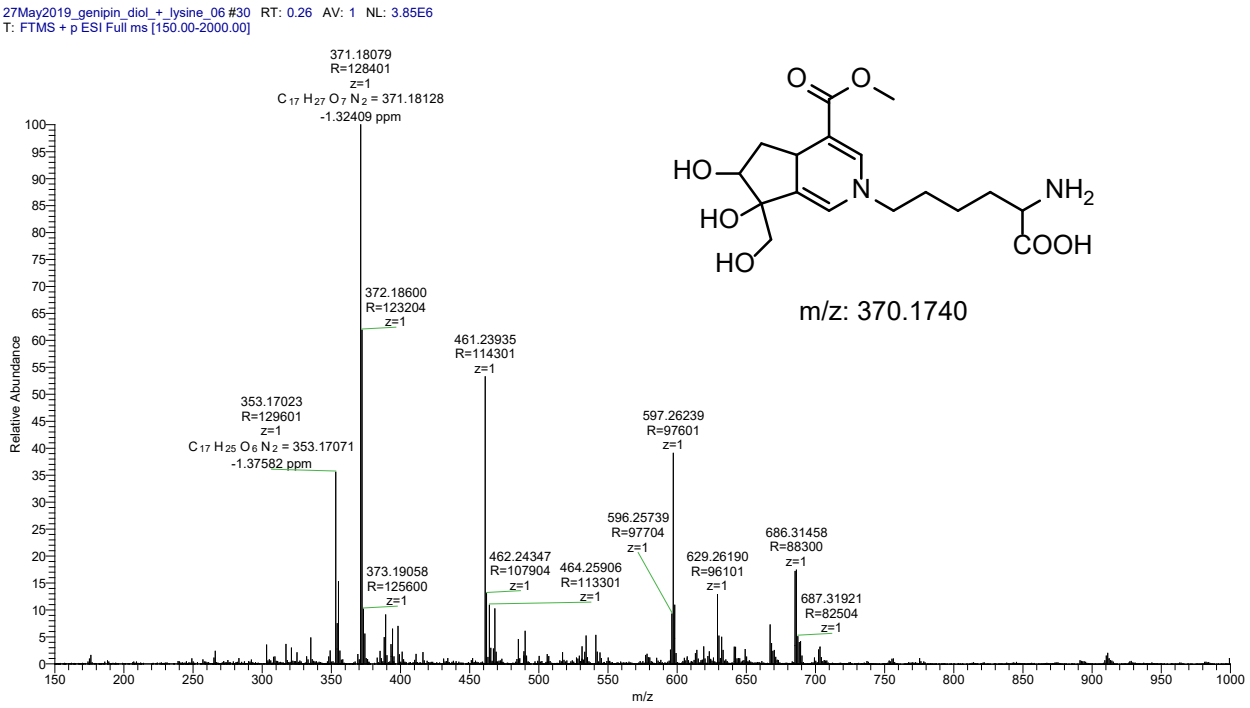

Figure A41. ESI-MS of **32** in positive mode. 371.08079 m/z – **32** $[M+H]^+$.